research report

WYLE LABORATORIES

TESTING DIVISION, HUNTSVILLE FACILITY

WYLE LABORATORIES - RESEARCH STAFF

REPORT WR 71-10

PREDICTION OF IN-FLIGHT FLUCTUATING PRESSURE ENVIRONMENTS INCLUDING PROTUBERANCE INDUCED FLOW

By

J.E. Robertson

Work Performed Under Contract NAS8-25700

March 1971

WYLE LABORATORIES

RESEARCH DIVISION, HUNTSVILLE FACILITY

COPY NO. 12

FOREWORD

This report was prepared by Wyle Laboratories, Research Division, Huntsville, Alabama for the Unsteady Gasdynamics Branch, Aero-Astrodynamics Laboratory, Marshall Space Flight Center (MSFC), National Aeronautics and Space Administration (NASA), Huntsville, Alabama under Contract NAS8-25700. This work was performed under the direction of Messrs. G. Wilhold — Deputy Chief of the MSFC Unsteady Gasdynamics Branch, and J. Jones — Technical Monitor of the contract.

This report contains an analysis of various fluctuating pressure environments for the purpose of formulating prediction methods and includes protuberance induced flows. Key features of the present investigation are the bringing together of data from disparate sources, combining the results to show general trends for the various unsteady flow environments, and, based on the combined results, the development of prediction methods.

The author wishes to express his appreciation and to extend thanks to Messrs. Gil Wilhold and Jess Jones of MSFC for their direction during the course of this study, and to Dr. B.J. Tu of Wyle Laboratories for his assistance in analyzing portions of the data presented in Section 3.0.

ABSTRACT

In recent years, considerable effort has been devoted to the study of unsteady flows over the surface of many different vehicles — aircraft, launch vehicles, underwater craft, etc. The fluctuating pressures resulting from unsteady flows can be an important source of vibration and sound and thus significantly affect the performance and environments of these vehicles. Fluctuating pressures may arise from several modes of disturbances, however, they are most often introduced by the passage of turbulence over the external surface. Particular phenomena which can be of significance in various circumstances include: attached boundary layers, separated boundary layers, oscillating shock waves (often referred to as shock-boundary layer interaction), protuberance flows, jet impingement, cavity response phenomena, and base or wake flow. Many of the phenomena above involve forms of turbulent separated boundary layer flows, and this report is centered around a description of these.

One of the critical flight regimes for aircraft and space vehicles is in the transonic speed range, and a major portion of this effort is devoted to an investigation of the transonic fluctuating pressure environments. Based on test results from many sources, prediction methods for various unsteady flow environments are formulated. In particular, prediction methods are proposed for (1) basic fluctuating pressure phenomena which will occur on virtually all aerospace vehicles during some phase of launch and (2) protuberance induced fluctuating pressure phenomena which are typical of three-dimensional protuberances attached to the external surfaces of a vehicle. The prediction methods for the basic fluctuating pressure phenomena were developed for two-dimensional and axisymmetric configurations; however, the conclusions are of fairly general application. The prediction of overall levels, spectra and cross-spectra for both basic and protuberance induced fluctuating pressure phenomena are compared to show characteristics unique to the particular unsteady flow condition. Key features of the present investigation are the bringing together of data from disparate sources, combining the results to show general trends for the various unsteady flow phenomena, and, based on the combined results, the development of prediction methods. It is anticipated that the results of this study will be a useful tool in the prediction of full-scale fluctuating pressure environments of future aerospace vehicles such as Space Shuttle as well as in the interpretation of the model and full scale test results.

TABLE OF CONTENTS

		Page
FOREWORD		ii
ABSTRACT		iii
TABLE OF CONTENTS		iv
LIST OF FIGURES		v
1.0	INTRODUCTION	1
2.0	BASIC FLUCTUATING PRESSURE ENVIRONMENTS	4
2.1	Attached Turbulent Boundary Layers	5
2.2	Separated Flow	10
2.3	Shock-Wave Oscillation	16
2.4	Non-Homogeneous Attached and Separated Flows	22
3.0	PROTUBERANCE INDUCED FLUCTUATING PRESSURE ENVIRONMENTS	27
3.1	General Characteristics of Protuberance Induced Flow	27
3.2	Protuberance Induced Separated Flow	30
3.3	Protuberance Induced Shock-Wave Oscillation	35
3.4	Protuberance Induced Wake Flow	38
3.5	Comparisons of Generalized and Specific Geometry Protuberances	40
4.0	CONCLUDING REMARKS	41
4.1	Power Spectra	41
4.2	Cross-Power Spectra	42
REFERENCES		44
FIGURES		46

LIST OF FIGURES

Figure		Page
1.	Subsonic, Transonic, and Supersonic Flow Fields for Basic Vehicle Configurations	46
2.	Comparison of Pressure Fluctuation Measurements by Various Investigators for Attached Turbulent Boundary Layers	47
3.	Power Spectra for Turbulent Boundary Layer Fluctuating Pressures	48
4a.	Narrow Band Longitudinal Space Correlation Coefficient for Boundary Layer Fluctuating Pressures	49
4b.	Narrow Band Lateral Space Correlation Coefficient for Boundary Layer Fluctuating Pressures	49
5.	Axial Distributions of Fluctuating Pressures for Blunt Body Separated Flow (Ref. 18)	50
6.	Axial Distributions of Static and Fluctuating Pressures for Flare Induced Separation (Ref. 14)	51
7.	Variation of Normalized RMS Fluctuating Pressure Level with Local Mach Number for Expansion Induced Separated Flow	52
8.	Variation of Fluctuating Pressure Level for Separated Flow with Mach Number	53
9.	Power Spectrum of Fluctuating Pressures within Separated Flow Regions	54
10.	Typical Longitudinal Cross-Spectra of Pressure Fluctuations for Separated Flow (Ref. 14)	55
11.	Axial Distribution of Fluctuating Pressures for Cone-Cylinder Body	56
12.	Comparison of Power Spectra for Shock-Wave-Oscillation Induced by Two- and Three-Dimensional Protuberances	57
13.	Longitudinal Distribution of Pressure Fluctuations and Typical Power Spectra in Vicinity of Supersonic Flow Separation Ahead of a 45° Wedge	58
14.	Correlation of Pressure Fluctuations Between Shock Wave and Adjacent Attached and Separated Flows (Reference 20)	59

LIST OF FIGURES (Continued)

Figure		Page
15.	Typical Oil Flow Pattern of the Protuberance Flow Field	60
16.	Variation of Separation Length with Protuberance Height	61
17.	Composite Schematic of Protuberance Flow Field Characteristics, $M_\infty = 1.60$, $h/D = 2.0$	62
18.	Comparison of Two- and Three-Dimensional Separated Flows	63
19.	Smoke Filament Flow Pattern Upstream of a Cylindrical Protuberance at Low Speed	64
20.	Comparison of the Axial Distributions of RMS Fluctuating Pressure Coefficient for the Various Cylindrical Protuberances	65
21.	Power Spectra for the Outer Region of Separated Flow Induced by Cylindrical Protuberances Showing the Data Collapse Using ℓ_s and U_∞ as Normalizing Parameters	71
22.	Comparison of Empirical Predictions with Experimentally Measured Power Spectra for the Outer Region of Separated Flow, $M_\infty = 1.60$, $h/D = 2.0$	72
23.	Power Spectra for the Inner Region of Separated Flow Induced by Cylindrical Protuberances Showing the Data Collapse Using ℓ_s and U_∞ as Normalizing Parameters	75
24.	Comparison of Empirical Prediction with Experimentally Measured Power Spectra for the Inner Region of Separated Flow, $M_\infty = 1.60$, $h/D = 2.0$, $r/D = 1.25$	76
25.	Variation of Longitudinal Cross-Spectra Within the Upstream Separated Flow Field, $M_\infty = 1.60$, $h/D = 2.0$	77
26.	Comparison of Predicted and Measured Power Spectra for Shock-Wave Oscillation Upstream of Two- and Three-Dimensional Separated Flow Fields	79
27.	Comparison of Predicted and Measured Power Spectra for Various Regions of the Wake Downstream of a Cylindrical Protuberance ($M_\infty = 1.60$, $h/D = 1.0$, $D = 8$ in.)	80

LIST OF FIGURES (Continued)

Figure		Page
28.	Variation of Longitudinal Cross-Spectra within the Downstream Wake Flow Field, $M_\infty = 1.60$, $h/D = 2.0$	83
29.	Comparison of Coherence Function for Various Fluctuating Pressure Environments, $M_\infty = 1.60$	85
30.	Comparison of the Axial Distribution of RMS Fluctuating Pressure Coefficient for the RCS Protuberance and a Cylindrical Protuberance	86
31.	Comparison of the Axial Distribution of RMS Fluctuating Pressure Coefficient for the APU Protuberance and a Cylindrical Protuberance	87

1.0 INTRODUCTION

When a vehicle moves through air there are two basic means by which it can produce noise: (1) by its propulsion mechanisms (motor-jet, rocket, etc.) and (2) by its interaction with its surroundings. At low speeds, for example, during and immediately after lift-off, the first of these is by far the dominant one while near or above the speed of sound, mechanism (2) becomes most important.

During any flight cycle for an aerospace vehicle, there are four important phases of the flight which should be investigated in order to assess the environmental trends due to acoustics and fluctuating pressures. These are listed in the chronological order in which they occur.

- Lift-off phase during which acoustic excitation results from the rocket exhaust noise.
- Launch flight to orbit phase, during which rocket exhaust noise diminishes and aerodynamic fluctuating pressures (pseudo-sound) start to dominate. From an aerodynamic noise viewpoint, this phase becomes most critical at transonic Mach numbers ($0.60 \leq M \leq 1.6$).
- Re-entry phase during which only aerodynamic fluctuating pressures are present.
- Flyback phase during which the noise from flyback engines dominate.

This report is devoted to the specification of surface fluctuating pressures resulting from unsteady aerodynamic flows which occur during the launch phase of flight. In-flight surface fluctuating pressures are distinctly different from acoustic disturbances originating from rocket exhaust flows and engine noise. In-flight disturbances, as considered herein, arise from several modes of disturbances — the principle source being the passage of a turbulence environment over the external surface. One other important source to be discussed is shock wave oscillation which is characterized by both turbulence (in close proximity to the foot of the shock wave) and pseudo-static disturbances resulting from the modulation of the pressure gradient through the shock wave. Thus, in-flight fluctuating pressure phenomena are near-field mechanisms acting on the surface of a vehicle with the distinction that the disturbances are generally convected at some fraction of the local mean flow velocity. On the other hand, rocket exhaust noise and engine noise are acoustic mode disturbances which generally originate away from the surface. Furthermore, acoustic mode disturbances consist of sound waves which propagate at the local speed of sound with a direction independent of the local velocity.

Two specific areas are considered in the present analysis: (1) basic fluctuating pressure environments which will occur on virtually all aerospace vehicles during some phase of launch, and (2) protuberance induced fluctuating pressure environments which occur in close proximity to three-dimensional projections on the external surface of vehicles. Distinction is made between the two areas since the "basic" fluctuating pressure phenomena are dictated by the aerodynamic flow field of the overall vehicle, whereas, protuberance induced phenomena are relatively localized fluctuating pressure mechanisms which are essentially superimposed within the basic flow field. Basic fluctuating pressure environments which are examined are: attached boundary layer flows; separated flows, and shock-boundary layer interactions. For protuberance induced flows, fluctuating pressures in both the upstream separated flow region and the downstream wake region are studied.

Aerodynamic fluctuating pressures are zero at launch and increase to peak values as the vehicle passes through the transonic Mach number range. Previous wind tunnel and flight data show that fluctuating pressures are proportional to free-stream dynamic pressure (q_∞) for a given unsteady flow phenomenon. However, peak fluctuating pressures do not necessarily occur at maximum q_∞ for certain regions of a vehicle due to the non-homogeneous nature of the flow field. For example, regions of the vehicle exposed to separated flow and the impingement of oscillating shock waves will experience fluctuating pressures at least an order of magnitude greater than regions exposed to attached flow. Thus, if separated flow and oscillating shock waves are present, say at Mach numbers other than the range of maximum q_∞, then peak fluctuating pressures will also be encountered at conditions other than at maximum q_∞. Thus, it is easily seen that vehicle configuration is very important in the specification of fluctuating pressure levels since the source phenomena are highly configuration dependent in addition to varying with Mach number and angle of attack.

In light of the foregoing discussion, one general statement can be made in regard to aerodynamic fluctuating pressures. Regions exposed to the same unsteady phenomenon will experience fluctuating pressure levels which are proportional to free-stream dynamic pressure. Thus, it can be readily seen that a fundamental parameter in the specification of the surface excitation is free-stream dynamic pressure and its variation with Mach number. For a given configuration, Mach number and angle of attack define the phenomena, and dynamic pressure defines the fluctuating pressure levels associated with the phenomena.

There are an infinite number of possible vehicle configurations and any discussion of their fluctuating pressure environments must be general. Practically all experimental data for unsteady aerodynamic flow have been acquired for bodies of revolution which are typical of missile configurations. As a result of these studies, it is well known to those working in this field, that certain basic unsteady flow conditions will occur regardless of the detailed geometry of the vehicle. It is convenient to discuss these

basic flow conditions for bodies of revolution; however, this is certainly no restriction on either the feasibility or the practicality of predicting their occurrence on more complicated configurations such as Space Shuttle. Thus, in Section 2.0, general features of typical bodies of revolution are defined and the unsteady flow fields which they encounter are discussed.

Similarly, the number of possible external protuberance geometries are unlimited. Thus, the three-dimensional flow fields induced by external protuberances will be discussed, primarily, for generalized protuberance shapes. The salient features of protuberance induced flows are basically the same regardless of the detailed geometry of the protuberances. However, there are regions in the protuberance flow field where free-interaction hypothesis becomes invalid. The analyses of surface fluctuating pressures for protuberance induced flows is presented in Section 3.0. Finally, concluding remarks are presented in Section 4.0.

2.0 BASIC FLUCTUATING PRESSURE ENVIRONMENTS

Examples of several bodies of revolution are shown in Figure 1. For the purpose of the present discussion, three basic configurations will be considered as specified below:

- Cone-cylinder
- Cone-cylinder-flare
- Cone-cylinder-boattail

Virtually all axisymmetric vehicles fall into one of these categories although numerous modifications to the basic geometry have been employed in the past.

Several fluctuating pressure environments having different statistical properties may exist over a vehicle at any given instant in the flight trajectory. It is convenient to consider three separate Mach number ranges — subsonic, transonic, and supersonic — for each of the three basic shroud configurations. Further, the flow fields will depend on the angle of attack of the vehicle which causes nonsymmetrical loading (both statically and dynamically); however, for the purpose of this discussion, nonsymmetrical loading will not be discussed.

Schematics of subsonic, transonic and supersonic flow fields for the basic configurations are shown in Figure 1. At subsonic speeds, all three configurations experience regions of attached flow and separated flow. The cone-cylinder portion of each configuration induces separated flow immediately aft of the cone-cylinder juncture for cones having half-angles greater than approximately 15 degrees. Re-attachment occurs within approximately one diameter aft of the shoulder (depending on cone angle) for the cone-cylinder and boattail configurations, whereas for the flare body, separation may continue over the flare. Both the flare and boattail induce separation for typical configurations. At high transonic speeds, the flow negotiates the shoulder of a cone-cylinder body without separating, reaches supersonic speed immediately aft of the shoulder and produces a near-normal, terminal, shock wave a short distance aft of the shoulder. The boundary layer immediately aft of the shock may or may not separate depending on the strength of the shock wave. At transonic speeds, the boattail and flare region produce separated flow which may be accompanied by weak shock waves in the vicinity of the separation and reattachment points. At supersonic speeds, the cone-cylinder configurations produce regions of attached flow. For the flare configuration, the separated flow is bounded by shock waves at the separation and reattachment points, whereas for the boattail configuration, separation occurs at the shoulder of the boattail (expansion region) and is bounded at the reattachment point by a shock wave.

It is evident that even simple vehicle shapes, such as cone-cylinders, produce complex and highly nonhomogeneous flow fields at certain Mach numbers — particularly at subsonic and transonic speeds. The unsteady flow phenomena are of particular

importance at transonic speeds, since in this range, fluctuating pressures reach maximum values due to their proportionality to dynamic pressure. In order to assess the fluctuating pressure environment of a vehicle of any arbitrary geometry, it is convenient to discuss the statistical properties of the fluctuating pressures for each of the basic types of unsteady flow condition. From Figure 1 it will be noted that the following flow conditions may occur for various regions of a vehicle.

- Attached flow
- Separated flow
- Shock-boundary layer interaction

The surface fluctuating pressures for each of the above flow conditions exhibit different statistical characteristics. Attached flow pressure fluctuations result from the disturbances within turbulent boundary layers. Separated flow pressure fluctuations result from disturbances within the separated shear layer and instabilities associated with the separation and reattachment points. Pressure fluctuations for shock-boundary layer interaction result from the movement of the shock wave and the static pressure discontinuity associated with the shock wave. The statistical characteristics of each fluctuating pressure environment that are important in the analysis of structural response may be classified under three parameters:

- The overall level
- The power spectrum
- The cross-power spectrum (or narrow band cross correlation)

The surface fluctuating pressures for each unsteady flow condition with their unique statistical characteristics will be discussed separately in the following subsections.

2.1 Attached Turbulent Boundary Layers

The surface fluctuating pressures beneath attached turbulent boundary layers have been the subject of both theoretical and experimental study for a number of years. The turbulent boundary layer extends over a considerable portion of the surface of vehicles in flight and, thus, it is considered to be one of the principle sources of aero-acoustic excitation to the vehicle structure. Several years ago, workers such as Kraichnan, Lilley, and Hodgson developed theoretical formulations for the fluctuating pressures under turbulent boundary layers and, more recently, several carefully planned experiments have provided additional information on the statistical characteristics of the pertubations. Lowson, Reference 1, presents a good summary of the results of studies on this subject, with the exception of some recent measurements by NASA-Ames. In Lowson's report, the basic mechanism underlying the production of the surface pressure fluctuations beneath turbulent boundary layers is discussed, together with a presentation of empirical and semi-empirical prediction techniques. This section of the present discussion is a brief overview of Lowson's

prediction formulae with the exception of the power spectra, which has been modified to be more consistent with the power spectra at low Strouhal numbers. The following discussion presents a review of the experimental results and prediction formulae in terms of the most important statistical parameters.

Overall Level

The correct method of presenting overall fluctuating pressure levels for surfaces beneath the convected turbulence in boundary layers is in terms of the root-mean-square fluctuating pressure level, $\sqrt{\overline{p^2}}$. Free-stream dynamic pressure, q_∞, local dynamic pressure, q_ℓ, and wall shear stress, τ_ω, have been used to normalize $\sqrt{\overline{p^2}}$ so that meaningful data collapse can be realized throughout the Mach number range. The most generally accepted normalizing parameter is q_∞ and thus, it will be used in the current expressions.

The effects of Mach number on the normalized rms intensities of the fluctuating pressures in attached flows are shown in Figure 2. There is significant scatter in the data which may be attributed to several factors: (1) background noise and free-stream turbulence in the testing medium; (2) instrumentation quality and the precision of the experimental technique; and (3) data acquisition and reduction techniques, etc. For the range of Mach numbers covered in the data of Figure 2, the normalized RMS value of the fluctuating pressure varies from $\sqrt{\overline{p^2}}/q_\infty \approx 0.006$ at subsonic Mach numbers to 0.002 at supersonic Mach numbers. Lowson, Reference 1, proposed the following semi-empirical prediction formula which appears to agree with the general trend in the data:

$$\sqrt{\overline{p^2}}/q_\infty = 0.006/(1 + 0.14 M_\infty^2) \qquad (1)$$

It is important to note that this formula has some theoretical basis and is not strictly an empirical approximation of measured results (see Reference 1). The use of this formula at high supersonic and hypersonic Mach numbers should be done so with the understanding that it has not been verified in this Mach number range and may lead to significant error. However, in the Mach number range up to, say $M_\infty = 3.0$, it is in good agreement with experimental results.

It should be noted that the results presented in Figure 2, particularly the wind tunnel results, were obtained for both homogeneous and stationary flows at free-stream conditions and in the absence of external pressure gradients. Consideration should be given to local conditions which deviate from free-stream conditions.

Power Spectra

Power spectra represent the distributions of the mean square fluctuating pressure with frequency. Power spectra for attached turbulent boundary layers are found to scale on a Strouhal number basis; that is, the frequency is normalized by multiplying by a typical length and dividing by a typical velocity. The advantages of using normalized spectra are obvious since it enables similar, homogeneous, flows to be represented by a single spectrum regardless of the scale of the flow field or the free-stream velocity.

Numerous studies have been conducted to determine the proper parameters to be used to nondimensionalize the spectra for various aero-acoustic environments. Unfortunately, the choice of parameters which best collapses the data appear to be dependent on the nature of the fluctuating pressure environment. In general, free-stream velocity is used as the normalizing velocity parameter, although a typical eddy convection velocity (itself a function of frequency) has been used occasionally. The local convection velocity appears to correspond more closely with the physical situation for fluctuating pressures due to turbulent eddies. Selection of a typical length is more difficult. Boundary layer thickness (δ), displacement thickness (δ^*), wall shear stress (τ_ω) and momentum thickness (θ) have all been used by various investigators. The most generally used typical lengths are δ and δ^*.

Lowson, Reference 1, proposed an empirical formula for the power spectrum for attached turbulent boundary layers based, primarily, on the experimental results of Speaker and Ailman. In comparing this formula with other data, and in particular, with recent measurements at supersonic speeds by NASA-Ames, the Lowson prediction appears to underestimate the spectral levels at low Strouhal numbers and also gives too large a roll-off at high Strouhal numbers. Therefore, a new formula is presented which appears to be more representative of experimental findings throughout the Mach number range. In this formula, it will be noted that δ^* and U_∞ have been used as normalizing parameters.

$$\frac{\Phi(\omega)\, U_\infty}{q_\infty^2\, \delta^*} = \frac{(\overline{P^2}/q_\infty^2)}{\frac{\omega_0\, \delta^*}{U_\infty}\left\{1+(\omega/\omega_0)^{0.9}\right\}^{2.0}} \qquad (2)$$

where $\omega_0 = 0.5\,\frac{U_\infty}{\delta^*}$

$$\overline{p^2}/q_\infty^2 = \frac{(0.006)^2}{(1+0.14M^2)^2}$$

A comparison of the predicted power spectrum with experimental spectra is presented in Figure 3.

Cross-Power Spectra

The final requirement in determining the characteristics of the fluctuating pressure field of the turbulent boundary layer is to define the narrow band, space correlation function or co-power spectral density. This parameter is the key function needed to describe an impinging pressure field on a structure in order to calculate the induced mean-square response of the structure (see, for example, Reference 17 for the structural response computational technique). The spatial correlation properties of a fluctuating pressure field can be obtained only from a careful and detailed examination of the field at a large number of points. Measurements by several investigators have shown that the co-power spectral density of the turbulent boundary layer pressure fluctuations in the direction of the flow can be approximated by an exponentially damped cosine function, and the lateral co-spectral density can be approximated by an exponential function. The general form of the cross-power spectral density is:

$$S_{pp}(\xi, \eta, \omega) = \phi(\omega)\, A(\xi, \eta, \omega) \cos\left(\frac{\omega \xi}{U_c}\right) \qquad (3)$$

Here, it is assumed that the pressure field is homogeneous, in the sense that the cross-power spectral density is a function only of the separation distances (ξ in the longitudinal direction and η in the lateral direction) so that it is independent of the actual positions (say x and $x + \xi$ longitudinally and y and $y + \eta$ laterally). Further, ω and U_c are the circular frequency and convection velocity, respectively.

Assuming that $A(\xi, \eta, \omega)$ is separable into its longitudinal and lateral components, and normalizing by the power spectral density of the homogeneous field gives:

$$G_{pp}(\xi, \eta, \omega) = G_\xi(\xi, \omega)\, G_\eta(\eta, \omega) = A_\xi(\xi, \omega)\, A_\eta(\eta, \omega) \cos \frac{\omega \xi}{U_c} \qquad (4)$$

where $A_\xi(\xi, \omega)$ and $A_\eta(\eta, \omega)$ are the correlation coefficients in the longitudinal and lateral directions, respectively. The assumed separable form leads to the prediction that the magnitude of A is constant along straight lines on the surface,

forming a diamond pattern surrounding the origin. This characteristic is somewhat physically unreasonable (see Reference 2); however, for purposes of calculating the induced structural response the assumption of separability greatly simplifies the mathematics and, hence, it is generally accepted. However, Lowson (Reference 1) notes that a more likely form for the lines of constant amplitude would be elliptic, suggesting that the usual separable solution underestimates the correlation area by $\pi/2$. Thus, integration of formula containing the cross-spectral density function should be multiplied by a factor of $\pi/2$ to allow for its probable underestimate of the correlation area at any frequency.

Measurements of the correlation coefficients have been made by Bull and others (see Reference 1) and the results are presented in Figures 4a and 4b. It is seen that the data in Figures 4a and 4b have been collapsed based on Strouhal numbers $\frac{\xi\,\omega}{U_c}$ and $\frac{\eta\,\omega}{U_c}$. From these data, empirical expressions have been derived for the correlation coefficients, these being

$$A_\xi(\xi, \omega) = \exp\left(-0.10\,|\xi|\,\omega/U_c\right) \tag{5}$$

$$A_\eta(\eta, \omega) = \exp\left(-0.715\,|\eta|\,\omega/U_c\right) \tag{6}$$

Typical values of the convection velocity (itself a function of frequency) for subsonic flow are $U_c = 0.6\,U$ for the small scale eddies near the wall and $U_c = 0.9\,U$ for the large scale eddies near the outer edge of the boundary layer.

The accuracy of Equations (5) and (6) break down at small values of $\frac{\omega\,\xi}{U_c}$; however, in Reference 3, Bull presents measured asymptotic values of the correlation coefficients for small values of $\frac{\omega\,\xi}{U_c}$ and $\frac{\eta\,\xi}{U_c}$. Based on these data, the Equations (5) and (6) may be corrected to include the lower frequencies, and the resulting expressions are:

$$A_\xi(\xi, \omega) = \exp\left(-0.10\,|\xi|\,\omega/U_c\right) \cdot \exp\left(-0.27\,|\xi|/\delta\right) \tag{7}$$

$$A_\eta(\eta, \omega) = \exp\left(-0.72\,|\eta|\,\omega/U_c\right) \cdot \exp\left(-2.0\,|\eta|/\delta\right) \qquad (8)$$

These expressions appear to be valid at both subsonic and supersonic speeds.

2.2 Separated Flow

Separated flows as induced by steps, wedges, flares and other, basically two-dimensional geometric changes have undergone considerable study only in recent years. Considerably less data is available on the fluctuating pressure environments within separated flow regions than is the case with attached boundary layers. Furthermore, there are various types of separated flows and little is known of the similarities and differences of their statistical properties. Example separated flow environments are listed below:

- Blunt body-induced separation (as occur at cone-cylinder and flare-cylinder expansion corners at subsonic Mach numbers)
- Flare-induced, step induced, and wedge-induced separation (as occur in compression corners)
- Shock-induced separation (as occur on cylinders, airfoils, etc., beneath terminal shock waves at transonic speeds and due to shock wave impingement at supersonic speeds)
- Boattail-induced and rearward facing-step-induced separation (such as occur in the base region of launch vehicles)

All of the foregoing environments differ to some degree in their aerodynamic structure. However, some basic comments can be made in regard to their fluctuating pressure characteristics. First, all of these environments may be regarded as two-dimensional type separated flows having mean separation and reattachment lines which are normal to the free-stream. Second, a general characteristic is that if the flow separates from an expansion corner, the separation line is quite stable in that oscillations which produce fluctuating pressures are not generated. However, if separation occurs, say, on the cylindrical portion of a payload shroud (flare induced separation) the separation point is unstable and may produce significant fluctuating pressures, particularly at supersonic speeds where the separation is accompanied by an oblique shock wave.

Third, the reattachment point of the separated flow field produces rather large fluctuating pressure levels for virtually all types of separated flow fields. The region within the separated flow field (between the separation and reattachment points) is a fairly homogeneous environment which is characterized by fluctuating pressure levels

greater than those for attached flow but less than those encountered at the separation and reattachment points. Example data for various separated flow fields are presented in the following sections.

Overall Level

A typical example of the fluctuating pressures resulting from blunt-body separation is shown in Figure 5 (results taken from Reference 18). These data were obtained at high subsonic Mach numbers for a 25-degree cone-cylinder configuration. The axial distribution of $\sqrt{\overline{p^2}}/q_\infty$ shows a relatively nonhomogeneous environment with a peak level which moves aft with increasing Mach number. The peak in $\sqrt{\overline{p^2}}/q_\infty$ results from the reattachment of the separated flow from the shoulder. Thus, the extent of the separated region increases with increasing Mach number. Peak levels of rms fluctuating pressure reach 11 percent of free-stream dynamic pressure at a free-stream Mach number of 0.70, and results from the instability of the reattachment point. It will be noted that the fluctuating pressure levels near the shoulder (X/D = 0) are relatively low (same order of magnitude as generally found within the homogeneous region of two-dimensional separated flows and typical of the environment for separated shear layers) thus indicating that the separation point which occurs at the shoulder is relatively stable. Separated flow over the boattail region of a bulbous vehicle may be expected to exhibit fluctuating pressure characteristics very similar to the cone-cylinder; however, the blunt-body separation on a cone-cylinder body is limited to the subsonic speed range, whereas, the boattail configuration may induce separation at all Mach numbers.

Typical fluctuating pressure data for flare-induced separation are presented in Figure 6 (results taken from Reference 14). These data clearly show the region of homogeneous separated flow, bounded on the upstream by the oscillating shock wave (forward peak in $\sqrt{\overline{p^2}}/q_\infty$), and on the downstream by the reattachment pertubations (aft peak in $\sqrt{\overline{p^2}}/q_\infty$). Surface fluctuating pressures for the separated flow region range from 1.5 to 2.7 percent of the free stream dynamic pressure. Levels associated with the upstream shock wave generally range from 4 to 8 percent of the free-stream dynamic pressure (see Reference 14); whereas, levels in the region of reattachment may range from 6 to 12 percent of q_∞ and agree reasonably well with the reattachment levels for blunt body separation. Further discussion of shock-wave oscillation data is presented in a later section.

The variation of fluctuating pressure level, normalized by free-stream dynamic pressure, with local Mach number for various separated flow environments downstream of expansion corners is presented in Figure 7. The regions aft of cone-cylinder junctures, and rearward-facing steps and in the near wake of boattail configurations are represented by the data presented in Figure 7. These environments will be

referred to as expansion induced separated flows and it will be noted that the attendant fluctuating pressures exhibit the same general trend with local Mach number. The largest levels occured at low Mach numbers and decreased as local Mach numbers increased. These data represent the region of plateau static pressure and the tolerance brackets on the data represent the variations due to nonhomogeneous flow within the region of constant static pressure rather than scatter in the measurements. A good empirical approximation to the experimental measurements is:

Expansion Induced Separated Flow:

$$\sqrt{\overline{p^2}}/q_\infty = \frac{0.045}{1 + M_\ell^2} \qquad (9)$$

This equation is similar in form with that previously proposed for attached turbulent boundary layers.

Fluctuating pressure measurements for the region of plateau static pressure upstream of compression corners are presented in Figure 8. Also, fluctuating pressures for expansion induced separated flow are presented in this figure for comparison. In general, the compression corner data show an increase in fluctuating pressure level with increasing free-stream Mach number in the range, $1.0 \leq M_\infty \leq 2.0$ — reaching a constant level at Mach numbers above 2.00. Free-stream Mach number is used here because adequate data is not available for determining the local Mach number in the vicinity of the compression induced separated flow region. Also, derivation of empirical prediction formula for the fluctuating pressure level within compression induced separated flows are not proposed at this time.

Power Spectra

The most comprehensive available data for power spectra of the fluctuating pressure within separated flows was obtained for the homogeneous region of compression corners at supersonic Mach numbers (References 14, 19, 20 and 21). These data, presented in Figure 9, were obtained for forward facing steps, wedges and conical frustums. All data, represented by the cross-hatched band, showed a distinct similarity in spectral characteristics when compared using normalized spectral level and frequency expressed as functions of local velocity, free-stream dynamic pressure, and local boundary layer thickness. A number of velocity, length and pressure parameters were used to collapse the data; however, local velocity, local boundary layer thickness and free-stream dynamic pressure appeared to be adequately representative of the parameter dependence of the fluctuating pressures for the configurations studied. Power spectra of the fluctuating pressures within the homogeneous region of separated flows may be represented by the following empirical formula:-

$$\frac{\phi(f)\, U_\ell}{q_\infty^2\, \delta_\ell} = \frac{\overline{P^2}/q_\infty^2}{\frac{f_0\, \delta_\ell}{U_\ell}\left\{1 + \left(f/f_0\right)^{0.83}\right\}^{2.15}} \qquad (10)$$

where $f_0 = 0.17 \frac{U_\ell}{\delta_\ell}$

$\overline{P^2}/q_\infty^2 = \frac{0.045}{1+M_\ell^2}$, Figure 7, for expansion induced separated flows.

$\overline{P^2}/q_\infty^2$ = the results as determined in Figure 8 for compression induced separated flows.

It is anticipated that Equation (10) can be used with good accuracy to predict the power spectra for fluctuating pressures within the homogeneous region of expansion induced separated flows although it was derived based on data taken in compression corners.

Cross-Power Spectra

Typical cross-power spectra for the homogeneous region of two-dimensional separated flows are presented in Figure 10. Again, noting that the co-spectral density is the same as the narrow-band spatial correlation, it is seen that the separated flow exhibits spatial coherence very similar to that of attached turbulent boundary layers. The damping of the sinusoidal cross spectra for separated flow is exponential at high values of $\omega \xi/U_c$ as is the case for attached flow. Thus as a first approximation, the normalized longitudinal co-spectra may be represented by:

$$C(\xi, f) = e^{-a\,\omega\,\xi/U_c} \cos \frac{\omega \xi}{U_c} \qquad (11)$$

The damping coefficient, a, is dependent on free-stream Mach number according to the results presented in Reference 14. The Chyu and Hanely results show damping coefficients ranging from approximately 0.13 at $M_\infty = 2.5$ to a value of 0.33 at $M_\infty = 1.6$. This suggests that the turbulence structure in separated flows decays

somewhat more rapidly than for attached flow which has a coefficient of exponential decay of 0.10. It should be noted that the exponential decays represent the envelope of the cross-spectra for various spatial distances, ξ. For a given value of ξ, the cross-spectra can be represented by the exponential envelope only at high frequencies, the lower limits of which increase with increasing distance between measurement points.

The loss of coherence at low frequencies precludes a general collapse of the data using a constant damping coefficient. This problem was overcome by Coe and Rechtien, Reference 20, by introducing an attenuation coefficient which is related to the normalized modulus of the cross-power spectral density by

$$\left| G\left(\xi, \frac{f\,\delta_\ell}{U_\ell}\right) \right|_{norm} = e^{-\alpha \xi} \tag{12}$$

The normalized modulii for available or selected transducer spacings, ξ, were curve-fitted by an exponential function using the method of least squares to obtain a non-dimensional attenuation-coefficient function $\alpha\left(\xi, f\,\delta_\ell / U_\ell\right) \leftarrow h$ in References 19-21. The parameter h is the height of the protuberances used to generate the separated flow field. Empirical approximations of the attenuation coefficients, based on the experimental results of Coe and Rechtien, are:

$$\alpha\left(\xi, \frac{f\,\delta_\ell}{U_\ell}\right) = 0.75/\text{in.} \quad , \frac{f\,\delta_\ell}{U_\ell} < 6 \times 10^{-3} \tag{13}$$

$$\alpha\left(\xi, \frac{f\,\delta_\ell}{U_\ell}\right) = 0.75 \left[\frac{f\,\delta_\ell/U_\ell}{\left(f\,\delta_\ell/U_\ell\right)_0}\right], \tag{14}$$

$$6 \times 10^{-3} \leq \frac{f\,\delta_\ell}{U_\ell} \leq 6 \times 10^{-2}$$

where $$\left(\frac{f\,\delta_\ell}{U_\ell}\right)_0 = 6 \times 10^{-3}$$

$$\alpha \left(\xi, \frac{f\delta_\ell}{U_\ell} \right) = 1.5 \text{ / in.} \quad , \frac{f\delta_\ell}{U_\ell} > 6 \times 10^{-2} \tag{15}$$

Lateral Direction

$$\alpha \left(\eta, \frac{f\delta_\ell}{U_\ell} \right) = 0.75 \text{ / in.} \quad , \frac{f\delta_\ell}{U_\ell} < 6 \times 10^{-3} \tag{16}$$

$$\alpha \left(\eta, \frac{f\delta_\ell}{U_\ell} \right) = 0.75 \text{ / in.} \left[\frac{f\delta_\ell / U_\ell}{(f\delta_\ell / U_\ell)_0} \right]^{0.3} , \frac{f\delta_\ell}{U_\ell} \geq 6 \times 10^{-3} \tag{17}$$

where $$\left(\frac{f\delta_\ell}{U_\ell} \right)_0 = 6 \times 10^{-3}$$

It will be noted that the longitudinal and lateral attenuation coefficients are the same at Strouhal numbers, $f\delta_\ell / U_\ell < 6 \times 10^{-2}$ and that the lateral attenuation coefficient becomes larger than the longitudinal value at $f\delta_\ell / U_\ell \geq 6 \times 10^{-2}$. It was pointed out in Reference 19 that this spatial characteristic indicates that the predominant turbulence is nonconvective at the lower frequencies and that contours of equal correlation would be circular; whereas, at $f\delta_\ell / U_\ell > 6 \times 10^{-2}$ the divergence of the longitudinal and lateral attenuation coefficients indicate a progressively extended correlation pattern in the direction of the free-stream with increasing frequency. This statement is not entirely true since the usual separable form of the cross-power spectral density leads to the prediction that the magnitude of the normalized modulus is constant along straight lines on the surface, forming a diamond pattern surrounding the origin rather than a circular or elliptic pattern. Under the assumption of separability of the longitudinal and lateral cross-power spectra, the following equations (which employ the attenuation coefficient) may be used as prediction formula for the normalized longitudinal and lateral co-spectra.

Longitudinal Co-Spectra

$$C\left(\xi, \frac{f\delta_\ell}{U_\ell}\right) = e^{-\alpha_\xi \xi} \cos \frac{\omega \xi}{U_c} \qquad (18)$$

Lateral Co-Spectra

$$C\left(\eta, \frac{f\delta_\ell}{U_\ell}\right) = e^{-\alpha_\eta \eta} \qquad (19)$$

where $\alpha_\xi = \alpha\left(\xi, \frac{f\delta_\ell}{U_\ell}\right)$ as defined in Equations 13, 14 and 15.

$\alpha_\eta = \alpha\left(\eta, \frac{f\delta_\ell}{U_\ell}\right)$ as defined in Equations 16 and 17.

2.3 Shock-Wave Oscillation

Generally, shock-wave oscillation produces the most intense fluctuating pressure levels that are usually encountered by a vehicle. As for the case of separated flow, there are many types of shock-wave oscillation and little is known in regard to similarities and differences of their statistical parameters. Typical shock waves encountered by vehicles are:

- Terminal shock waves for regions of transonic flow.
- Displaced oblique shock waves as induced by the separated flow in compression corners at local supersonic speeds.
- Reattachment shock waves in the vicinity of the reattachment point for separated flows generated by both compression and expansion corners.
- Impingement shock waves as caused by local bodies such as strap-on rockets.

All shock waves may be expected to produce similar fluctuating pressure environments since the movement of the shock wave results from the interaction with the separated flow at the foot of the shock wave (see Reference 19) and the fluctuating pressure is

the result of the modulation of the pressure gradient through the shock wave. A special case of shock wave oscillation is referred to as an alternating flow condition, whereby, the flow at an expansion corner intermittently fluctuates between a separated and attached condition. This environment is illustrated schematically in Figure 11 together with the more common terminal shock-wave oscillation case. Example data for various shock wave oscillation environments are presented in the following sections.

Overall Level

The axial distribution of rms fluctuating pressure resulting from terminal shock wave oscillation is shown in Figure 11 (from Reference 18). A special case of terminal shock wave oscillation results when the terminal shock wave moves forward to the expansion shoulder of a cone-cylinder. For this case, the flow intermittently fluctuates between the blunt-body separated flow condition and the attached flow condition at high subsonic (low transonic) Mach numbers. This condition represents an alternating unbalance between the large pressure rise through the shock wave that exceeds the values required to separate the flow and the small pressure rise that is too small to maintain fully separated conditions.

Extremely large fluctuating pressures result from this condition; however, it should be noted that this phenomenon occurs over a small Mach number range and generally is of very low frequency. Thus for large Mach number transients, this phenomenon may not occur. On the other hand, some experimental studies using aeroelastic wind tunnel models indicate that this phenomenon may become coupled with the vibrational response of vehicles such that flutter in the lower order bending modes would result for certain configurations — particularly for bulbous shaped payloads on rather slender launch vehicles.

As Mach number is increased above the range of alternating flow, the localized oscillation of the shock wave produces intense fluctuating pressures for the region in close proximity to the shock wave as shown in Figure 11. The shock wave moves aft with diminishing strength with increasing Mach number such that the rms fluctuating pressure level also decreases. In addition to the results presented in Figure 11, the fluctuating pressures which occur at the separation and reattachment points for separated flow over compression corners (Figure 6) are fairly complete examples of shock-wave oscillation data.

Power Spectra

Only recently has comprehensive data been presented on the spectral characteristics of shock-wave oscillation. Much of the previous data were presented in linear-linear graphical form rather than using log-log scales. As a result, much resolution was lost at the high frequencies. Recent experimental data by Coe and Rechtien (Reference 20) gives a clearly defined spectrum for shock wave oscillation at $M_\infty = 2.0$; however, data at other Mach numbers have not been published. Data

obtained for three-dimensional protuberance flows do agree with the Coe and Rechtien data and thus substantiates their limited published results. The normalized power spectra for shock-wave oscillation for both two- and three-dimensional protuberances (References 18 and 19) are presented in Figure 12. The power spectrum shows a relatively steep roll-off starting at a Strouhal frequency $\left(f\,\delta_0 / U_\infty\right)$ of 1×10^{-2}. The roll-off is 8 dB per octave for the range $1 \times 10^{-2} \leq f\,\delta_0 / U_\infty \leq 2 \times 10^{-1}$ and above this range the roll-off changes suddenly to 4 dB per octave. These unique spectral characteristics of shock-wave induced fluctuating pressures are explained by the physical behavior of the shock-wave oscillation and the resulting pressure time history. The shock wave is basically a pressure discontinuity which becomes slightly distorted by the boundary layer such that a finite gradient through the shock wave is observed at the surface. Oscillation of the shock wave produces a wave form which approaches a random-rectangular wave as the displacement of the oscillation increases. Superimposed upon this signal is the low amplitude, high frequency disturbance associated with the attached boundary layer (for that portion of the signal when the shock wave is aft of the measurement point) and the moderate amplitude and frequency disturbances associated with separated flow (for that portion of the signal when the shock wave is forward of the measurement point). The roll-off rate of the power spectrum for a random-rectangular wave form is 6 dB per octave which is 2 dB lower than the experimentally observed value. Above $f\,\delta_0 / U_\infty = 2 \times 10^{-1}$, the power spectral density for the random modulation of the shock wave diminishes below the power spectral density for the turbulence portion of the signal. Thus, the roll-off rate changes to a value roughly equal to that for separated flow since this environment is the larger of the two turbulence generating mechanisms (the other being attached flow).

Noting that the power spectra for shock-wave oscillation is composed of (1) low frequency spectral energy of the shock wave and (2) high frequency spectral energy of the separated flow and attached boundary layer, the resulting empirical formula for the power spectra may be written as a combination of power spectra of the contributing sources:

$$\left[\Phi(f)\right]^{H}_{SW} = \left[\Phi(f)\right]^{I,\,H}_{SW} + k_1 \left[\Phi(f)\right]^{H}_{S} + k_2 \left[\Phi(f)\right]^{H}_{A} \qquad (20)$$

where the subscripts and superscripts denote the following:

Subscripts:

SW - shock wave

S - separated flow

A - attached flow

Superscripts: I -- absence of viscosity (inviscid)

H - homogeneous flow

The constants, k_1 and k_2 are weighting functions which account for that portion of the total energy resulting from the presence of viscous flow in the form of separated flow and attached flow respectively. It should be noted that the two secondary environments (separated flow and attached flow) are not simultaneously superimposed on the shock wave signal but rather are time shared. This, together with the fact that these environments may be correlated with the gross motion of the shock wave results in values of k_1 and k_2 less than 1.0. Finally, for peak overall levels of shock wave oscillation (corresponding to a point located at the mean position of the shock wave) the contribution of attached flow is negligible in comparison to that for separated flow. Thus, Equation 20 may be simplified to

$$\left[\Phi(f)\right]_{SW}^{H} = \left[\Phi(f)\right]_{SW}^{I,H} + k_1 \left[\Phi(f)\right]_{S}^{H} \qquad (21)$$

Based on experimental data of Reference 19, the power spectra $\left[\phi(f)\right]_{SW}^{I,H}$ for shock wave oscillation in the absence of viscous flow normalized by local inflowing boundary layer thickness and velocity and free-stream dynamic pressure is given by:

$$\left[\frac{\Phi(f)\, U_0}{q_\infty^2\, \delta_0}\right]_{SW}^{I,H} = \frac{\left(\overline{p^2}/q_\infty^2\right)_{SW}^{I,H}}{\left(\frac{f_0\, \delta_0}{U_0}\right)_{SW} \left\{1 + \left(f/f_0\right)^{1.55}\right\}^{1.7}} \qquad (22)$$

where:

$$\left[\overline{p^2}/q_\infty^2\right]_{SW}^{I,H} = \left[\overline{p^2}/q_\infty^2\right]_{SW}^{H} - k_1 \left[\overline{p^2}/q_\infty^2\right]_{S}^{H}$$

$\left[\overline{p^2}/q_{\infty}^2\right]_{SW}^{H}$ - overall level of shock oscillation peak corresponding to the mean location of the shock wave.

$\left[\overline{p^2}/q_{\infty}^2\right]_{S}^{H}$ - overall level of homogeneous separated flow as defined from Figures 7 and 8.

The subscript 0 denotes local velocity and boundary layer thickness upstream of the shock wave.

$$\left(\frac{f_0\,\delta_0}{U_0}\right)_{SW} = 1 \times 10^{-2}$$

$$k_1 = 0.25$$

} determined empirically from experimental data of Reference 19

Substitution of Equations (10) and (22) into Equation (21) gives the final expression for the power spectra for shock wave oscillation.

$$\left[\frac{\Phi(f)\,U_0}{q_{\infty}^2\,\delta_0}\right]_{SW}^{H} = \frac{\left(\overline{p^2}/q_{\infty}^2\right)_{SW}^{I,H}}{\left(\frac{f_0\,\delta_0}{U_0}\right)_{SW}\left\{1+\left(f/f_0\right)^{1.55}\right\}^{1.7}} + 0.25\,\frac{\left(\overline{p^2}/q_{\infty}^2\right)_{S}^{H}}{\left(\frac{f_0\,\delta_0}{U_0}\right)_{S}\left\{1+\left(f/f_0\right)^{0.83}\right\}^{2.15}} \qquad (23)$$

where $(f_0\,\delta_0/U_0)_S$ is now defined for conditions upstream of the shock wave.

A comparison of the predicted power spectra for shock-wave oscillation with experimental measurements is presented in Figure 13. It should be noted that this prediction formula holds true only at a point corresponding to the mean location of the shock wave. On either side of the shock wave, the influence of the shock diminishes rapidly due to its small displacement such that the environment is basically either attached or separated flow with some low frequency intermittency due to the shock wave. It is convenient to refer to these regions as non-homogeneous attached and separated flows and they will be discussed later in Section 2.4.

Cross-Power Spectra

Very little data have been published in the form of cross-power spectra of fluctuating pressures beneath oscillating shock waves. Because oscillating shock waves at a given flight condition are confined to relatively small areas of the vehicle surface, it is extremely difficult to define the spatial characteristics of the attendant fluctuating pressures. Fluctuating pressures in the vicinity of the shock wave are highly non-homogeneous; although they do appear to be related in both spectral shape and spatial coherence. The only significant results on the spatial coherence of fluctuating pressures in the vicinity of shock-waves are those by Coe and Rechtien (Reference 20). Their data indicate that the fluctuating pressures generated by the shock wave are related only at frequencies below $f\delta_0/U_0 = 0.08$ for the region immediately downstream of the mean location of the shock wave (Figure 14). For the region immediately upstream of the shock-wave, a small degree of coherence is also evident in this frequency range as well as at $f\delta_0/U_0 \geq 0.2$. A comparison of the power spectra and coherence function shows some very interesting characteristics of shock-induced fluctuating pressures. First, the power spectra of fluctuating pressures on each side of the peak level point show large low frequence energy which can be identified as having the same basic characteristics as the shock wave spectrum for $f\delta_0/U_0 \leq 0.08$. This is confirmed by the coherence of the data over the same frequency range $\left(f\delta_0/U_0 \leq 0.08\right)$. For $f\delta_0/U_0 \geq 0.08$, power spectra immediately upstream and downstream of the shock wave show spectral characteristics identical to attached turbulent boundary layer and separated flow, respectively. Thus, for $f\delta_0/U_0 \geq 0.8$, the spatial correlation of fluctuating pressure immediately upstream of the peak should be characteristic of the attached flow; whereas, immediately downstream of the peak they should be characteristic of separated flow. However, when the spatial correlation is normalized by the power spectral densities to obtain the coherence function, this coherence appears to be minimized due to the large spectrum level for the point of peak fluctuating pressure. Further discussion on this characteristic will be given later in the section on non-homogeneous attached and separated flows.

The spatial decay of the low frequency, shock induced fluctuating pressure in the longitudinal direction as shown in Figure 14 may be represented by an exponential coherence function as follows:

$$\gamma^2\left(\xi, \frac{f\delta_0}{U_0}\right) = e^{-8.0\, f\delta_0/U_0} \qquad (24)$$

A comparison of this empirical prediction with experimental data is presented in Figure 14. It should be noted that, as separation distance is increased, the above formula fails to account for the low coherence at low frequencies. However, because the large non-homogeneous effects associated with the flow in close proximity of the shock wave, the application of classical statistical methods to define the spatial characteristics for large separation distances may be questionable. Thus, for regions under the peak, Equation (24) is felt to be an accurate representation of the spatial characteristics of the fluctuating pressures in the longitudinal direction.

The longitudinal co-spectra may be written:

$$C(\xi_1, f) = e^{-4.0\, f\delta_0/U_0} \cos 2\pi \frac{f\delta_0}{U_0} \qquad (25)$$

Published data is not available on the transverse spatial characteristics of shock-induced fluctuating pressures. However, it is anticipated that these disturbances will be reasonably correlated over much larger distances in the transverse direction than in the longitudinal direction because of the continuity of the shock wave in the plane normal to the flow.

2.4 Non-Homogeneous Attached and Separated Flows

Non-homogeneous attached and separated flows are defined as environments which are basically attached or separated; however, the statistical properties of their attendant fluctuating pressures vary with spatial location. Examples to be considered herein are attached and separated flows immediately upstream and downstream of oscillating shock waves, respectively. The non-homogeneity may result from intermittency of the shock wave oscillation or from a more basic modification to the turbulence structure of attached and separated flow due to the motion of the shock wave. The variations in both the overall level and power spectra with position relative to the shock wave are evident in Figure 13. These data are shown in comparison with homogeneous attached and separated flow data to illustrate the presence of low frequency energy due to the shock wave. Again, basic characteristics of the overall levels, power spectra, and cross-power spectra will be discussed for the

purpose of defining empirical prediction techniques for the non-homogeneous attached and separated flows.

Overall Level

The overall fluctuating pressure levels for attached and separated flow in close proximity to an oscillating shock wave are bounded on the low side by the levels of fluctuating pressures corresponding to homogeneous environments and are bounded on the high side by the peak fluctuating pressures corresponding to shock wave oscillation. In essence, this means that the differences between the homogeneous and non-homogeneous fluctuating pressure levels may be attributed directly to fluctuating pressures induced by the oscillating shock wave for the case considered here. Thus, normalized fluctuating pressure levels for non-homogeneous flows may be defined as:

$$\left(\frac{\sqrt{\overline{p^2}}}{q_\infty}\right)_A^H \leq \left(\frac{\sqrt{\overline{p^2}}}{q_\infty}\right)_A^{NH} \leq \left(\frac{\sqrt{\overline{p^2}}}{q_\infty}\right)_{SW}^H \tag{26}$$

$$\left(\frac{\sqrt{\overline{p^2}}}{q_\infty}\right)_S^H \leq \left(\frac{\sqrt{\overline{p^2}}}{q_\infty}\right)_S^{NH} \leq \left(\frac{\sqrt{\overline{p^2}}}{q_\infty}\right)_{SW}^H \tag{27}$$

where the subscripts and superscripts are defined as follows:

Subscripts:	A	attached flow
	S	separated flow
	SW	shock wave
Superscripts:	H	homogeneous condition
	NH	non-homogeneous condition

Under the assumption of statistical independence between the various sources, i.e., attached flow, separated flow and shock wave oscillation, the fluctuating pressure levels may be expressed as:

$$\left(\frac{\sqrt{\overline{p^2}}}{q_\infty}\right)^{NA}_{A} = \sqrt{\left[\left(\frac{\sqrt{\overline{p^2}}}{q_\infty}\right)^{H}_{A}\right]^2 + c_1\left[\left(\frac{\sqrt{\overline{p^2}}}{q_\infty}\right)^{H}_{SW}\right]^2} \qquad (28)$$

$$\left(\frac{\sqrt{\overline{p^2}}}{q_\infty}\right)^{NH}_{S} = \sqrt{\left[\left(\frac{\sqrt{\overline{p^2}}}{q_\infty}\right)^{H}_{S}\right]^2 + c_2\left[\left(\frac{\sqrt{\overline{p^2}}}{q_\infty}\right)^{H}_{SW}\right]^2} \qquad (29)$$

where c_1 and c_2 are weighting functions less than 1.0, which represent the contribution of the shock wave to the overall fluctuating pressure level. The values of c_1 and c_2 vary with spatial location relative to the shock wave and therefore, are difficult to predict. However, the above method of representation is useful in the prediction of power spectra for non-homogeneous flows as will be shown in the next section.

Power-Spectra

To predict the power spectra for non-homogeneous flows, a prior knowledge of the overall fluctuating pressure levels is required. Under the assumption of statistical independence between the various contributing sources, the power spectra for non-homogeneous environments may be written as the summation of power spectra of the contributing sources. Using the same symbolic representation as for the overall level, the power spectra for non-homogeneous environments may be written as:

$$\left[\Phi(f)\right]^{NH}_{A} = \left[\Phi(f)\right]^{H}_{A} + c_1\left[\Phi(f)\right]^{I,H}_{SW} \qquad (30)$$

$$\left[\Phi(f)\right]^{NH}_{A} = \left[\Phi(f)\right]^{H}_{A} + c_2\left[\Phi(f)\right]^{I,H}_{SW} \qquad (31)$$

From Equations (30) and (31), c_1 and c_2 are given as:

$$c_1 = \frac{\left(\frac{\overline{p^2}}{q_\infty^2}\right)_A^{NH} - \left(\frac{\overline{p^2}}{q_\infty^2}\right)_A^{H}}{\left(\frac{\overline{p^2}}{q_\infty^2}\right)_{SW}^{I,H}} \tag{32}$$

$$c_2 = \frac{\left(\frac{\overline{p^2}}{q_\infty^2}\right)_S^{NH} - \left(\frac{\overline{p^2}}{q_\infty^2}\right)_A^{H}}{\left(\frac{\overline{p^2}}{q_\infty^2}\right)_{SW}^{I,H}} \tag{33}$$

To determine the power spectra for non-homogeneous attached flow as caused by shock-wave oscillation in the vicinity of the attached flow region, Equations (2), (22), and (32) are substituted into Equation (30), which gives a form normalized by local conditions upstream of the shock wave:

$$\left[\frac{\Phi(f)\ U_0}{q_\infty^2\ \delta_0}\right]^{NH} = \frac{\left(\frac{\overline{p^2}}{q_\infty^2}\right)^{H}_{A}}{\left(\frac{f\ \delta_0}{U_0}\right)_A \left\{1 + \left(f/f_0\right)^{0.9}\right\}^2} +$$

$$\frac{\left(\frac{\overline{p^2}}{q_\infty^2}\right)^{NH}_{A} - \left(\frac{\overline{p^2}}{q_\infty^2}\right)^{H}_{A}}{\left(\frac{f\ \delta_0}{U_0}\right)_{SW} \left\{1 + \left(f/f_0\right)^{1.55}\right\}^{1.7}} \qquad (34)$$

Similarly, substitution of Equations (10), (22) and (33) into Equation (31), leads to the following expression for non-homogeneous separated flow:

$$\left[\frac{\Phi(f)\ U_0}{q_\infty^2\ \delta_0}\right]^{NH}_{S} = \frac{\left(\frac{\overline{p^2}}{q_\infty^2}\right)^{H}_{S}}{\left(\frac{f\ \delta_0}{U_0}\right)_S \left\{1 + \left(f/f_0\right)^{0.83}\right\}^{2.15}} +$$

$$\frac{\left(\frac{\overline{p^2}}{q_\infty^2}\right)^{NH}_{S} - \left(\frac{\overline{p^2}}{q_\infty^2}\right)^{H}_{S}}{\left(\frac{f\ \delta_0}{U_0}\right)_{SW} \left\{1 + \left(f/f_0\right)^{1.55}\right\}^{1.7}} \qquad (35)$$

Comparison of these predictions with expreimental measurements are shown in Figure 13.

3.0 PROTUBERANCE INDUCED FLUCTUATING PRESSURE ENVIRONMENTS

Recognizing the impracticality of investigating the fluctuating pressure environment of every protuberance which may be attached to the external surface of a launch vehicle, a systematic study was conducted by Wyle Laboratories in cooperation with NASA-MSFC to investigate the flow fields induced by generalized protuberance geometries. The results of this study are reported in References 22 and 23. The first objective of this study was to investigate general features of protuberance flows at transonic speeds using generalized protuberance geometries consisting of right circular cylinders of various heights and diameters which projected into the flow with the axis of the cylinder normal to the flow direction. In view of the free-interaction hypothesis first advanced by Chapman, Kuehn and Larson (Reference 24) it was anticipated that the use of generalized protuberance shapes was a reasonable approach in the study of protuberance induced flows and attendant fluctuating pressures. Essentially, this hypothesis states that boundary layers undergo separation in a manner which is independent of the original cause. The separation commenses well ahead of the protuberance, which leads to the conclusion that the flow near the separation point was unaffected by the detail geometry of the protuberance. This hypothesis was verified to some exrent; however, it was noted in References 22 and 23, that distinct differences do exist between two- and three-dimensional protuberance flow fields. These differences are discussed herein. Also, in close proximity to the protuberance, the local flow characteristics must depend on the detailed protuberance geometry. The validity of the free-interaction hypothesis as applied to the wake region of the protuberance induced flow field appears to be subject to restrictions similar to those for the upstream separated flow region. In the far-wake, the hypothesis is valid; whereas, in the near-wake the detailed protuberance geometry must be considered.

Analyses of protuberance induced fluctuating pressures as presented herein will encompass both the generalized cylindrical protuberance and two typical specific geometry protuberances.

3.1 General Characteristics of Protuberance Induced Flow

Before discussing the prediction methods, some general comments in regard to protuberance induced flow fields should be made. A photograph of a typical oil flow pattern around a cylindrical protuberance is shown in Figure 15. The oil flow pattern was obtained by injecting oil of different colors into the attached boundary layer upstream of the perturbed flow region as well as in close proximity to the protuberance. Any protuberance, regardless of geometry, which extends into or through an attached boundary layer will 1) tend to induce separated flow upstream of the protuberance and 2) generate a wake downstream of the protuberance. Both the separated flow and wake regions are clearly defined in Figure 15. These two regions will be discussed separately.

Oil injected through the three upstream orifices flowed aft and was deflected around the protuberance by the separated flow field. Oil injected into the separated flow region flowed in a direction counter to the free stream - indicating a reverse flow

environment, and transverse to the free stream - indicating circumferential flow due to the side relief afforded by the three-dimensional nature of the flow field. Furthermore the upstream separation line or front is parabolic in shape as may be anticipated for a three-dimensional protuberance, particularly for one having a cylindrically shape. The important feature of the oil flow pattern in the separated flow region is the concentration of oil along a secondary front which is downstream of the front caused by separation of the boundary layer. This suggests a condition of low velocity at angles perpendicular to the secondary front. The presence of the low velocity region imbedded within the separated flow has not been observed in two-dimensional separated flow and is apparently unique to the three-dimensional case.

The length of the upstream separated flow region at the longitudinal centerline was evaluated from oil-flow studies of the 4-inch diameter protuberance for the Mach number range from 0.60 to 1.40 and h/D range from 0 to 2.0. The separation point is identified in Figure 15. The resulting variations of normalized separation length, ℓ_s/D, with h/D for the various Mach numbers of the test are presented in Figure 16. The curve presented for $M_\infty = 1.60$ was determined by extrapolation of the lower Mach number data to $M_\infty = 1.60$. An increase in either protuberance height or Mach number resulted in an increase in separation length. The trend in the data indicates that the separation length will approach asymptotic values for large protuberance heights. Also, even though oil flow studies were not conducted for other protuberance diameters, the static- and fluctuating-pressure data indicate that protuberance diameter is the appropriate normalizing parameter.

Oil injected at strategic points around the base of the protuberance resulted in the flow pattern for the wake. The wake flow is characterized by a short converging region which is terminated by a narrow neck followed by a diverging region. The converging region will be denoted as the near wake and the diverging region as the far wake with the neck region separating the two. The neck and far wake are clearly shown in Figure 15; however, the near wake is partially obscured by the protuberance due to the slight downstream angle of the camera view. In the wake, it is obvious that the flow will be perturbed for many diameters downstream of the protuberance. Generally, the neck region which separates the near- and far-wake regions appeared to occur at approximately one diameter aft of the protuberance ($r/D \approx 1.5$) for $M_\infty \geq 1.20$. For lower Mach numbers, the wake was ill defined by the oil flow pictures; however, the fluctuating pressure measurements indicate that the neck region moved aft with decreasing Mach number.

A composite schematic showing typical axial distributions of static pressure coefficients and root-mean-square fluctuating pressure coefficients, and a possible model of the flow field upstream of the protuberance is presented in Figure 17. Sufficiently upstream of the protuberance, the flow is attached which results in static pressure coefficients of approximately zero, and fluctuating pressure coefficients of approximately 0.01. The latter results primarily from tunnel background noise as discussed in Reference 22. For the case shown, which is the $M_\infty = 1.60$, $h/D = 2.0$ condition, the most upstream boundary of the perturbed flow is the shock wave. The shock wave induces a nonlinear

increase in static pressure coefficient and a relatively small peak in the fluctuating pressure coefficient. The mean shock wave location corresponds to the inflection point in the static pressure data. Immediately aft of the shock wave, the boundary layer undergoes separation which, in turn, results in a region of relatively constant, plateau, static pressure. In the plateau region, a gradual increase in fluctuating pressure level with decreasing distance from the protuberance is observed. In contrast to these data, the two-dimensional protuberance (or step) case of References 19 and 20 show a region of plateau fluctuating pressure corresponding to the region of plateau static pressure (as shown in Figure 18). This latter discrepancy between two- and three-dimensional separated flows is the first indication (as the flow is examined moving downstream toward the protuberance) of dissimilarities between the two cases. Further, the fluctuating pressure levels for the three-dimensional case are an order of magnitude greater than that for the two-dimensional separated flow region. Immediately downstream of the plateau region, the flow exhibits a sudden reduction in static pressure, and the beginning of this sudden reduction corresp[onds to a] peak in the fluctuating pressure level. Corresponding to the region of low sta[tic pressu]re is what may be envisioned as a plateau region of fluctuating pressure for the $M_\infty = 1.60$ condition; however, this is not typical of all Mach numbers, since the fluctuating pressure decreases toward the protuberance for the region of low static pressure as discussed in Reference 22. The distinct nature of the sudden static pressure reduction and the strong levels of fluctuating pressure are unique to the three-dimensional separated flow case as shown in Figure 18.

Based on the characteristics of the induced separated flow as exhibited by the static pressures, fluctuating pressures, and oil flow pictures, a model of the upstream perturbed flow can be postulated. Consider a system of horse-shoe vortices, which when viewed in the plane of symmetry appear as shown in Figure 17. Two major vortices are assumed to be rotating such that a condition of reverse flow exists near the wall of the test panel with a third, smaller, vortex trapped near the wall between the two major vortices and rotating in the opposite direction. Thus, the boundary conditions at the inner region of the separated shear layer and within the separated flow are satisfied. Also observe that the upstream vortex may be elongated which would result in a relatively constant static pressure, plateau, region. The aft vortex, because of the geometry of the flow, may be more circular which would induce a nonlinear variation of the wall pressures as observed in the static pressure distribution. Further, because of the different static pressure levels associated with the two vortices, it may be postulated that the inner vortex has a higher tangential velocity at the wall than does the forward, elongated vortex. Finally, the shearing mechanism that would result due to the opposite velocity vectors in the region between the two vortices would cause a discontinuity in the wall shear stress which would enable oil to be trapped in this region (corresponding to the secondary front noted in the oil flow pictures) and also disturbances from the shear interaction could generate high level fluctuating pressures as noted in the axial distribution of $\sqrt{\overline{P'^2}}/q_\infty$, Figures 17 and 18. The direction of rotation of the vortices is verified from the oil flow patterns over the surface of the test panel (Figure 15) as well as in photographs of titanium dioxide studies of the protuberance flow pattern. It is interesting to note that the titanium dioxide flow patterns (side view) showed the separation of the flow from the wall of the protuberance near the 90-degree ray very clearly as was observed in the static and

fluctuating pressure measurements over the wall of the 8-inch diameter protuberance presented in Reference 22. One final sample of data which adds support to the validity of the postulated model of the upstream separated flow is presented in Figure 19. Here, the flow pattern upstream of a cylindrical protuberance has been photographed using thin filaments of smoke for flow visualization (Reference 25). The multiple vortex pattern upstream of the protuberance is clearly defined. This condition was extremely low speed (on the order of 5 ft/sec); however, the present data suggests that the basic features of the flow field remain unchanged at transonic Mach numbers. Other fluctuating pressure data which distinctly show similarities and differences between two- and three-dimensional separated flows are the power spectra and cross-power spectra which will be discussed in the following subsections.

The flow structure in the wake of the protuberance consists of a converging, near wake, region; a neck region of nearly parallel flow; and a diverging, far wake region as previously noted in Figure 15. Fluctuating pressures in the wake generally reach maximum values in the neck region. ($r/D \approx 1.5$ for $M_\infty = 1.6$) as shown in Figure 15. Additional insight into the flow structure of protuberance wake flows will be forthcoming in the discussions of power spectra and cross-power spectra in the following subsections.

Analyses for the purpose of deriving prediction formula for protuberance induced flows are based on data taken along the longitudinal conterline (in the plane of symmetry). Generally, the most severe fluctuating pressures for protuberance flows occur in the plane of symmetry. Comprehensive data for regions around the protuberances are presented in Reference 23. It suffices to note here that the region around the protuberance is characterized by a gradual transition from upstream separated flow to downstream wake flow. Both static and fluctuating pressures exhibited gradual changes from one region to the other; however, relatively severe fluctuating pressures were observed near the edge of the wake as well as along the longitudinal centerline (see Reference 23).

In the following subsections, separate analyses are presented for 1) the protuberance induced separated flow field, 2) the protuberance induced shock wave oscillation and 3) the protuberance induced wake flow field.

3.2 Protuberance Induced Separated Flow

Overall Levels — As noted in the foregoing discussion, the separated flow field induced upstream of a three-dimensional protuberance will consist of two distinct regions which are referred to as the inner and outer regions. According to the Chapman, Kuehn, and Larson free-interaction hypothesis, the outer region of the separated flow field for a three-dimensional protuberance should exhibit fluctuating pressure characteristics similar to those observed for two-dimensional and axisymmetric flows. Immediately aft of the induced shock wave at the separation point, the rms fluctuating pressure levels are in fairly close agreement as shown in Figure 18. However, deviations between the two cases occur a short distance aft of the shock wave and grow increasingly greater in the direction of the protuberance. Prediction of the rms fluctuating pressure

levels is complicated by their dependence on free-stream Mach number, protuberance diameter, protuberance height and location in the perturbed flow field. Thus, it does not appear feasible to propose prediction methods for the overall levels. However, a representative set of data is presented in Figures 20a-f for Mach numbers from 0.6 to 1.6. Additional data is presented in References 22 and 23.

Data presented in Figures 20a-f show characteristics typical of both the upstream separated flow field and the downstream wake flow field. In the upstream separated flow region, it suffices to note that the region is extremely non-homogeneous with $\sqrt{\overline{P^2}}/q_\infty$ ranging from 0.04 to 0.12 in the outer region of separated flow and from 0.06 to 0.12 in the inner region of separated flow with peak levels between the two regions ranging up to approximately 0.22. Thus, the development of generalized prediction formulas of overall levels for the separated flow field is considered to be impractical and reference should be made to experimental data for any particular case of interest.

Power Spectra -- The derivations of prediction formula of the power spectra for the separated flow field requires separate analyses of the inner and outer regions. Both regions are non-homogeneous as evidenced by the variations in overall levels and, as a result, prediction formula will represent the spatial average spectrum shape within that region. However, it will be noted that the prediction formula for each region is derived as a function of mean square overall fluctuating pressure levels. Thus, under the assumption of similarity of spectrum shape with spatial location, the proposed prediction formula will contain the non-homogeneous effects as they affect the spectrum levels.

Normalized power spectra for the outer region of the separated flow field at a short distance aft of the shock wave (corresponding to $\sqrt{\overline{P^2}}/q_\infty \approx 0.04$) are presented in Figure . These data represent the same relative location in the separated flow field for $M_\infty = 1.4$ and 1.6, and $h/D = 1.0$ and 2.0. It was anticipated that these data were measured sufficiently aft of the shock waves to preclude any contribution of the shock wave to the power spectral density. Also, the measurement locations were sufficiently forward of the inner region of separated flow to preclude contributions to the power spectral density from this region.

It is interesting to note the excellent data collapse achieved by using the separation length, ℓ_s, as the typical length and free-stream velocity, U_∞, as the typical velocity. For the range of data presented in Figure 21, the separation length varied from 1.75 to 2.35 diameters. Other typical lengths which were considered were inflowing boundary layer thickness δ_0, boundary layer displacement thickness, δ^*, and protuberance diameter, D. It is not surprising that the best collapse was achieved using separation length since it is a direct measure of the scale of the separated flow field. Also, this parameter contains the effects of both protuberance height, h, and protuberance diameter, D. It will be noted in Figure 16 that both h and D have an effect on the separation length. At small values of h/D, protuberance height is the more influential parameter on separation

length; whereas, at large values of h/D, protuberance diameter is more influential. The dividing point between these two ranges occurs where $(h/D)/(\ell_s/D) = 1.0$, and thus it is a function of free-stream Mach number. At very low values of h/D, the power spectra should collapse using h as a typical length; whereas, at large values of h/D, the spectra should collapse using D as a typical length. Naturally, the choice of h or D is avoided if ℓ_s is used as proposed herein.

For the range of Mach numbers studied herein, it is not possible to evaluate the accuracy of U_∞ as the typical velocity. Other investigators have suggested local velocity, U_ℓ, as discussed in Section 2.2. As a matter of convenience, U_∞, will be employed herein; however, conversion of the prediction formula to another typical velocity can be achieved with relative ease. For the present analysis, the selection of a typical length was certainly the most critical task in order to achieve meaningful prediction formulas.

Power spectra for the region of minimum $\sqrt{\overline{P^2}/q_\infty}$ within the outer region of the separated flow field is closely represented by the following empirical formula:

$$\frac{\Phi(f)\, U_\infty}{q_\infty^2\, \ell_s} = \frac{\overline{P^2}/q_\infty^2}{\frac{f_0\, \ell_s}{U_\infty}\left\{1 + (f/f_0)^{1.71}\right\}^{1.15}} \qquad (36)$$

where

$$f_0 = 0.412\ \frac{U_\infty}{\ell_s}$$

A comparison between Equation (36) and the experimental data is shown in Figure 21. It will be noted that this equation is somewhat different than Equation (10) which was derived for two-dimensional separated flows in Section 2.2.

For a true comparison of the two prediction formula, Equation (10) was rederived in terms of separation length, ℓ_s, and free-stream velocity, U_∞, using the values given in Reference 21. The resulting equation is:

$$\frac{\Phi(f)\, U_\infty}{q_\infty^2\, \ell_s} = \frac{\overline{P^2}/q_\infty^2}{\frac{f_0\, \ell_s}{U_\infty}\left\{1 + (f\ f_0)^{0.83}\right\}^{2.15}} \qquad (37)$$

where

$$f_0 = 0.70\ \frac{U_\infty}{\ell_s}$$

A comparison of this equation with experimental data is also shown in Figure 21. Although the disagreement is not overly disturbing, it does suggest that the free-interaction hypothesis is questionable when applied to the fluctuating pressure environment in the outer region of separated flow.

To check the validity of Equation 36 for other areas of the outer separated flow region, comparisons are made with the power spectra for two protuberances of different diameter and various radial locations in Figures 22a-c. At r/D = 2.50, the measurements were taken immediately aft of the shock wave and, in fact, may be upstream of the outer vortex since the oil flow photographs indicated that separation occurred at r/D = 2.35 for this condition. However, the shock wave is known to be forward of the r/D = 2.50 location. Thus, the disturbances appear to have a spectral content between that defined for two- and three-dimensional separated flows as shown in Figure 22a. The influence of the shock wave on the low frequency spectral density is evident for the 8-inch protuberance data in Figure 22a. The location, r/D = 1.75, corresponded to the region where $\sqrt{\overline{P^2}}/q_\infty \approx 0.09$ and, thus, should exhibit the effects of non-homogeneity on the power spectra. The close agreement between Equation (36) and the experimental data shown in Figure 22b indicate that non-homogeneous effects in the outer region are essentially an increase in fluctuating pressure levels with little change in sepctral content. At r/D = 1.50, corresponding to the boundary between the inner and outer regions of the separated flow field, maximum fluctuating pressure levels are reached. A comparison between Equation (36) and experimental spectra show an under approximation at low frequencies and an over approximation at high frequencies. Since the spectrum level is a function of $\overline{P^2}/q_\infty^2$ in Equation (36), the over-approximation at high frequencies is attributed to the high level disturbances at low frequencies and their influence on $\overline{P^2}/q_\infty^2$. In other words, the spectra at r/D = 1.50 is believed to have the same basic shape as the outer region with the exception that low frequency modulation in a longituding direction of the flow structure increases the low frequency spectrum level. This low frequency energy is similar to that noted for a shock wave and apparantly results from a similar oscillation mechanism. It obviously does not result from a contribution of the inner vortex structure as will be shown later. Forward and aft movement of the vortex structure would cause a longitudinal modulation of the instantaneous static pressure distributions. Since, at r/D = 1.5, $M_\infty = 1.60$, h/D = 2.0, a large pressure gradient is present, modulation will result in a fluctuating pressure similar to that noted beneath oscillating shock waves. This may easily be the mechanism noted in Figure 22c.

A representative sampling of power spectra for the inner region of the separated flow field is presented in Figure 23. These data have little in common with the spectra measured at r/D ≥ 1.50. This is consistent with the postulated model of the separated flow field. Thus, a new prediction formula is required for r/D ≤ 1.50. The following equation is in close agreement with the power spectra for the experimentally measured data for a range of test conditions:

$$\frac{\Phi(f)\,U_\infty}{q_\infty^2\,\ell_s} = \frac{\overline{P^2}/q_\infty^2}{\frac{f_0\,\ell_s}{U_\infty}\left\{1 + (f/f_0)^{2.62}\right\}} \qquad (38)$$

where

$$\frac{f_0\,\ell_s}{U_\infty} = 1.3$$

A comparison of Equation 38 with experimental data for protuberances of 8-inch and 4-inch diameters, r/D = 1.25, is shown in Figure 24. The agreement is considered to be excellent. The power spectrum for two-dimensional separated flows as defined by Equation (37) is also shown in Figure 24. A comparison between this equation and experimental data reveals large differences between the two flow fields. Finally, it should be noted that the lack of a peak in the experimental spectra at low frequencies supports the preceding argument that the anomaly observed at low frequencies at r/D = 1.50 (Figure 22c) results from some mechanism other than the disturbances contained within the inner vortex.

In summary, the power spectra for the separated flow field upstream of a three-dimensional protuberance supports the postulated, multiple vortex, model of the separated region. In the outer region, corresponding to the outer vortex structure, the power spectra can be accurately represented by a single equation with non-homogeneous effects adequately contained in the mean-square-overall level parameter in the prediction equation. Immediately downstream of the shock wave, the spectra for two- and three-dimensional separated flows deviate from each other even though some similarity in shape is retained. Finally, in the inner region of separated flow drastic differences are observed between the power spectra for two- and three-dimensional separated flows for this region.

Cross-Power Spectra — Cross-spectra for a representative condition (M_∞ = 1.60, h/D = 2.0) are presented in Figure 25. It will be noted that reasonably good correlation is shown for microphone pairs located beneath the forward vortex, poor coherence for microphone pairs located near the region between the two major vortices, and fair correlation for microphone pairs located in the region of the inner vortex. Disturbances generated in the region of interaction between the two major vortices would not be convected directly across the microphones near the protuberance because of the direction of rotation of the inner vortex. Thus, some loss of coherence (compared to that for the outer vortex system) may be expected. Typical variation of the coherence function $\gamma^2(\xi, f)$ with Strouhal frequency ($f\,\xi/U_c$) have been analyzed for attached flow and two- and three-dimensional separated flows. These data show that the three-dimensional separated flow field loses coherence very rapidly in comparison with the other two cases, as may be expected from the spiral-horseshoe vortex structure in the separated flow field.

As a first approximation, the normalized longitudinal co-spectra may be represented by:

$$C(\xi, f) = e^{-a\omega\xi/U_c} \cos \frac{\omega \xi}{U_c} \qquad (39)$$

where a is the coefficient of exponential decay which will vary with spatial location within the separated flow field. On the average, the coefficient of exponential decay was approximately the same for both the inner and outer regions of separated flow; although, the coherence was more clearly defined for the outer region. Thus, a value of $a = 0.7$ should adequately represent these two regions. Between the inner and outer regions, the coherence should be assumed to be approximately zero or $a = \infty$.

3.3 Protuberance Induced Shock Wave Oscillation

Overall Levels — Oscillation of the shock wave immediately upstream of the protuberance induced separated flow field produced surface fluctuating pressures very similar to those observed upstream of two-dimensional separated flows as shown in Figures 12 and 18. The measurement of peak fluctuating pressure levels beneath oscillating shock waves is extremely difficult since the disturbances are highly localized and the shock must be centered directly over the measuring instrument. For the range of protuberance test conditions reported in References 22 and 23, only a few examples of shock wave oscillation were recorded. For these conditions, rms levels ranged up to 0.07 as shown in Figures 20a-f. These data are consistent with the levels measured by Coe and others in References 14, 19, 20, and 21.

Power Spectra — The power spectra for shock wave oscillation induced by three-dimensional protuberances are very similar to that reported by Coe for two-dimensional separated flow (see Figure 12). A comprehensive analysis of the spectrum shape, and the mechanisms which contribute to the fluctuating pressures beneath oscillating shock waves was presented in Section 2.3 and will not be repeated here. The similarity in the spectra for the two cases indicates that the region of shock wave oscillation is effectively a free-interaction region and the attendant fluctuating pressures are independent of the detailed geometry of the protuberance. The generalized prediction formula for shock wave oscillation as presented in Section 2.3 should be appropriate for the prediction of power spectra for regions beneath protuberance induced shock waves. However, one interesting anomaly is evident in the shock oscillation data presented in Figures 12 and 18. The normalized spectrum levels are generally greater for the three-dimensional protuberance than for the two-dimensional case (Figure 12); whereas, the overall levels (Figure 18) are less for the three-dimensional protuberance. This anomaly appears to result from either 1) the normalizing parameters, δ_0 and U_∞, are not correct or 2) the overall levels are incorrect. Since shock wave oscillation is a low frequency phenomenon, it is possible that the microphones employed in the study of three-dimensional protuberances reported in References 22 and 23 failed to record the low frequency fluctuating pressures due to response roll-off (see Reference 22). Consequently, the measured overall levels may be somewhat lower than the actual case.

However, a more significant effect appears to be the use of δ_0 as the typical length. Comparisons of power spectra using separation length ℓ_s appears to give a much closer collapse of the data as shown in Figure 26. The new prediction for that portion of the spectra resulting from inviscid shock wave oscillation, expressed in terms of ℓ_s, is:

$$\left[\frac{\Phi(f)\, U_\infty}{q_\infty^2\, \ell_s}\right]_{SW}^{I} = \frac{\left(\overline{P^2}/q_\infty^2\right)_{SW}^{I}}{\left(\frac{f_0\, \ell_s}{U_\infty}\right)_{SW} \left\{1 + (f/f_0)^{1.55}\right\}^{1.7}} \qquad (40)$$

where

$$\left(\frac{f_0\, \ell_s}{U_\infty}\right)_{SW} = 8.75 \times 10^{-2}$$

$$\left(\overline{P^2}/q_\infty^2\right)_{SW}^{I} = 4.5 \times 10^{-3}$$

The contribution of the separated flow in the immediate vicinity of the shock wave is given by the two-dimensional expression:

$$k\left[\frac{\Phi(f)\, U_\infty}{q_\infty^2\, \ell_s}\right]_S = k\, \frac{\left(\overline{P^2}/q_\infty^2\right)_S}{\left(\frac{f_0\, \ell_s}{U_\infty}\right)_S \left\{1 + (f/f_0)^{0.83}\right\}^{2.15}} \qquad (41)$$

where

$$\left(\frac{f_0\, \ell_s}{U_\infty}\right)_S = 0.70$$

$$\left(\overline{P^2}/q_\infty^2\right) = 1.6 \times 10^{-3}$$

As noted in Section 2.3, the value of k_1 may vary from approximately 0.25 to 1.00, depending on the mean location of the shock wave relative to the measurement location. For Coe's shock oscillation spectra, $k_1 \approx 0.25$.

For the cylindrical protuberance data presented in Figure 26, $k_1 = 0.25$, gives a good empirical fit to the experimentally observed spectra. It will be noted that the two-dimensional expression for the separated flow is employed here since the separated flow in the immediate vicinity of the shock wave appears to exhibit fluctuating

pressure characteristics typical of two-dimensional flows rather than characteristics typical of the outer vortex. In fact, it is highly possible that the flow undergoes separation a short distance aft of the shock wave rather than immediately aft of the shock wave since Equation (10) closely resembles that for attached turbulent boundary layers as mentioned in Section 2.2.

The final expression for the shock wave oscillation upstream of a cylindrical protuberance is the combination of Equations (40) and (41):

$$\left[\frac{\Phi(f)\ U_\infty}{q_\infty^2\ \ell_s}\right]_{SW} = \frac{\left(\overline{P^2}/q_\infty^2\right)_{SW}}{\left(\frac{f_0\ \ell_s}{U_\infty}\right)_{SW}\left\{1 + (f/f_0)^{1.55}\right\}^{1.7}} +$$

$$0.25\ \frac{\left(\overline{P^2}/q_\infty^2\right)_S}{\left(\frac{f_0\ \ell_s}{U_\infty}\right)_S\left\{1 + (f/f_0)^{0.83}\right\}^{2.15}} \qquad (42)$$

where

$$\left(\frac{f_0\ \ell_s}{U_\infty}\right)_{SW} = 8.75 \times 10^{-2}$$

$$\left(\frac{f_0\ \ell_s}{U_\infty}\right)_S = 0.7$$

Also for the case shown in Figure 26

$$\left(\overline{P^2}/q_\infty^2\right)_{SW}^{I} \approx 4.5 \times 10^{-3}$$

$$\left(\overline{P^2}/q_\infty^2\right)_S \approx 1.6 \times 10^{-3}$$

Equation (42) is in excellent agreement with experimental data as shown in Figure 26. As previously noted in Section 2.3, the prediction formula for the power spectra of shock wave oscillation holds true only at a point corresponding to the mean location of the shock wave.

Cross-Power Spectra — Cross-power spectra for protuberances induced shock wave oscillation were not computed in References 22 and 23. However, the close similarity of the overall levels and power spectra between two- and three-dimensional separated flows for the region of the shock wave indicates that the cross-spectra for three-dimensional protuberances will closely resemble those for the two-dimensional case. Thus, Equation (25) in Section 2.3 should be appropriate here with the possible exception that the typical length dimension should be ℓ_s rather than δ_0.

At this point in time, the spatial characteristics of fluctuating pressures remain open and will require additional study. Certainly, considerable insight has been gained as a result of the studies reported in References 19, 20, 22, and 23; however many questions in regard to shock oscillation phenomena remain unanswered.

3.4 Protuberance Induced Wake Flow

Overall Levels — Typical rms fluctuating pressure levels for the wake flow field downstream of cylindrical protuberances are presented in Figure 27 ($\theta^* = 180$ degrees). The fluctuating pressure field associated with the wake of a protuberance extends over a relatively large axial distance. It is difficult to distinguish the near-wake, neck, and far-wake regions in the overall levels, however, the general trend is that peak fluctuating pressure levels occur near the neck with decreasing levels in the near- and far-wake regions. For certain conditions the peak levels of fluctuating pressures occur three or four diameters aft of the protuberance. As noted in References 22 and 23, it is difficult to define consistent trends in the wake results and perhaps this confusion is a result of the complex flow structure that exists in the wake and the way it changes with variations in both Mach number and protuberance height.

Power Spectra — Power spectra for the wake exhibit characteristics of a non-homogeneous flow field which is gradually changing in space. It is difficult to determine precise trends in the power spectra with variations of either Mach number, protuberance height, or axial location (see References 22 and 23). Typical power spectra, normalized by protuberance diameter and free-stream velocity, are presented in Figure 27. The choice of diameter as the typical length was necessitated by the lack of a typical length scale for the wake flow field. In the upstream separated flow field, the separation length, ℓ_s, was found to be an appropriate normalizing parameter. However, in the wake the choice is more difficult since the geometry of the wake is relatively unknown. Perhaps the axial distance from the protuberance to the neck region is a typical dimension for the wake structure; however, this parameter is not clearly defined. The flow field in the wake is complicated by 1) the flow around the protuberance which will have a characteristic scale in proportion to protuberance diameter and 2) the flow over the top of the protuberance which will have a characteristic scale in proportion to protuberance height. Furthermore, the non-uniform distribution of velocity and flow direction upstream of the protuberance as caused by upstream separated flow further complicates the analysis for the wake. It is concievable that a characteristic dimension for the wake does not exist in the way that it was defined for the upstream flow field. For this reason, only one case will be analyzed corresponding to $M_\infty = 1.6$,

h/D = 1.0. For this condition, a single prediction formula appears to be representative of the power spectra for all three regions of the wake. The equation is given as:

$$\frac{\Phi(f)\, U_\infty}{q_\infty^2\, D} = \frac{\overline{P^2}/q_\infty^2}{\frac{f_0 D}{U_\infty}\left\{1 + (f/f_0)^{2.62}\right\}} \qquad (43)$$

where

$$\frac{f_0 D}{U_\infty} = 0.95$$

A comparison of Equation (43) with spectra for the near-wake, neck, and far-wake regions is shown in Figure 27. The agreement is considered to be excellent in the far-wake with increasing discrepancy occurring in the direction of the protuberance.

Cross-Power Spectra — Typical cross-spectral density results for the protuberance wake are presented as normalized co- and quad-spectra in Figure 28. Maximum coherence in the wake occurred in the neck and far-wake regions as evidenced by the lower decay rates of the cross-spectra. In the near-wake, $r/D \leq 1.50$, the cross-spectra decay very rapidly and in general show poor correlation. The correlation increases to a maximum in the neck region and this is attributed to the non-dispersive nature of the parallel flow in this region. In the far wake, the flow has a diverging pattern; however, good correlation was still attained. The larger separation of the microphones in the far wake resulted in a loss of coherence in the low frequency components. In general, the wake flow was characterized by positive convection velocities (convection in the direction of the free stream) as exhibited by the positive values of the normalized frequency parameter and the trend in the quad-spectral density.

The longitudinal co- and quad-spectra in the neck and far-wake regions for small spatial separations can be represented by exponentially damped sinusoids as follows:

$$C(\xi_1 f) = e^{-2\pi a f \xi/U_c} \cos 2\pi f \xi/U_c$$

$$Q(\xi_1 f) = e^{-2\pi a f \xi/U_c} \sin 2\pi f \xi/U_c$$

where the coefficient of exponential decay is given by $a \approx 0.19$.

Lateral cross-power spectra were not computed for the wake flow field in References 22 and 23, and consequently prediction fromula are not proposed.

Another way of expressing the spatial characteristics of a fluctuating pressure field is with the coherence function which is the square of the modulus for the cross-power spectra. A comparison of coherence functions for various basic and protuberance induced fluctuating pressure environments is presented in Figure 29.

3.5 Comparisons of Generalized and Specific Geometry Protuberances

Tests were performed as reported in Reference 22 to investigate similarities between generalized and specific geometry protuberance flow fields and attendant fluctuating pressures. This study was a cursory examination of specific geometry protuberances since only two configurations were studied. These configurations represented scaled models of the Reaction Control Systems (RCS) and Auxiliary Propulsion Unit (APU) on the Saturn V. The results presented herein represent only the salient characteristics of the induced fluctuating pressures since only rms levels are presented. A comparison of the axial distributions of rms fluctuating pressures for the RCS protuberance and a 2-inch diameter cylindrical protuberance with $h/D = 0.5$ is presented in Figure 30. The agreement is good, particularly in the upstream separated flow field and the far-wake region. A similar comparison, between the APU protuberance and a 4-inch diameter cylindrical protuberance with $h/D = 1.0$ is shown in Figure 31. The elongated shape of the APU protuberance resulted in peak fluctuating pressures at a distance further upstream than that observed for the cylindrical protuberance. Also, the wake disturbances are in agreement only in the far wake. However, in both the upstream and wake flow fields, the trends in the data are similar.

4.0 CONCLUDING REMARKS

Analyses of various unsteady flow environments have been performed for the purpose of defining empirical formula for estimating the statistical properties of the attendant fluctuating pressures. The surface fluctuating pressures for both basic unsteady flows — consisting of attached turbulent boundary layers, separated flows, and shock-wave oscillation — and protuberance induced flows have been reviewed. The resulting empirical formula are characterized by (1) the simplicity of their mathematical formulation, (2) the relation to the physical parameters of the flow, and (3) good agreement with the available experimental data. Of particular importance are the formula for the Power Spectra and Cross-Power Spectra which have been derived as functions of the overall mean square levels. These formula are summarized below.

4.1 Power Spectra

Prediction of the power spectra for the various unsteady flows with the exception of shock-wave oscillation have the following form:

$$\frac{\Phi(f)\,U}{q_\infty^2\,L} = \frac{P^2/q_\infty^2}{\frac{f_0 L}{U}\left\{1+\left(f/f_0\right)^n\right\}^k}$$

where U = characteristic velocity

L = characteristic length and

f_0 = characteristic frequency

For shock wave oscillation, the power spectra is a combination of power spectra for inviscid shock-wave motion as well as contributions from the separated flow near the foot of the shock wave. The prediction formula has the following form:

$$\left(\frac{\Phi(f)\,U}{q_\infty^2\,L}\right)_{SW} = \left(\frac{\Phi(f)\,U}{q_\infty^2\,L}\right)^{I}_{SW} + k_1 \left(\frac{\Phi(f)\,U}{q_\infty^2\,L}\right)_{S}$$

where $k_1 \approx 0.25$, the subscripts SW and S denote shock wave and separated flow respectively, and the superscript I denotes the absence of viscous effects.

Generally, a prior knowledge of $\overline{p^2}/q_\infty^2$ is required to predict the power spectra; however, prediction formula for the overall levels are presented for attached turbulent boundary layers and two-dimensional (or axisymmetric) separated flows.

The separated flow upstream of cylindrical protuberances consists of an inner and outer region which require separate prediction formula. These regions are non-homogeneous; however, the spectrum shapes remain fairly coherent within each region such that the non-homogeneous effect is contained in the mean-square overall level term of the power spectrum equations. Both shock-wave oscillation and the separated flow appear to have spectra which scale with free-stream velocity and separation length for the cylindrical protuberance case. Close agreement was achieved between the spectra for shock oscillation upstream of two- and three-dimensional separated flows using separation length and free-stream velocity as normalizing parameters. The wake downstream of cylindrical protuberances consists of near-wake, neck, and far-wake regions. Empirical formula representative of all three regions for $M_\infty = 1.6$, $h/D = 1.0$ were derived; however, this prediction is not considered to be general since protuberance diameter and free-stream velocity were employed in the normalization. Examination of the experimental data show large effects of both free-stream Mach number and protuberance height on the power spectra in the wake. Although protuberance diameter appears to be a typical length scale for a fixed protuberance height-to-diameter ratio, and at a given Mach number, it is not a typical length scale in the general sense as separation length was found to be for the upstream separated flow field.

4.2 Cross-Power Spectra

The spatial coherence of the fluctuating pressure environments as defined by the cross-power spectra were evaluated for the various unsteady flows. The cross-power spectra for attached turbulent boundary layers, two- and three-dimensional separated flows and protuberance induced wake flows appear to be fairly well defined at least in the longitudinal direction. Much uncertainty remains for transverse cross-power spectra in upstream separated flows, and protuberance wake flows. Both longitudinal and transverse cross-power spectra for the regions beneath oscillating shock waves require additional study.

In general the normalized cross-power spectra for the various fluctuating pressure environments can be defined as exponentially damped sinusoids as follows:

$$C(\xi, f) = e^{-a\,\omega\,\xi/U_c} \cos \frac{\omega\,\xi}{U_c}$$

$$C(\eta, f) = e^{-b\,\omega\,\eta/U_c}$$

where ω is the circular frequency, U_c is the convection velocity, and ξ and η are the longitudinal and transverse separation distances, respectively.

However, the coefficient of exponential decay is a function of the particular environment under study and may also depend on free-stream Mach number as well as local flow conditions. Derivations of the coefficient of exponential decay are presented for each unsteady flow condition where the data was sufficiently well defined to merit an analysis. For attached boundary layer flow, the coefficient of exponential decay in the longitudinal direction was found to be $a = 0.10$. For two-dimensional and axisymmetric separated flows, the values ranged from 0.13 at $M_\infty = 2.5$ to 0.33 at $M_\infty = 1.60$. The coefficient of exponential decay in the inner and outer regions of three-dimensional separated flows upstream of cylindrical protuberances were approximately the same in the longitudinal direction with a value of $a \approx 0.7$. In the protuberance wake, the spatial decays were clearly defined only in the neck and far-wake regions with a value of $a \approx 0.19$.

REFERENCES

1. Lowson, M. V., "Prediction of Boundary Layer Pressure Fluctuations," Wyle Laboratories Research Staff Report WR 67-15, October 1967.

2. Speaker, W. V. and Ailman, C. M., "Spectra and Space-Time Correlations of the Fluctuating Pressures at a Wall Beneath a Supersonic Turbulent Boundary Layer Perturbed by Steps and Shock Waves," NASA CR-486, May 1966.

3. Bull, M. K., "Properties of the Fluctuating Wall Pressure Field of a Turbulent Boundary Layer," AGARD Report 455, April 1963.

4. Bull, M. K., et al., "Wall Pressure Fluctuations in Boundary Layer Flow and Response of Simple Structure to Random Pressure Fields," University of Southampton, AASU Report 243, 1963.

5. Kistler, A. L. and Chen, W. S., "The Fluctuating Pressure Field in a Supersonic Turbulent Boundary Layer," Jet Propulsion Laboratory Technical Report No. 32-277, August 1962.

6. Belcher, P. M., "Predictions of Boundary Layer Turbulence Spectra and Correlations for Supersonic Flight," Presented at the 5th International Acoustic Congress, Liege, Belgium, September 1965.

7. Serafini, J. S., "Wall Pressure Fluctuations and Pressure Velocity Correlations in a Turbulent Boundary Layer," NASA TR R-165, December 1963.

8. Bakewell, H. P. Jr., et al., "Wall Pressure Correlation in Turbulent Pipe Flow," U. S. Navy Sound Laboratory Report No. 559, August 1962.

9. Shattuck, R. D., "Sound Pressures and Correlations of Noise on the Fuselage of a Jet Aircraft in Flight," NASA TN-D-1086, August 1961.

10. Willmarth, W. W. and Roos, F. W., "Resolution and Structure of the Wall Pressure Field Beneath a Turbulent Boundary Layer," J. Fluid Mech., Vol. 22, Part 1, pp. 81-94, 1965.

11. Maestrello, L., "Measurement of Noise Radiated by Boundary Layer Excited Panels," J. Sound Vib., 2 (2), 1965.

12. Hilton, D. A., "In-Flight Aerodynamic Noise Measurements on a Scout Launch Vehicle," NASA TN D-1818, July 1963.

13. Williams, D. J. M., "Measurements of the Surface Pressure Fluctuations in a Turbulent Boundary Layer in Air at Supersonic Speeds," University of Southampton, AASU Report No. 162, Department of Aeronautics and Astronautics, December 1960.

14. Chyu, W. J. and Hanly, R. D., "Power and Cross-Spectra and Space Time Correlation of Surface Fluctuating Pressures at Mach Numbers Between 1.6 and 2.5," AIAA Preprint No. 68-77, January 1968.

15. Maestrello, L., "Measurement and Analysis of the Response Field of Turbulent Boundary Layer Excited Panels," J. Sound and Vib., 2, No. 3, July 1965.

16. Willmarth, W. W. and Woolridge, C. E., "Measurements of the Fluctuation Pressure at the Wall Beneath a Thick Turbulent Boundary Layer," J. Fluid Mech., Vol. 14, pp. 187-210, 1962.

17. Bozich, D. J. and White, R. W., "Study of the Vibration Responses of Shells and Plates to Fluctuating Pressure Environments," Wyle Laboratories Research Staff Report WR 69-19, September 1969.

18. Robertson, J.E., "Wind Tunnel Investigation of the Effects of Reynolds Number and Model Size on the Steady and Fluctuating Pressures Experienced by Cone-Cylinder Missile Configurations at Transonic Speeds," AEDC-TR-66-266, March 1967.

19. Coe, Charles F., "Surface Pressure Fluctuations Associated with Aerodynamic Noise," Basic Aerodynamic Noise Research Conference Proceedings, NASA SP-207.

20. Coe, Charles F., and Rechtien, R. D., "Scaling and Spatial Correlation of Surface Pressure Fluctuations in Separated Flow at Supersonic Mach Numbers," Paper presented at the AIAA Structural Dynamics and Aeroelasticity Specialist Conference, New Orleans, La., April 16-17, 1969.

21. Rechtien, Richard D., "A Study of the Fluctuating Pressure Field in Regions of Induced Flow Separation at Supersonic Speeds," University of Missouri - Rolla UMR Research Report, May 1970.

22. Robertson, J.E., "Characteristics of the Static- and Fluctuating-Pressure Environments Induced by Three-Dimensional Protuberances at Transonic Mach Numbers," Wyle Laboratories Research Staff Report WR 69-3, June 1969.

23. Robertson, J.E., "Fluctuating Pressures Induced by Three-Dimensional Protuberances," Wyle Laboratories Research Staff Report WR 70-10, April 1970.

24. Chapman, D.R., Kuehn, D.M., and Larson, H.K., "Investigation of Separated Flows in Supersonic and Subsonic Streams with Emphasis on the Effects of Transition," NACA Report 1356.

25. Incompressible Aerodynamics, Oxford at the Claredon Press, 1960.

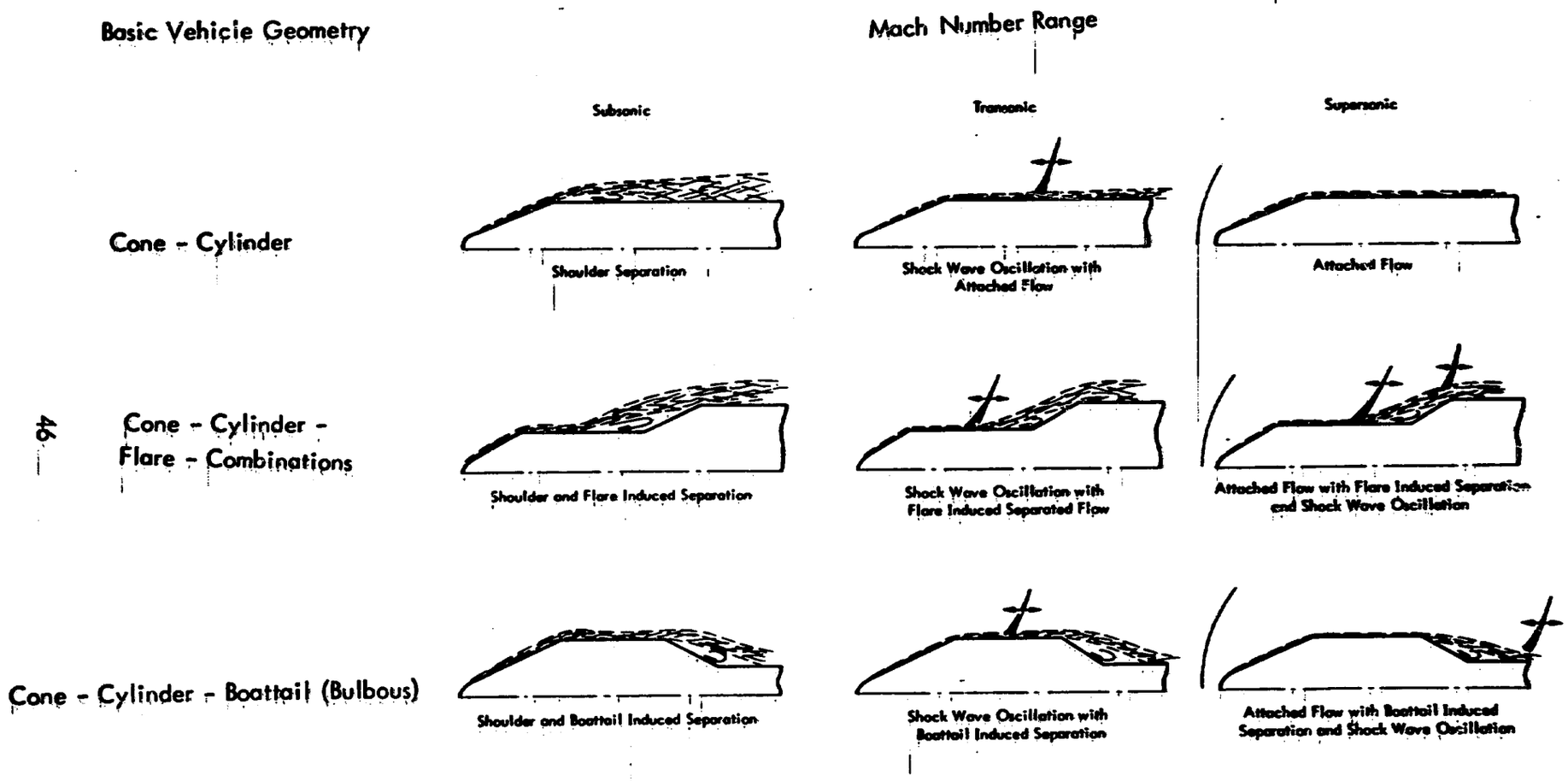

Figure 1. Subsonic, Transonic, and Supersonic Flow Fields for Basic Vehicle Configurations

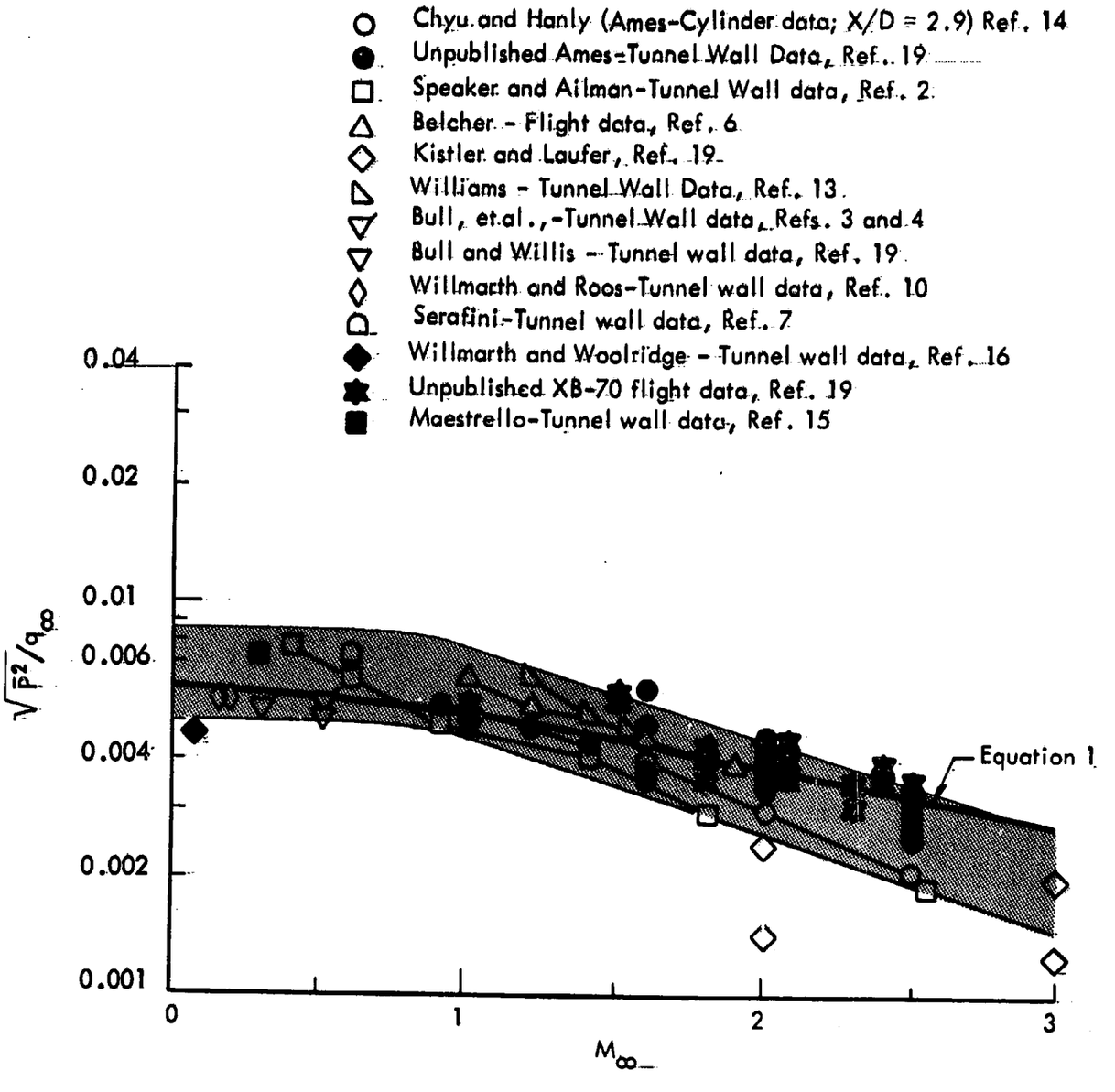

Figure 2. Comparison of Pressure Fluctuation Measurements by Various Investigators for Attached Turbulent Boundary Layers

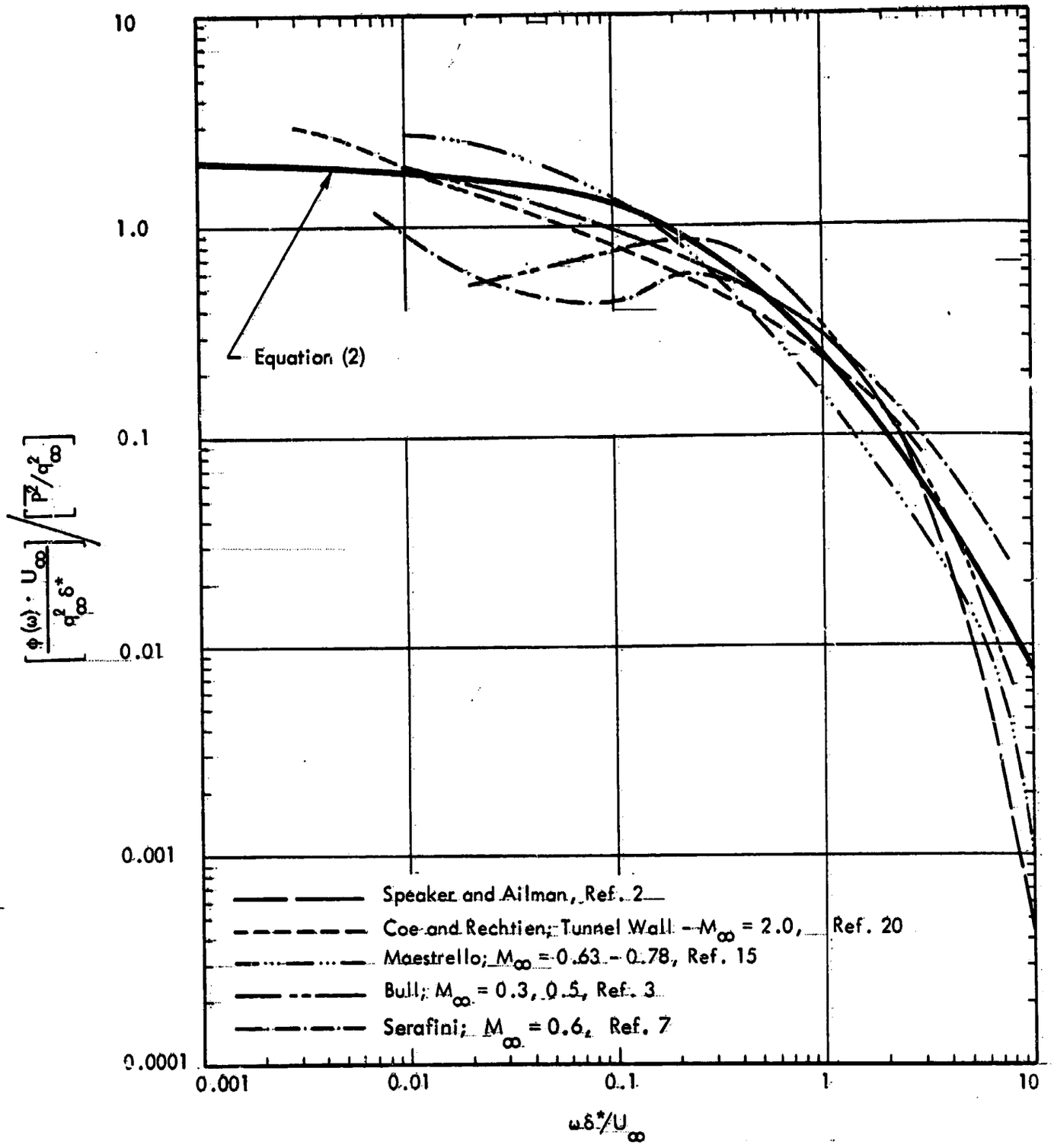

Figure 3. Power Spectra for Turbulent Boundary Layer Fluctuating Pressures

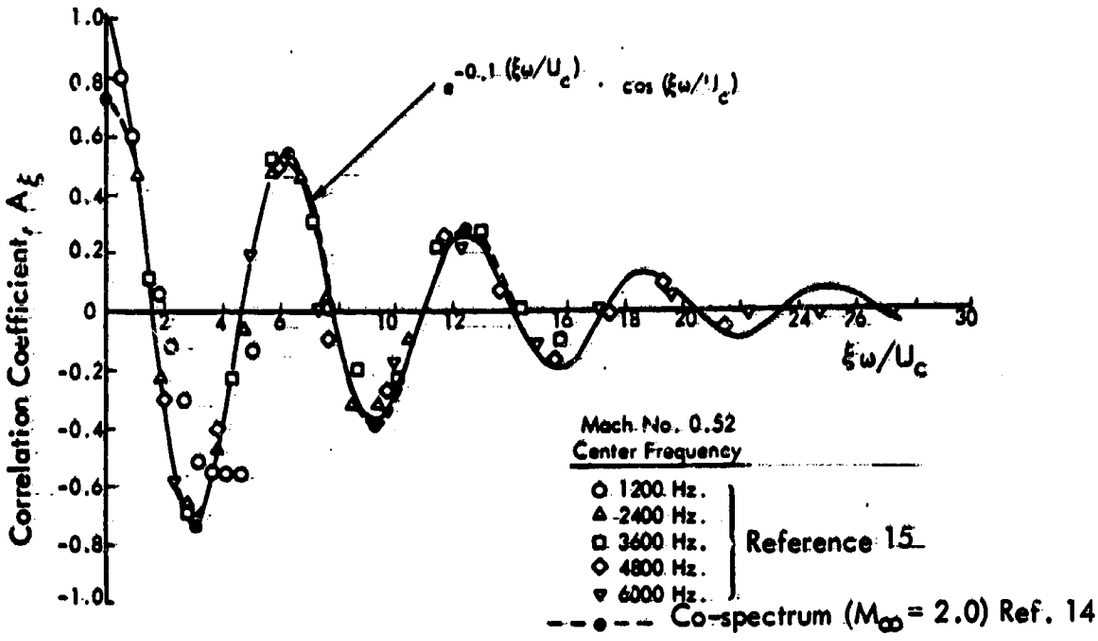

Figure 4a. Narrow Band Longitudinal Space Correlation Coefficient for Boundary Layer Fluctuating Pressures

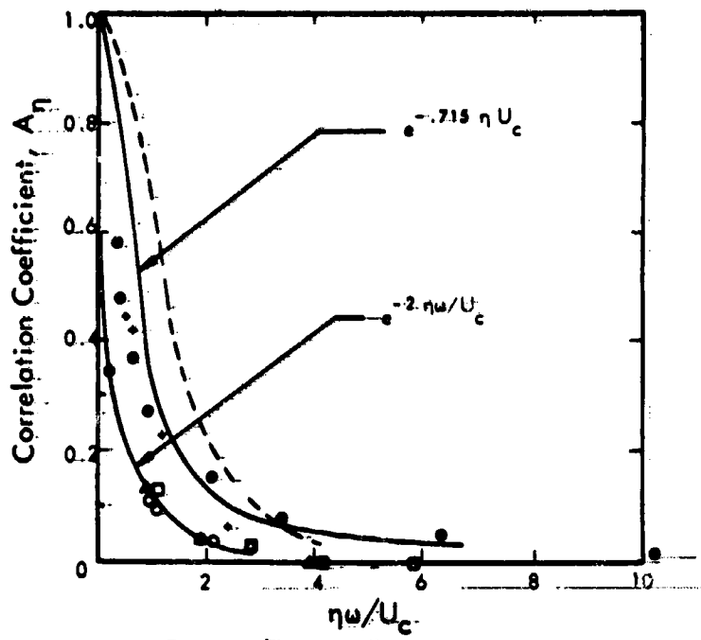

Figure 4b. Narrow Band Lateral Space Correlation Coefficient for Boundary Layer Fluctuating Pressures

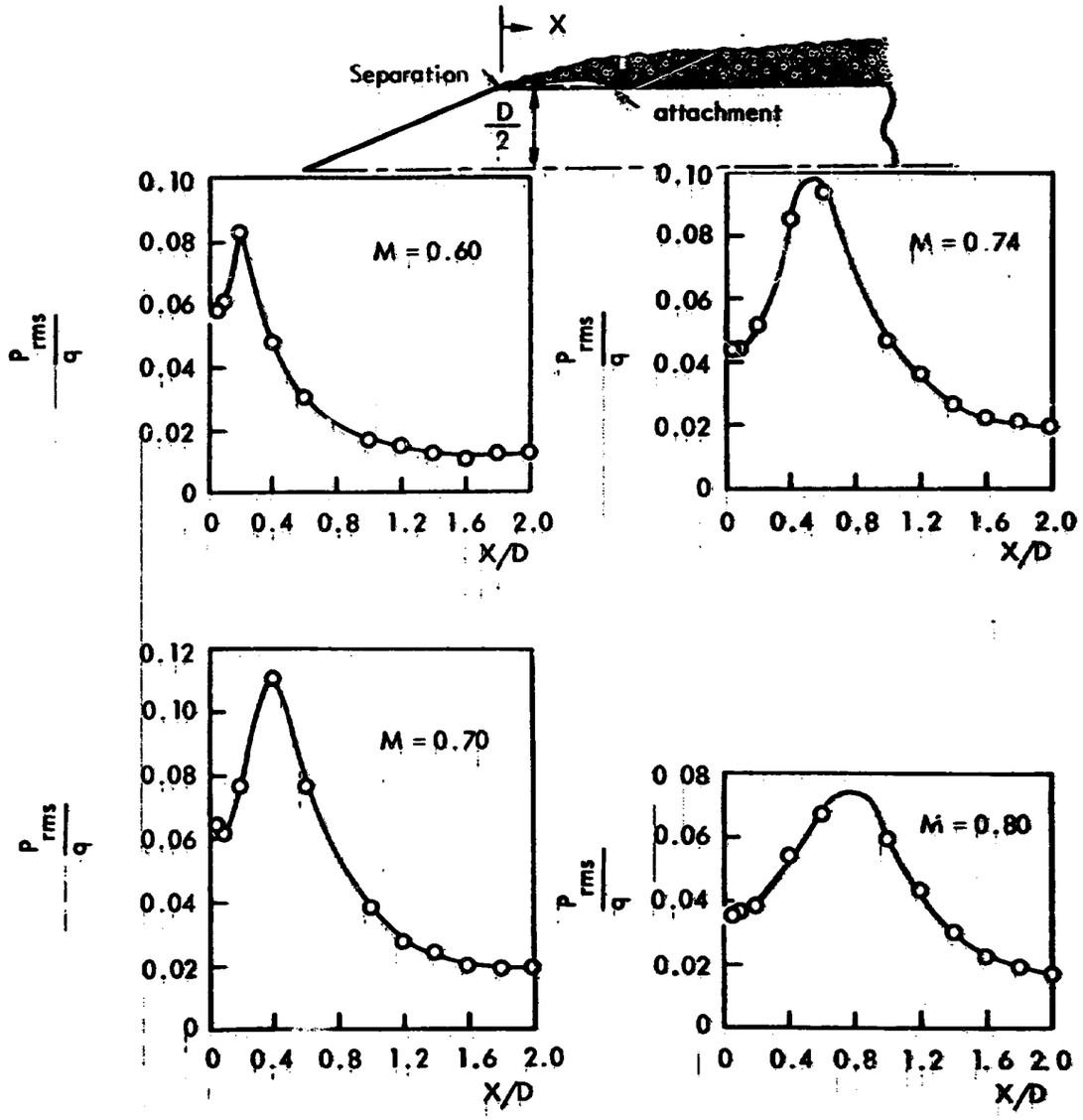

Figure 5. Axial Distributions of Fluctuating Pressures for Blunt Body Separated Flow (Ref. 18)

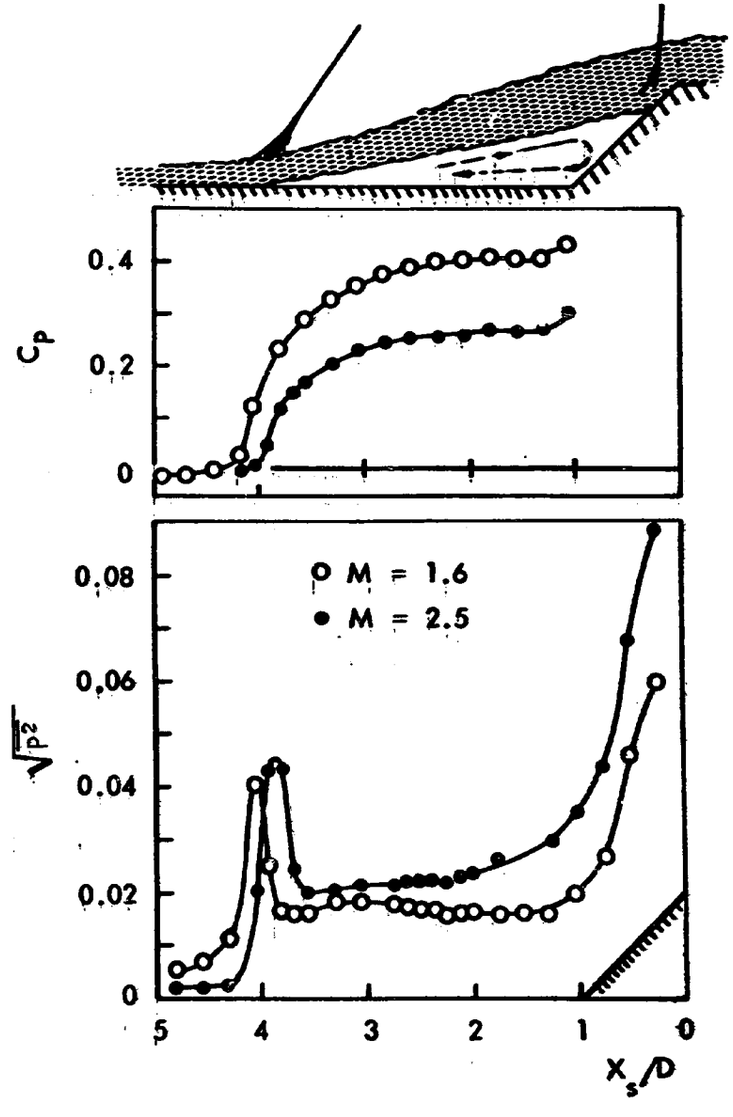

Figure 6. Axial Distributions of Static and Fluctuating Pressures for Flare Induced Separation (Ref. 14)

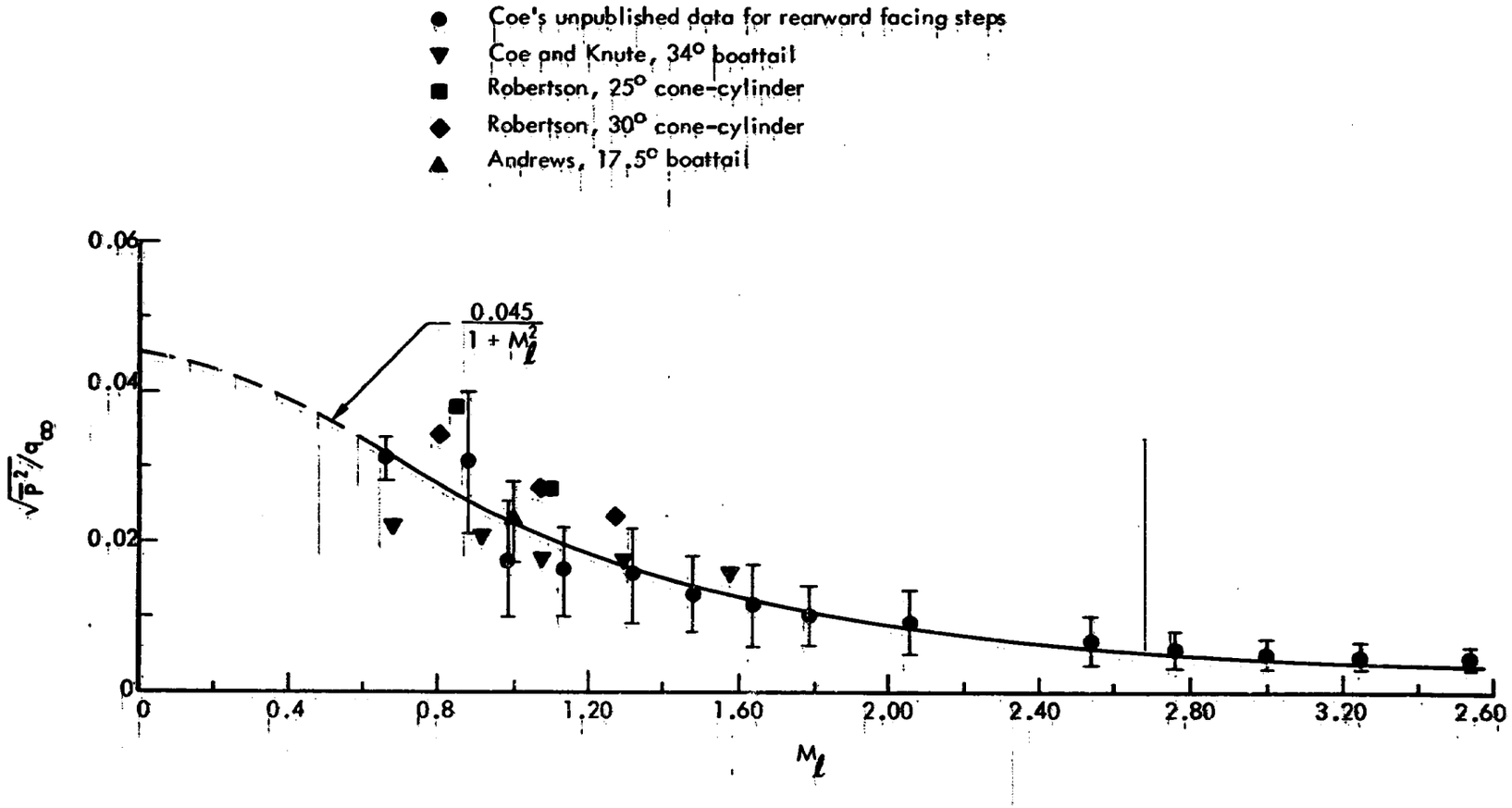

Figure 7. Variation of Normalized RMS Fluctuating Pressure Level with Local Mach Number for Expansion Induced Separated Flow

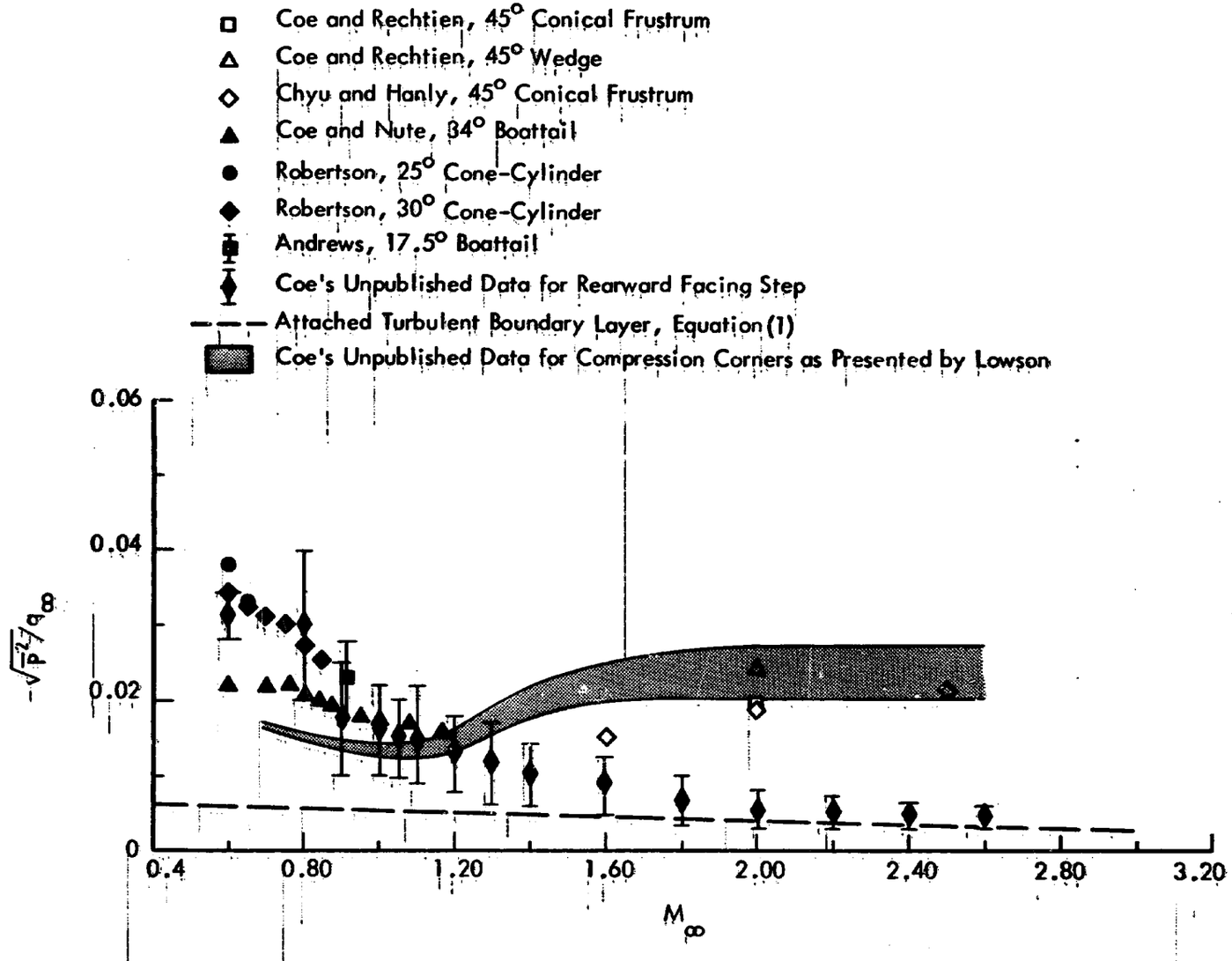

Figure 8. Variation of Fluctuating Pressure Level for Separated Flow with Mach Number

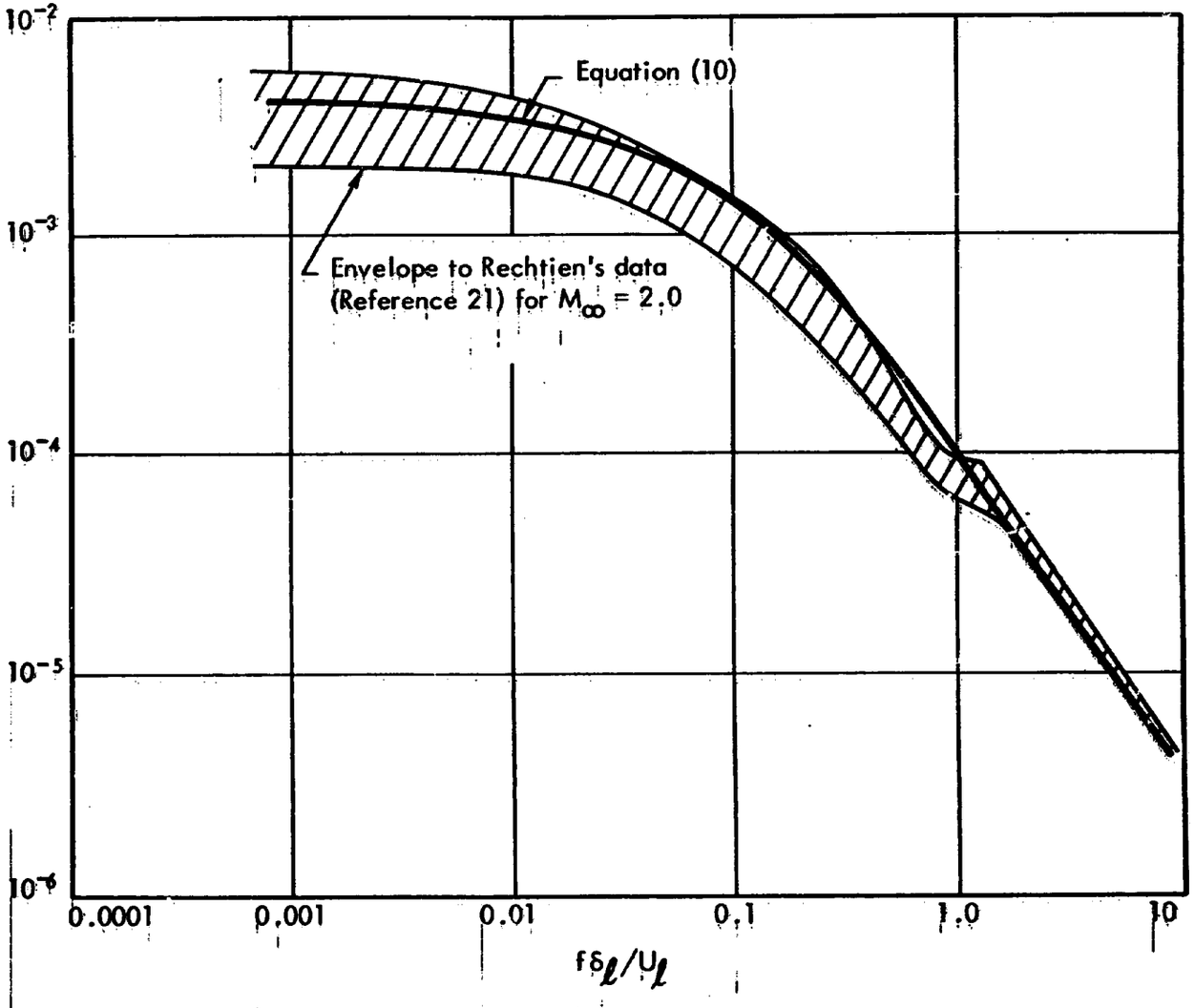

Figure 9. Power Spectrum of Fluctuating Pressures within Separated Flow Regions

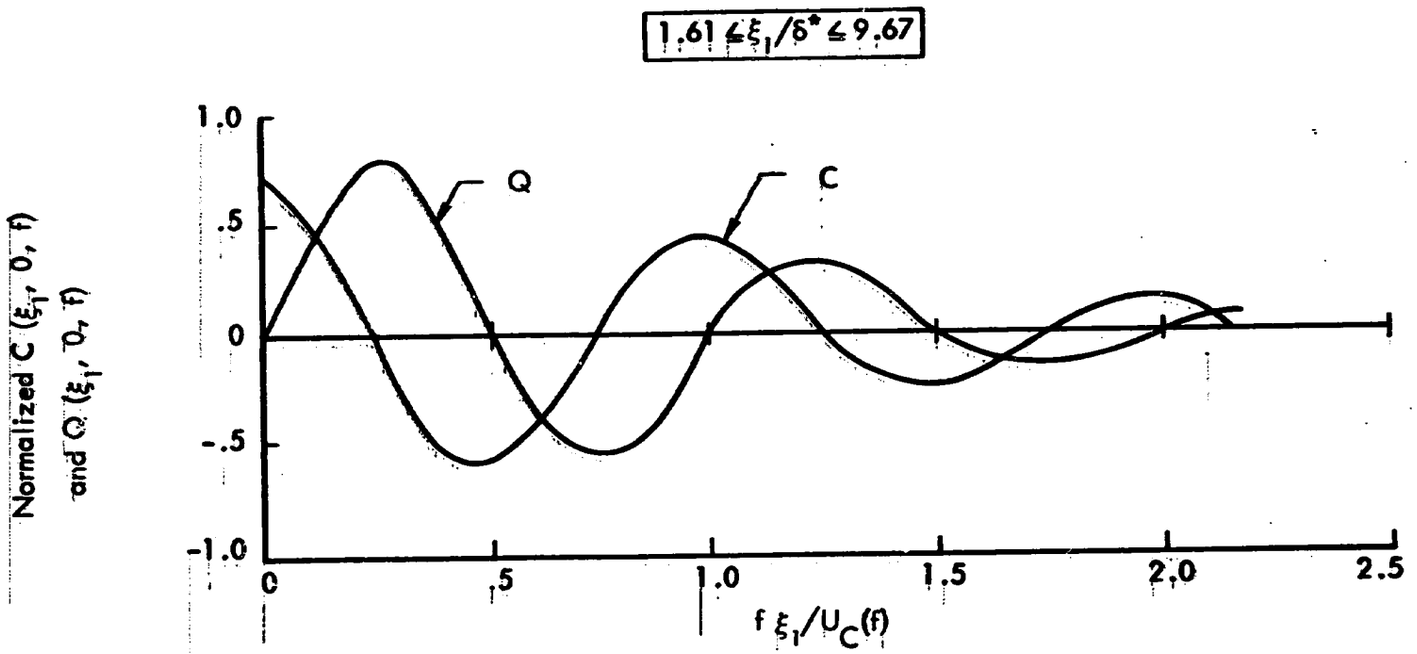

Figure 10. Typical Longitudinal Cross-Spectra of Pressure Fluctuations for Separated Flow (Ref. 14)

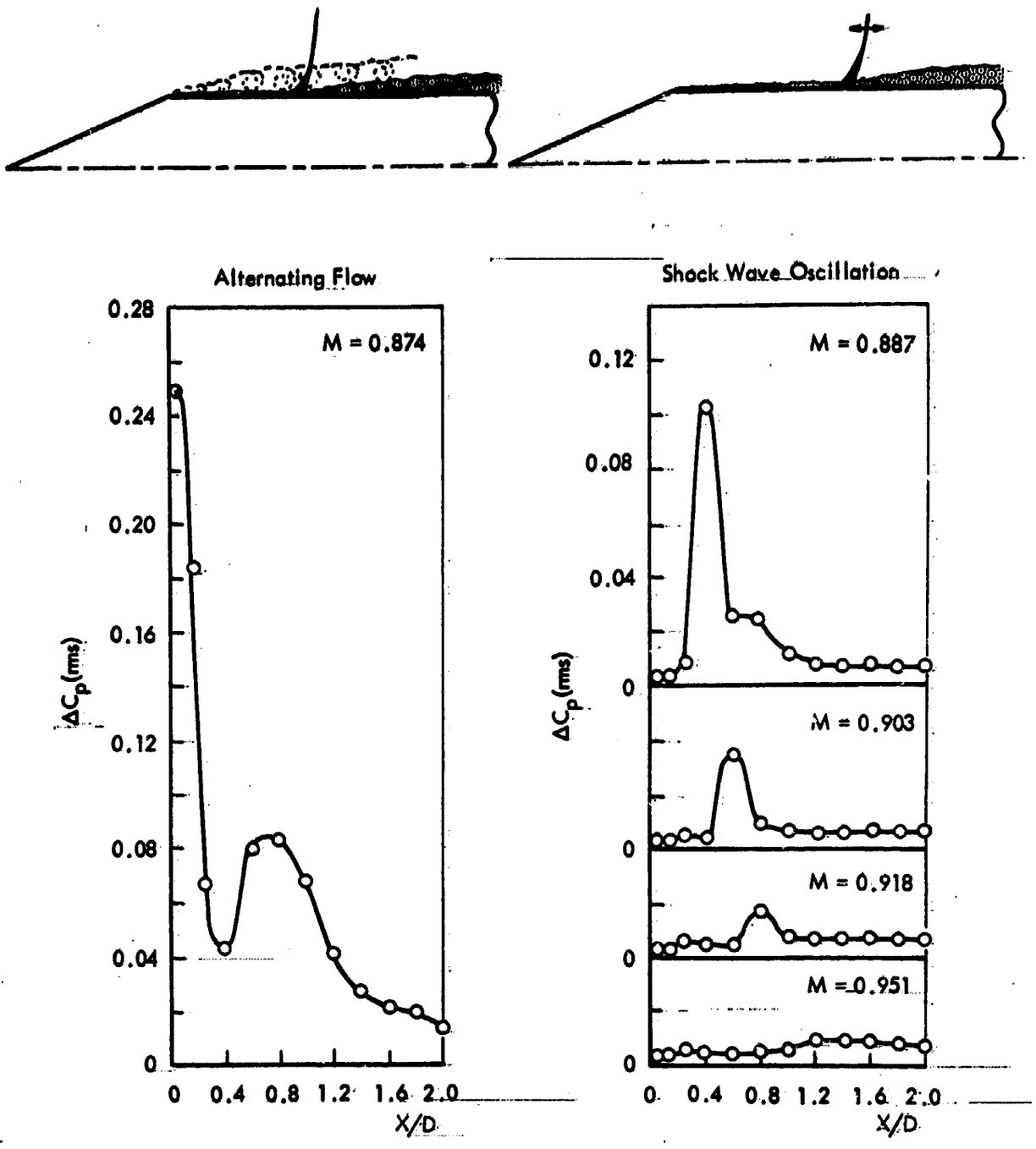

Figure 11. Axial Distribution of Fluctuating Pressures for Cone-Cylinder Body

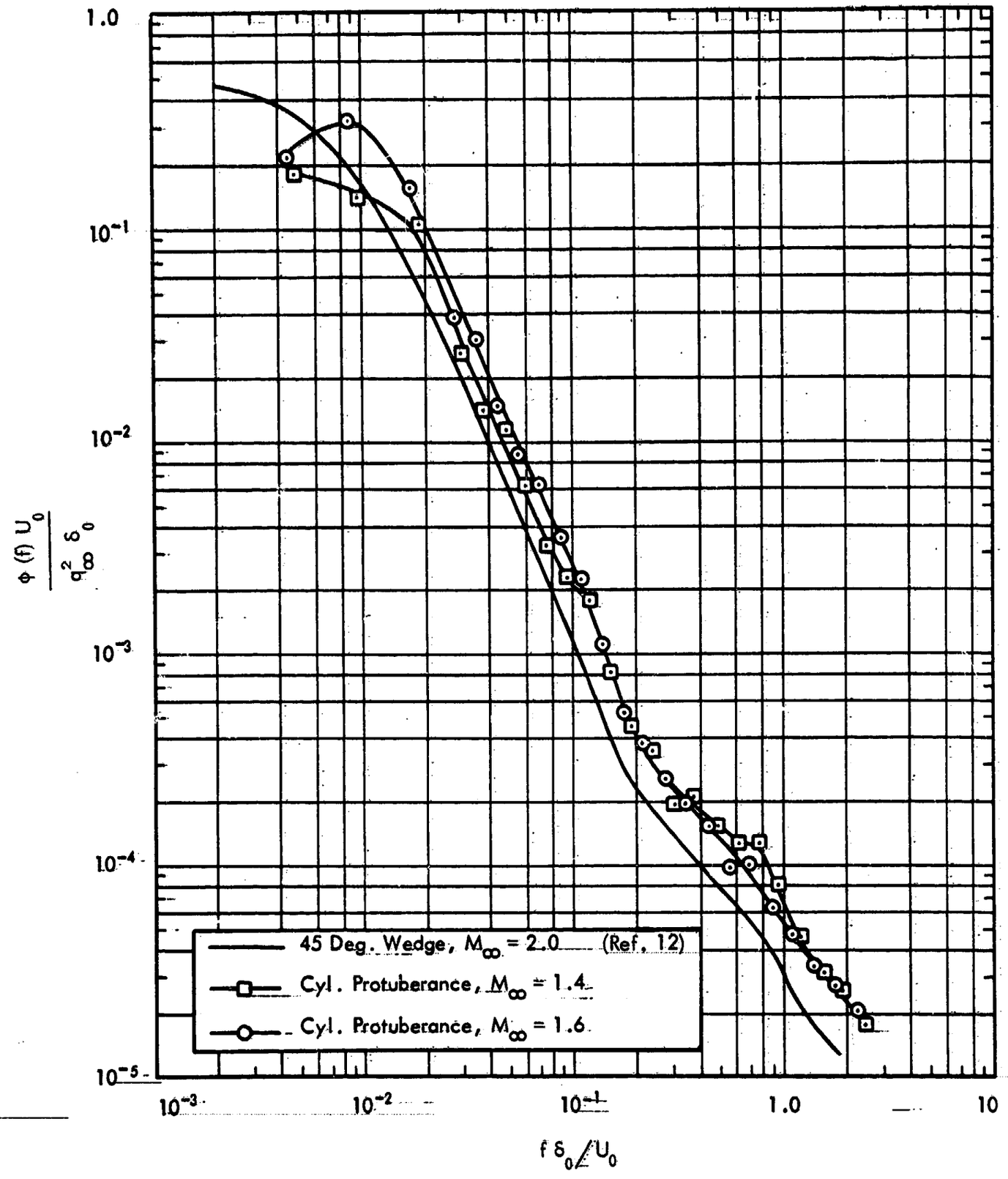

Figure 12. Comparison of Power Spectra for Shock-Wave Oscillation Induced by Two- and Three-Dimensional Protuberances

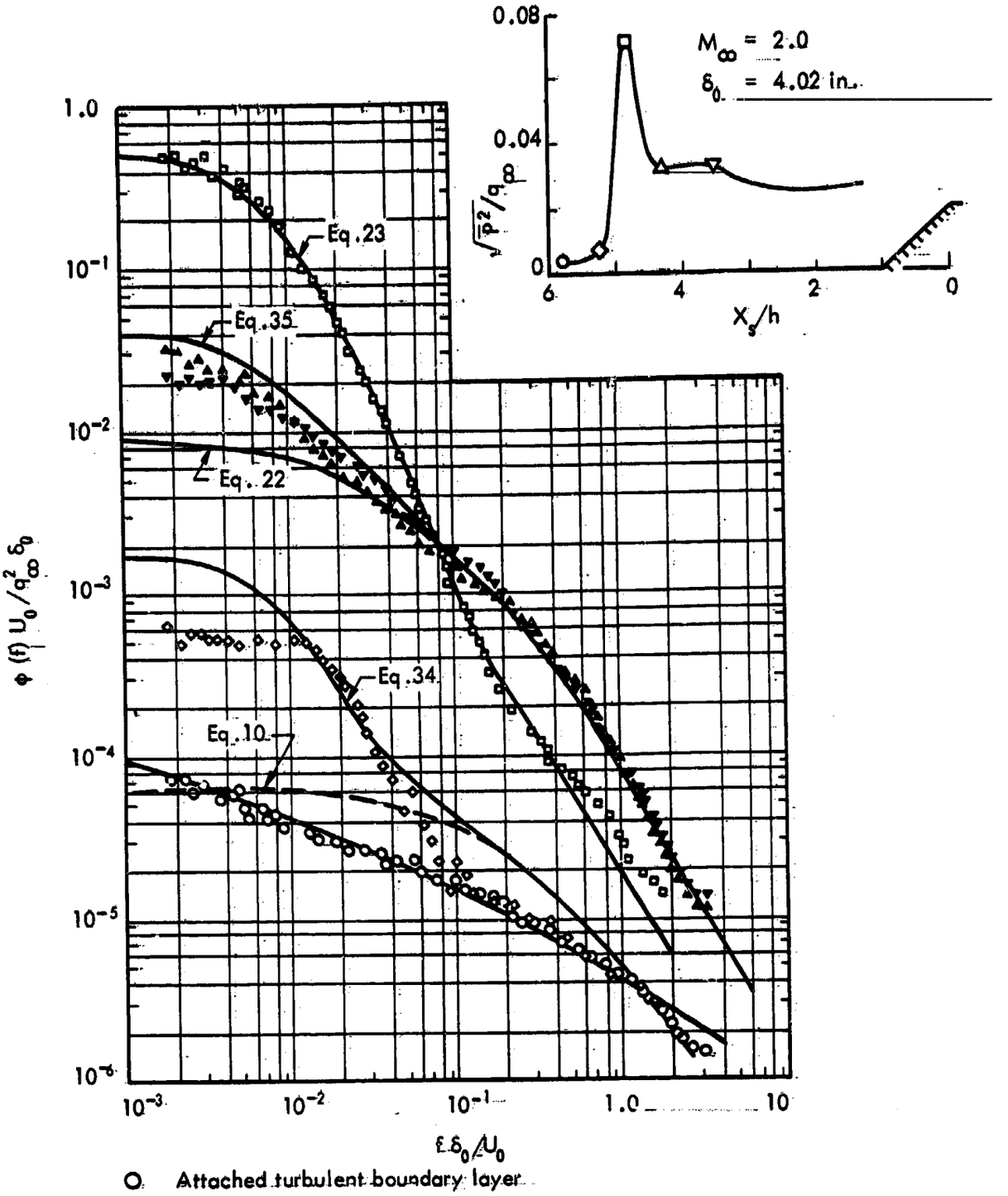

Figure 13. Longitudinal Distribution of Pressure Fluctuations and Typical Power Spectra in Vicinity of Supersonic Flow Separation Ahead of a 45° Wedge

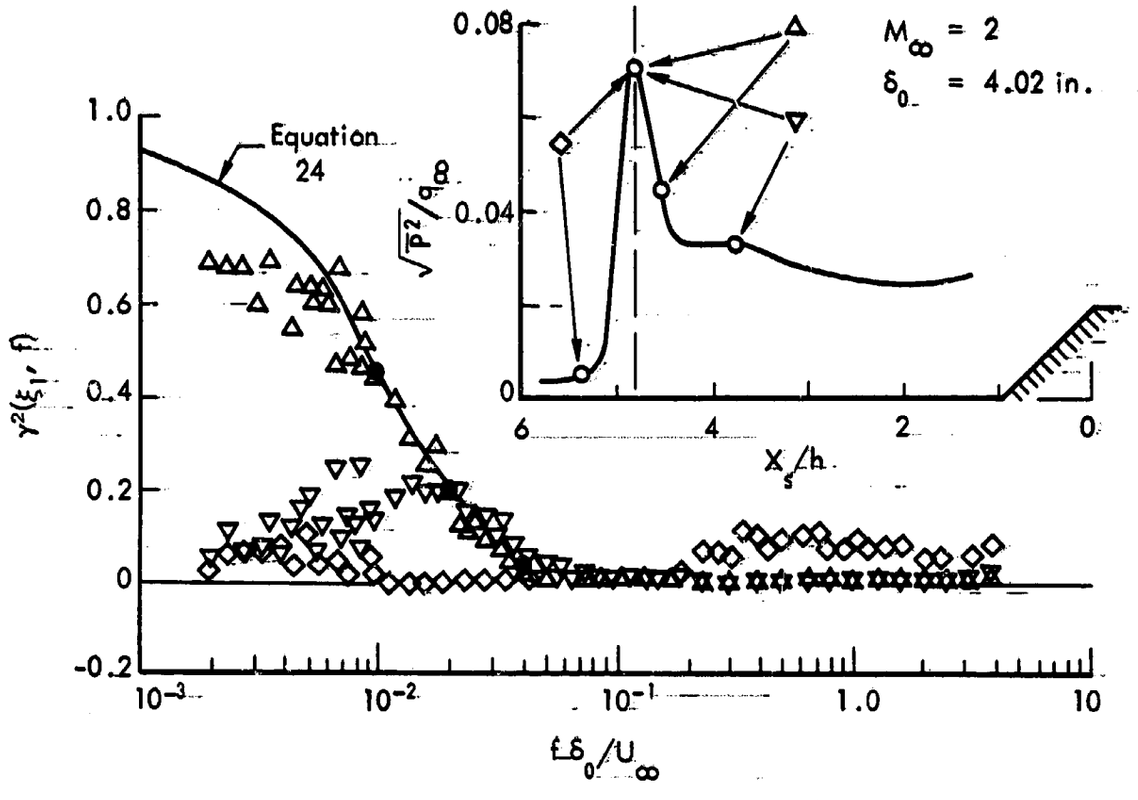

Figure 14. Correlation of Pressure Fluctuations Between Shock Wave and Adjacent Attached and Separated Flows (Reference 20)

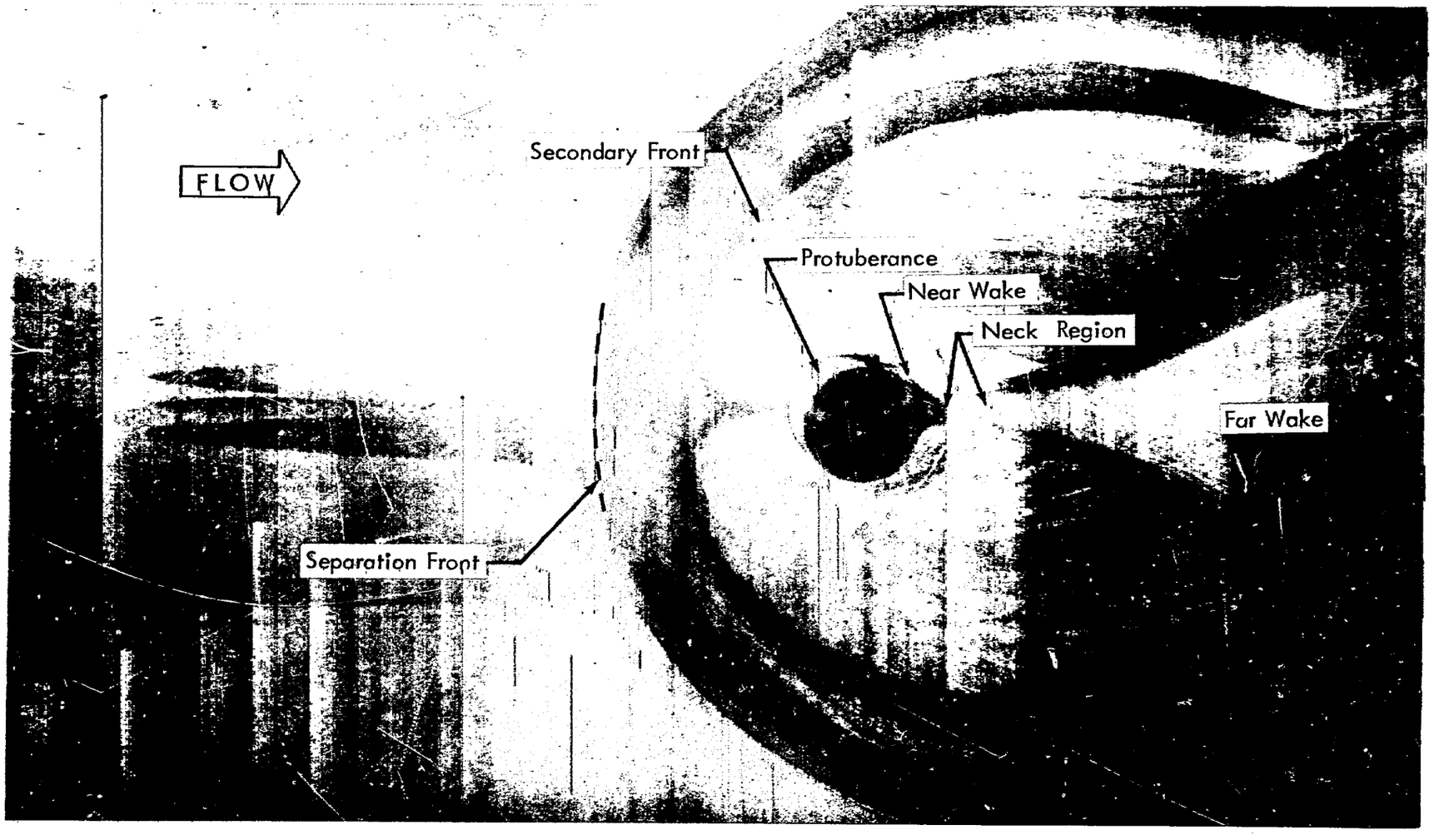

Figure 15. Typical Oil Flow Pattern of the Protuberance Flow Field

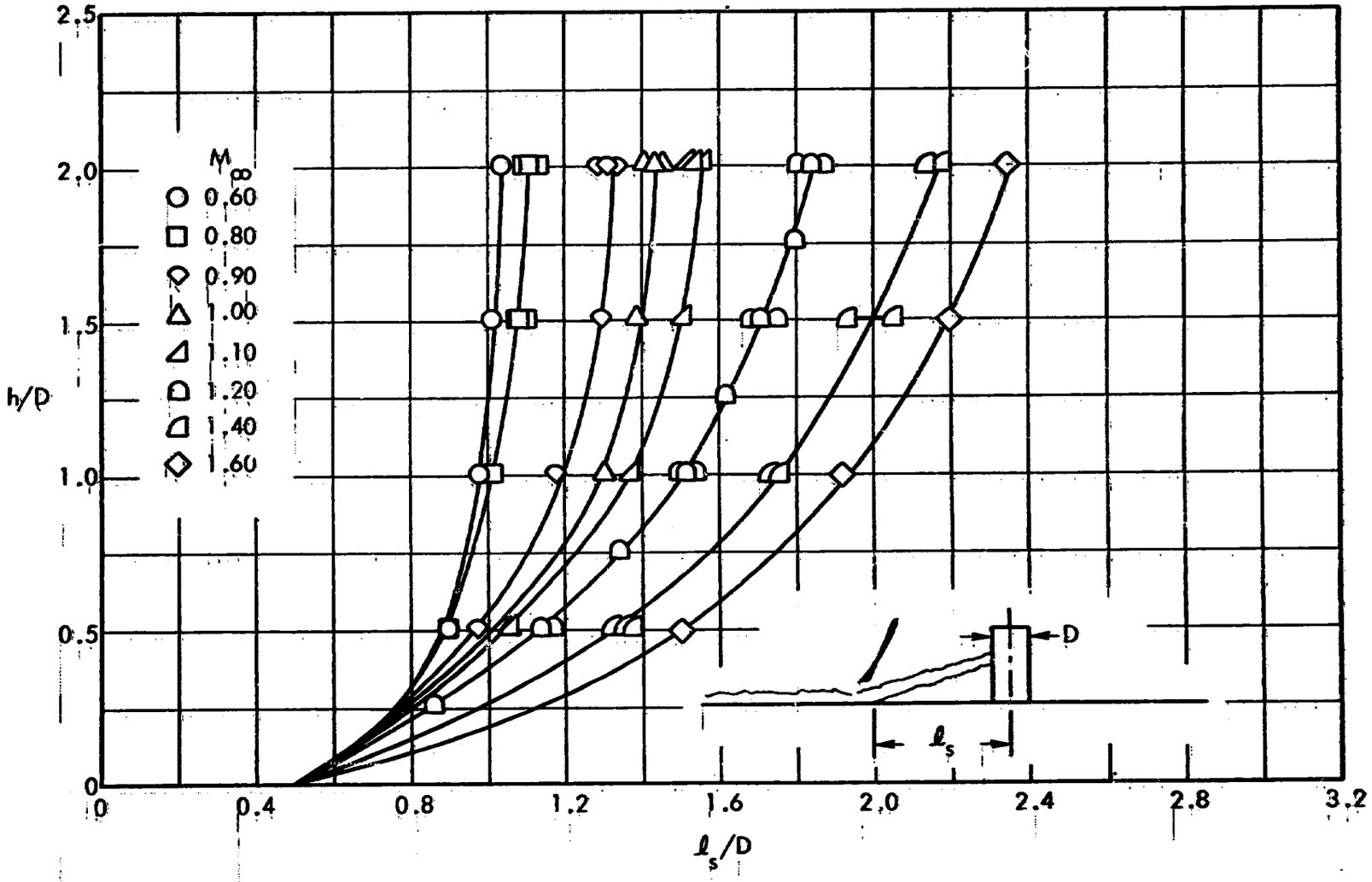

Figure 16. Variation of Separation Length with Protuberance Height

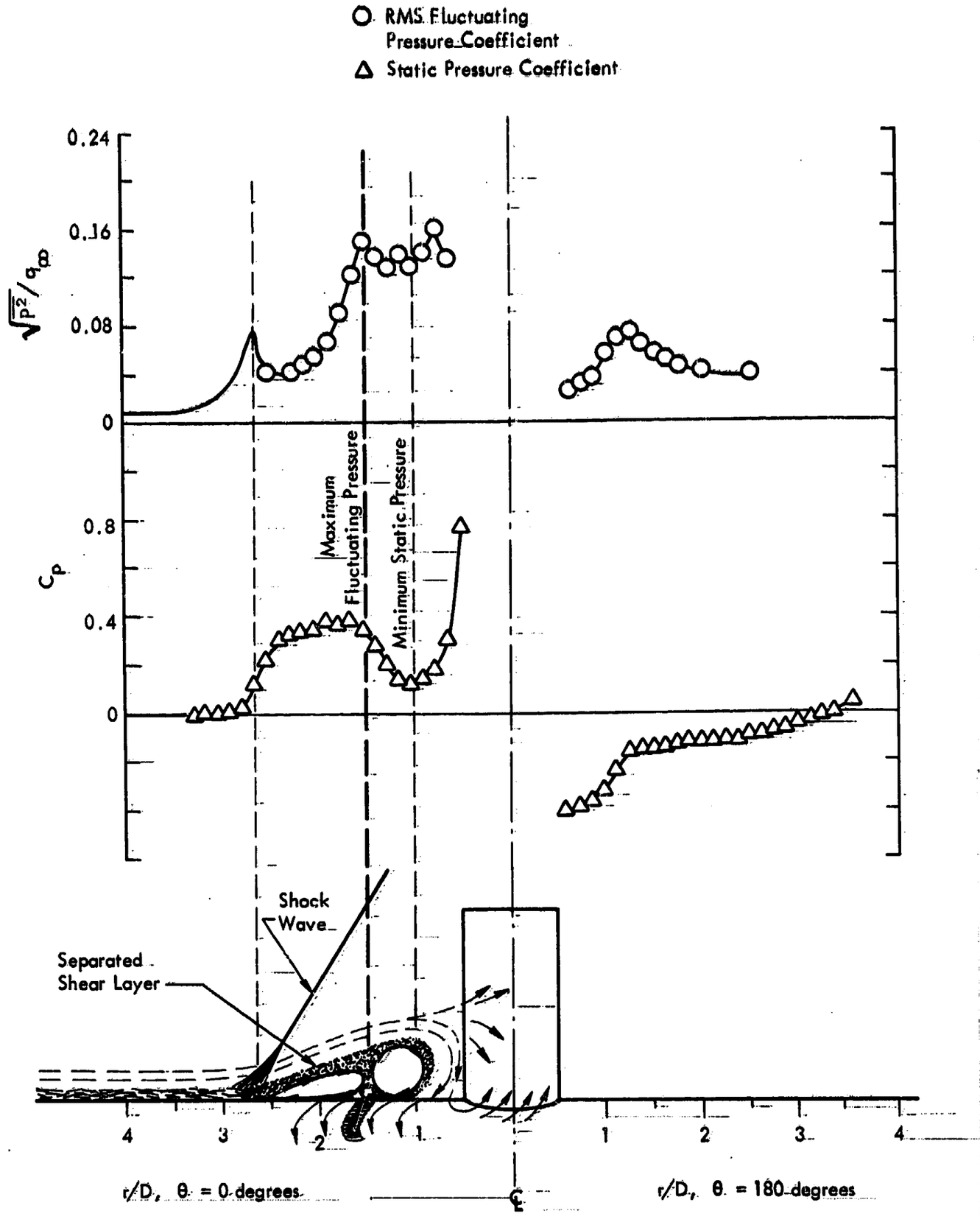

Figure 17.—Composite Schematic of Protuberance Flow Field Characteristics, $M_\infty = 1.60$, $h/D = 2.0$

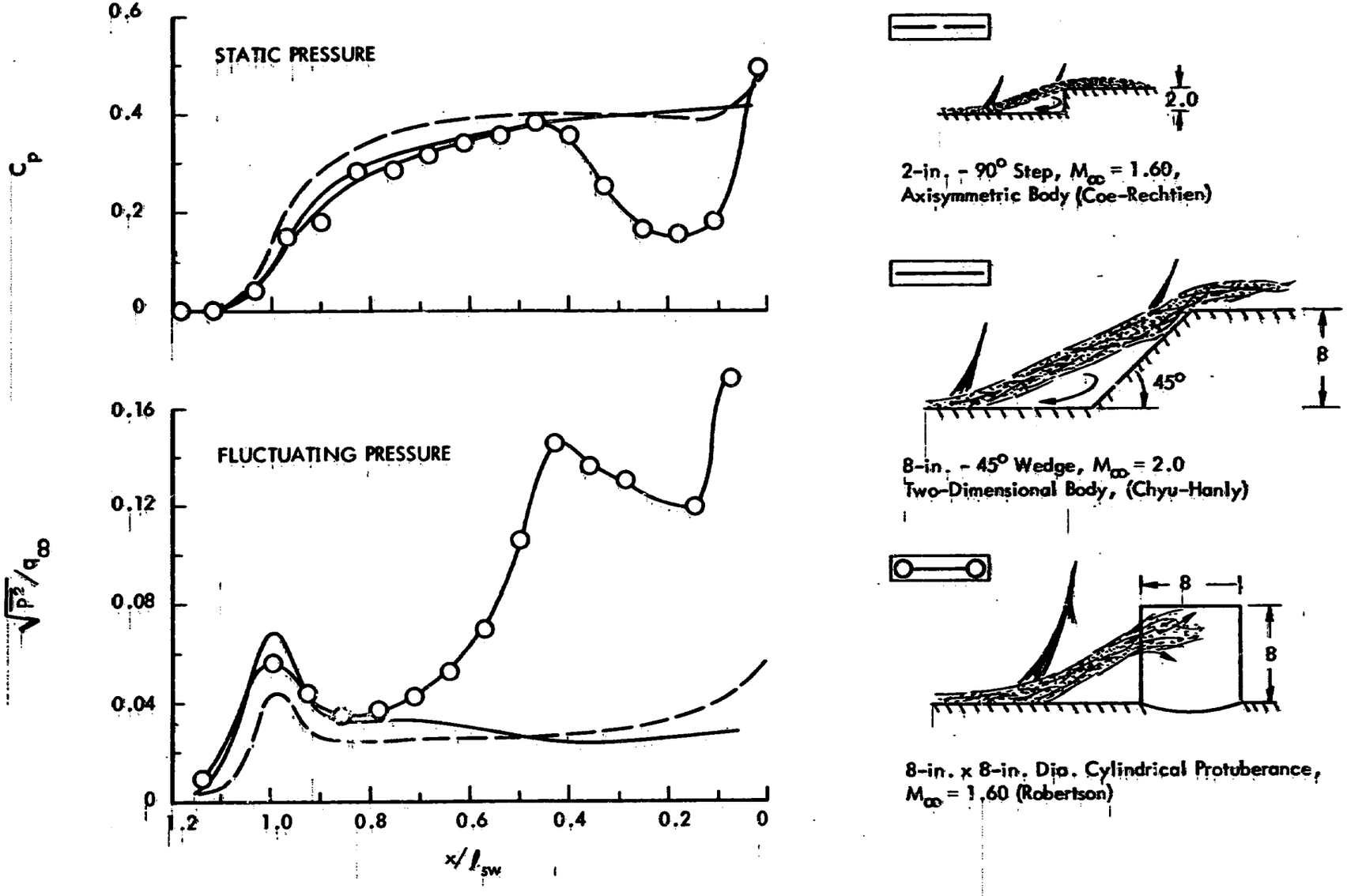

Figure 18. Comparisor of Two- and Three-Dimensional Separated Flows

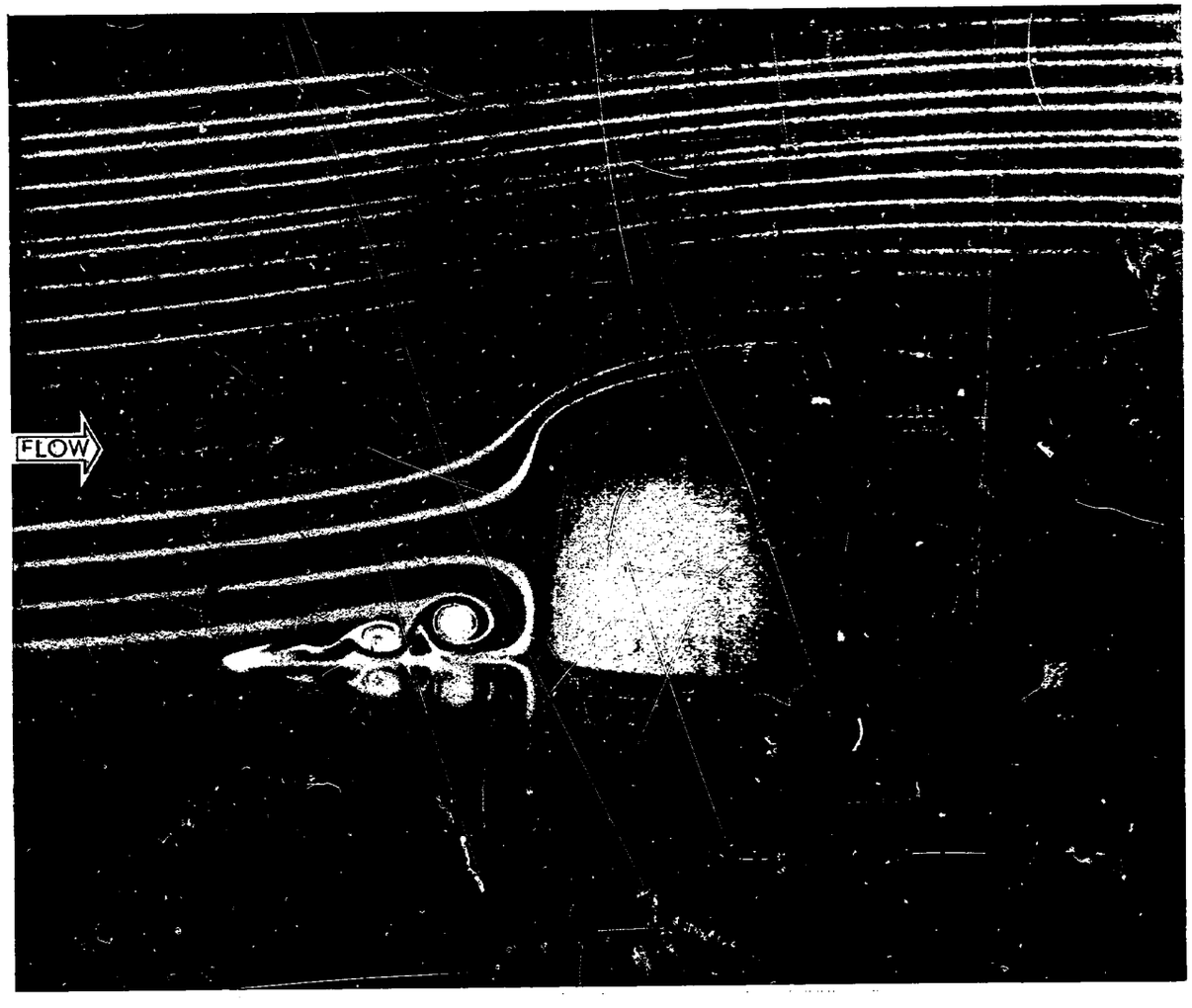

Figure 19. Smoke Filament Flow Pattern Upstream of a Cylindrical Protuberance at Low Speed

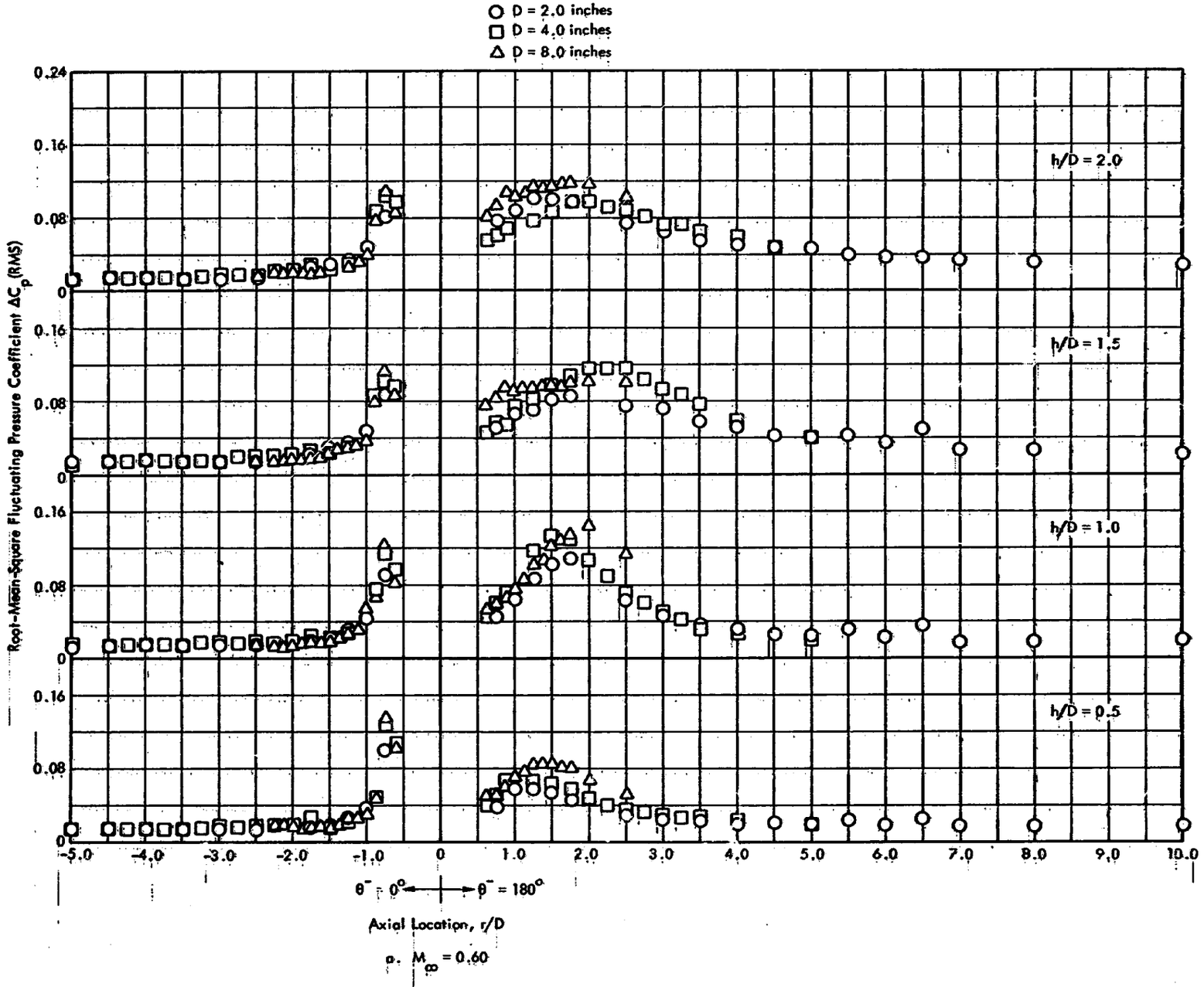

Figure 20. Comparison of the Axial Distributions of RMS Fluctuating Pressure Coefficient For the Various Cylindrical Protuberances

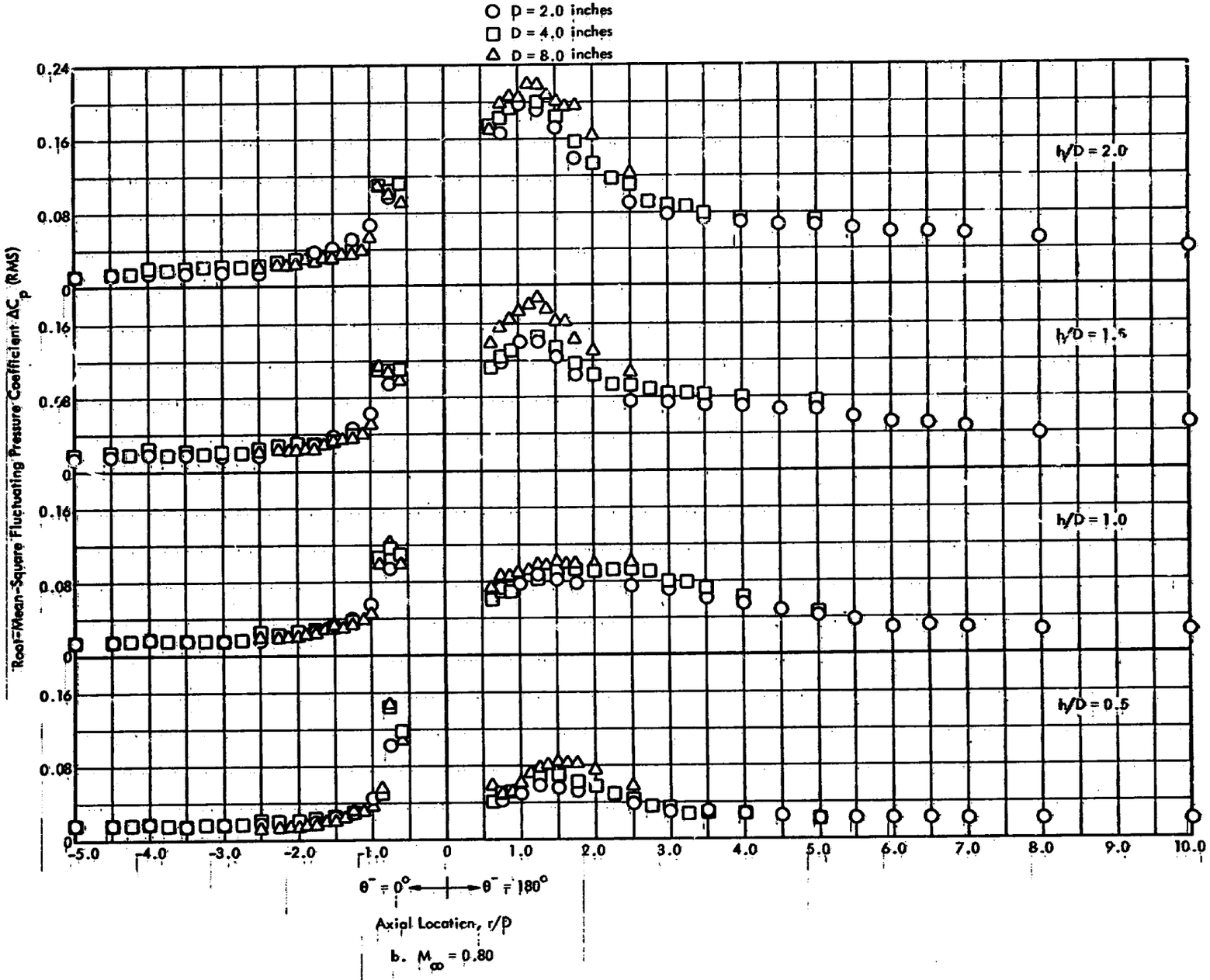

b. $M_\infty = 0.80$

Figure 20. Continued

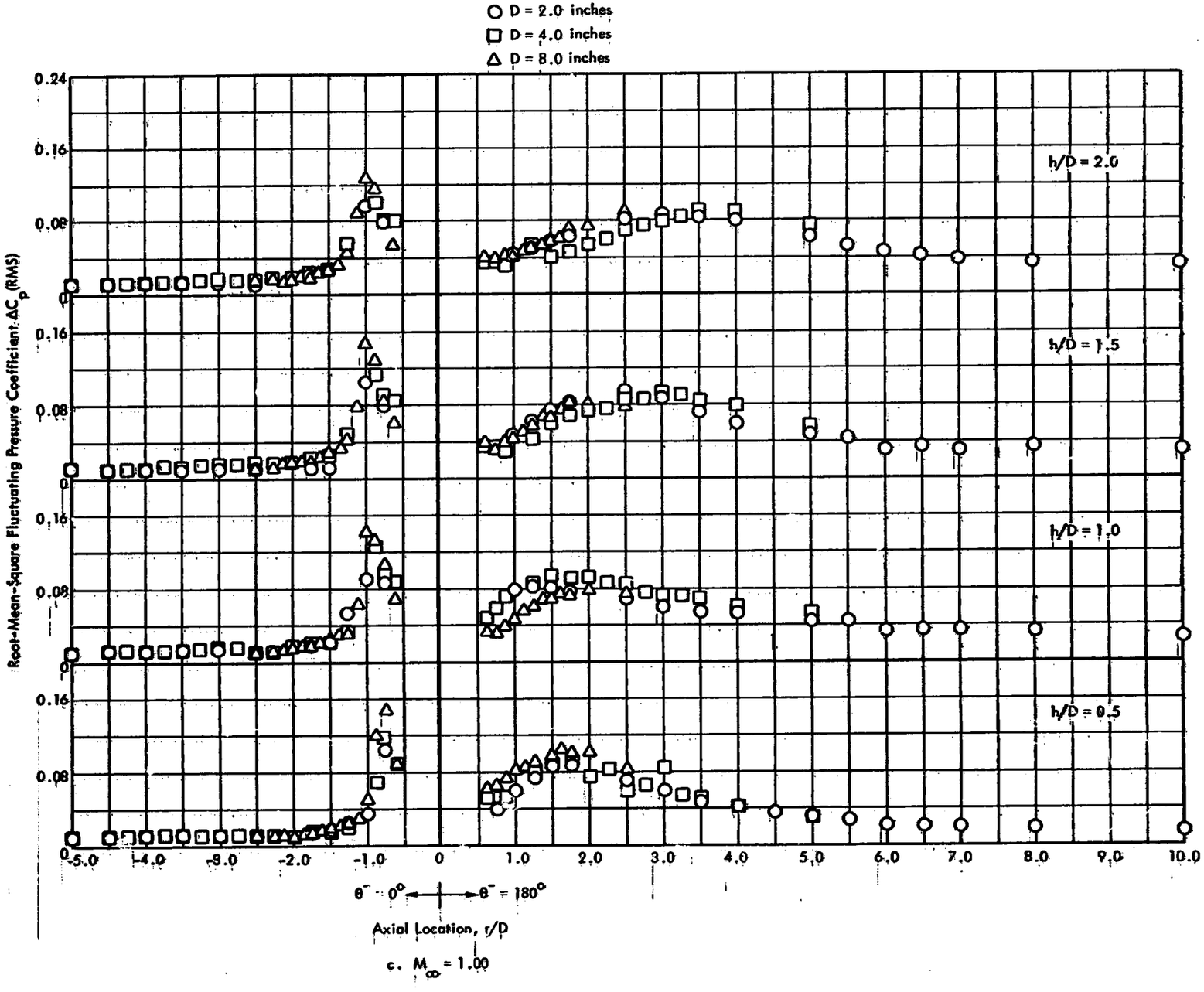

c. $M_\infty = 1.00$

Figure 20. Continued

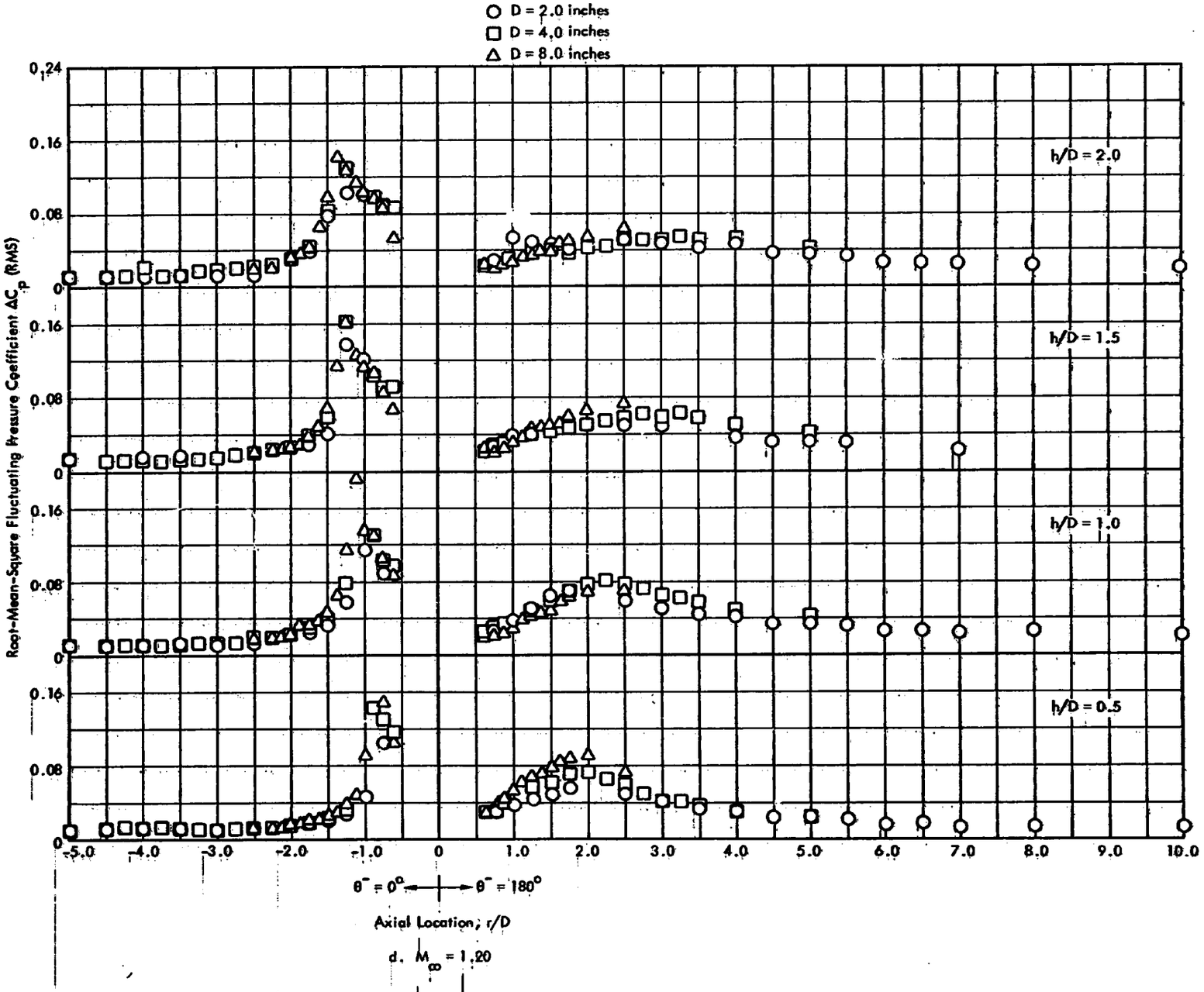

d. $M_\infty = 1.20$

Figure 20. Continued

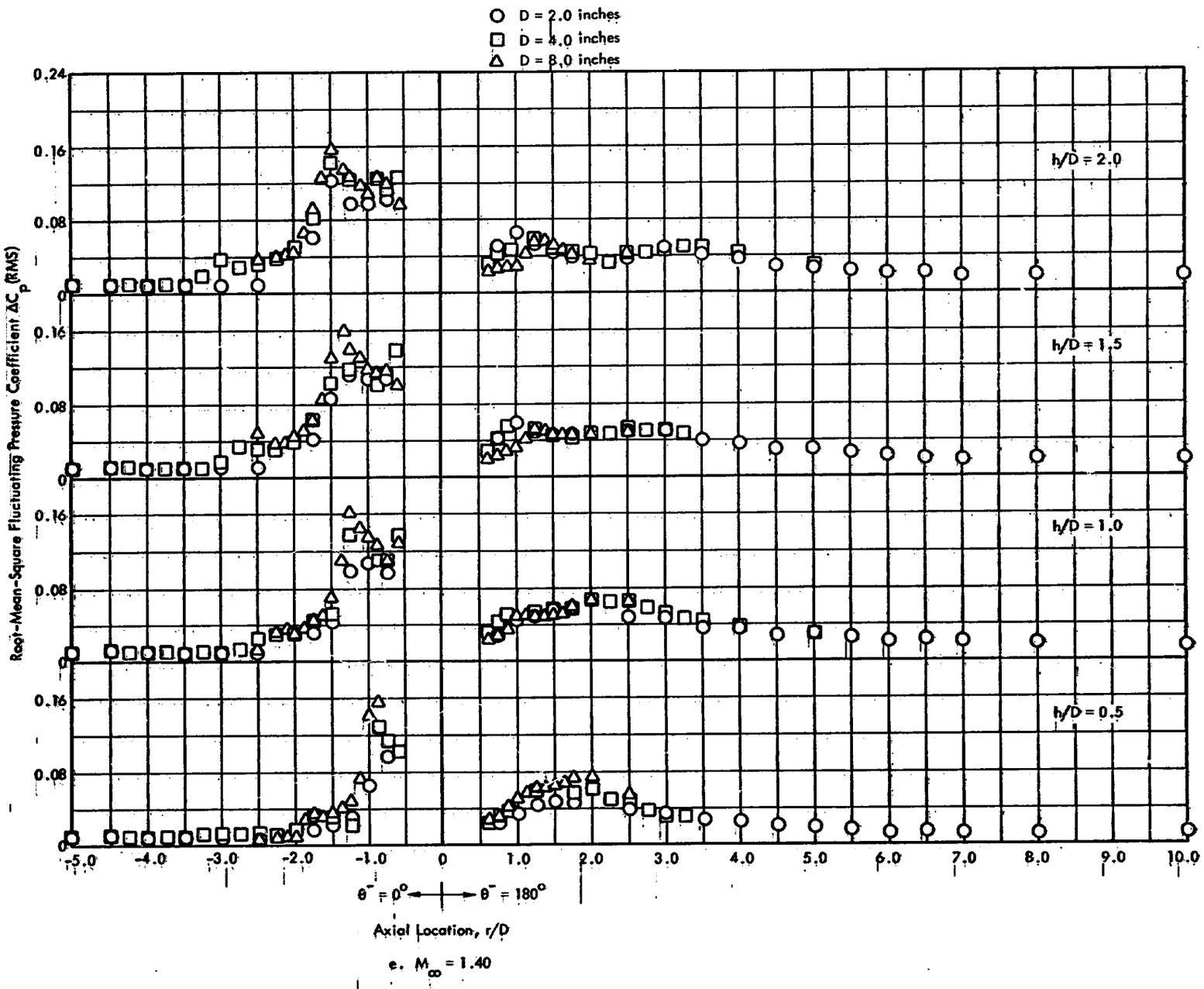

e. $M_\infty = 1.40$

Figure 20. Continued

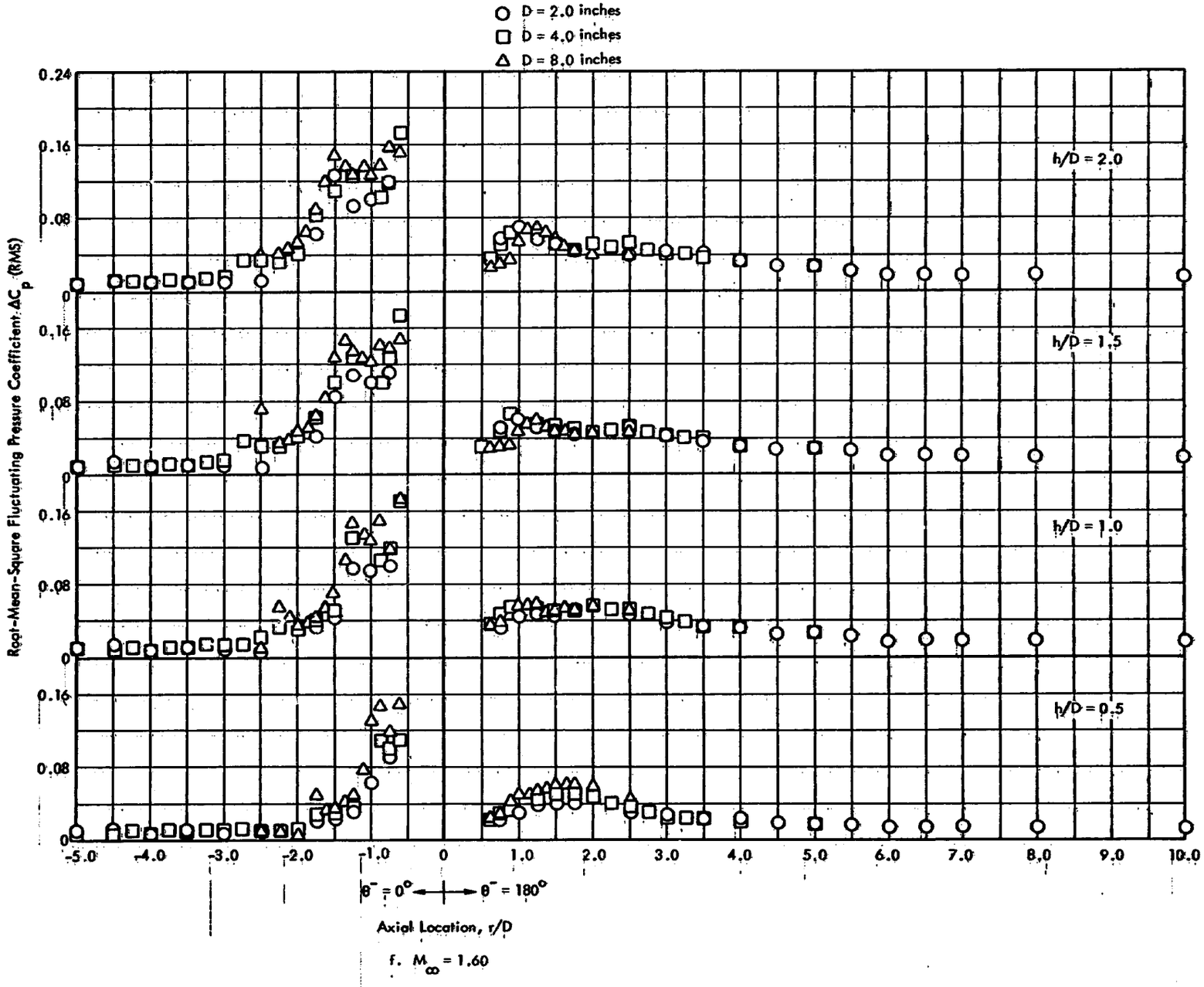

f. $M_\infty = 1.60$

Figure 20. Concluded

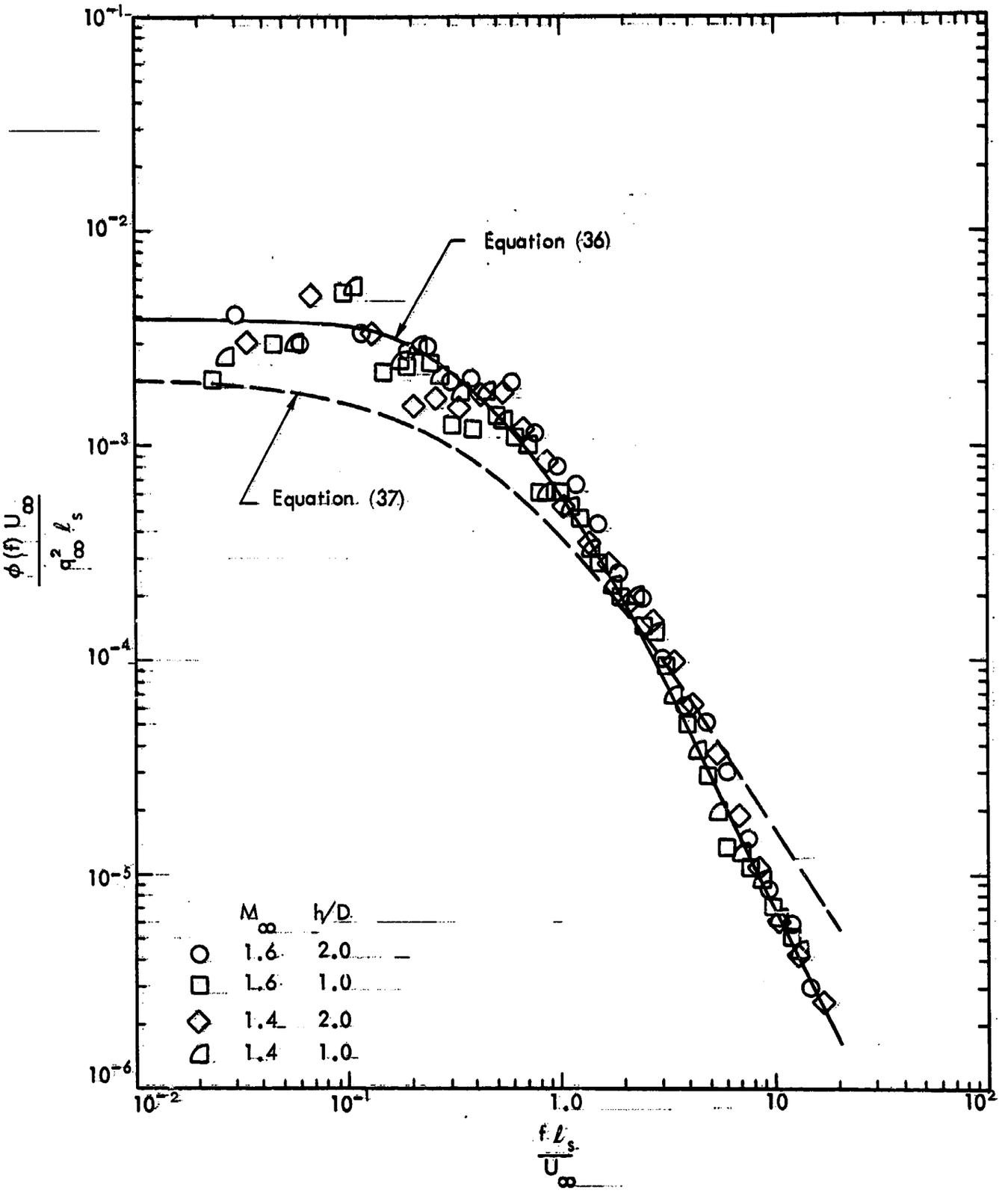

Figure 21. Power Spectra for the Outer Region of Separated Flow Induced by Cylindrical Protuberances Showing the Data Collapse Using ℓ_s and U_∞ as Normalizing Parameters.

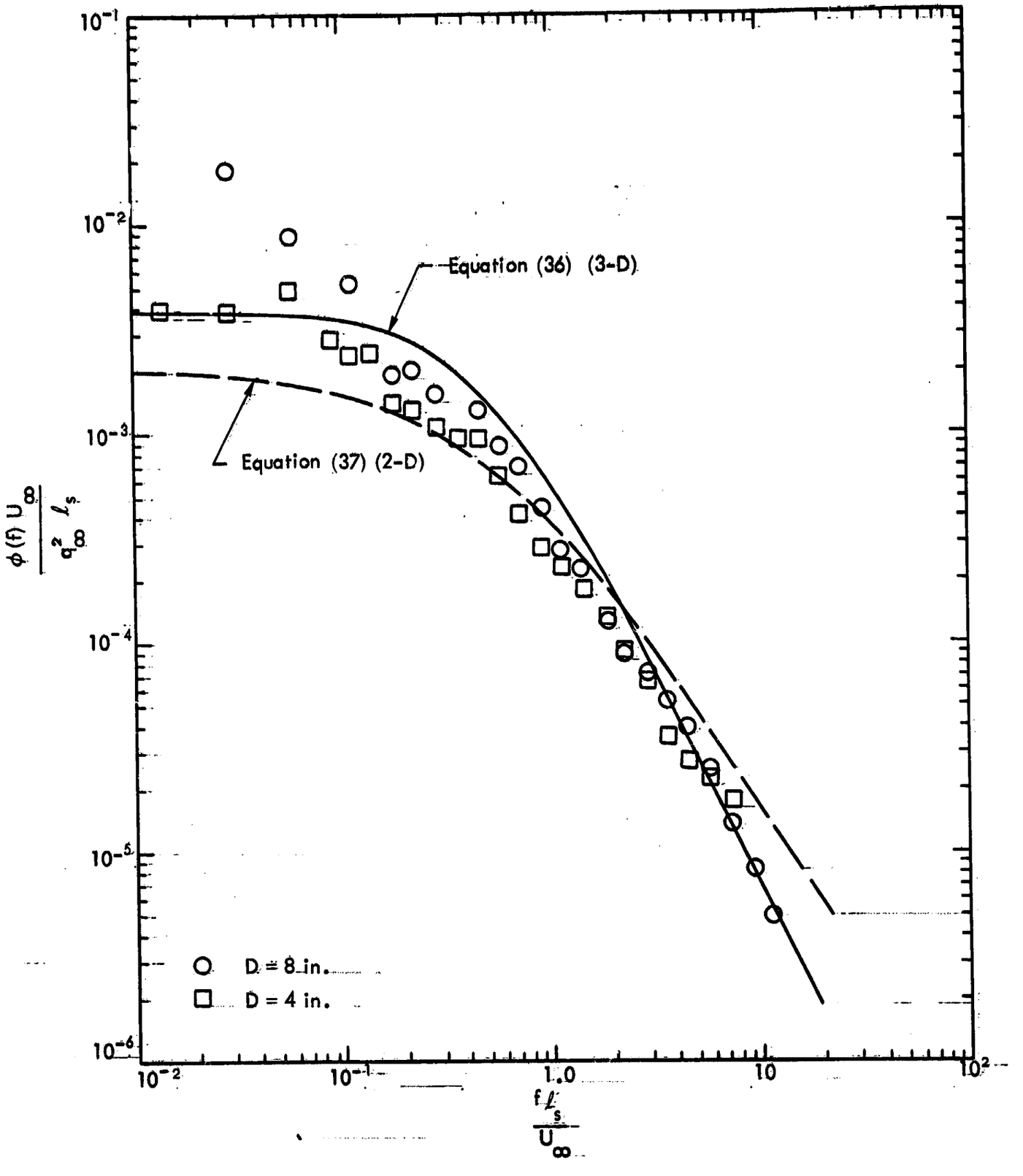

a. r/D = - 2.50

Figure 22. Comparison of Empirical Predictions with Experimentally Measured Power Spectra for the Outer Region of Separated Flow, M_∞ = 1.60, h/D = 2.0

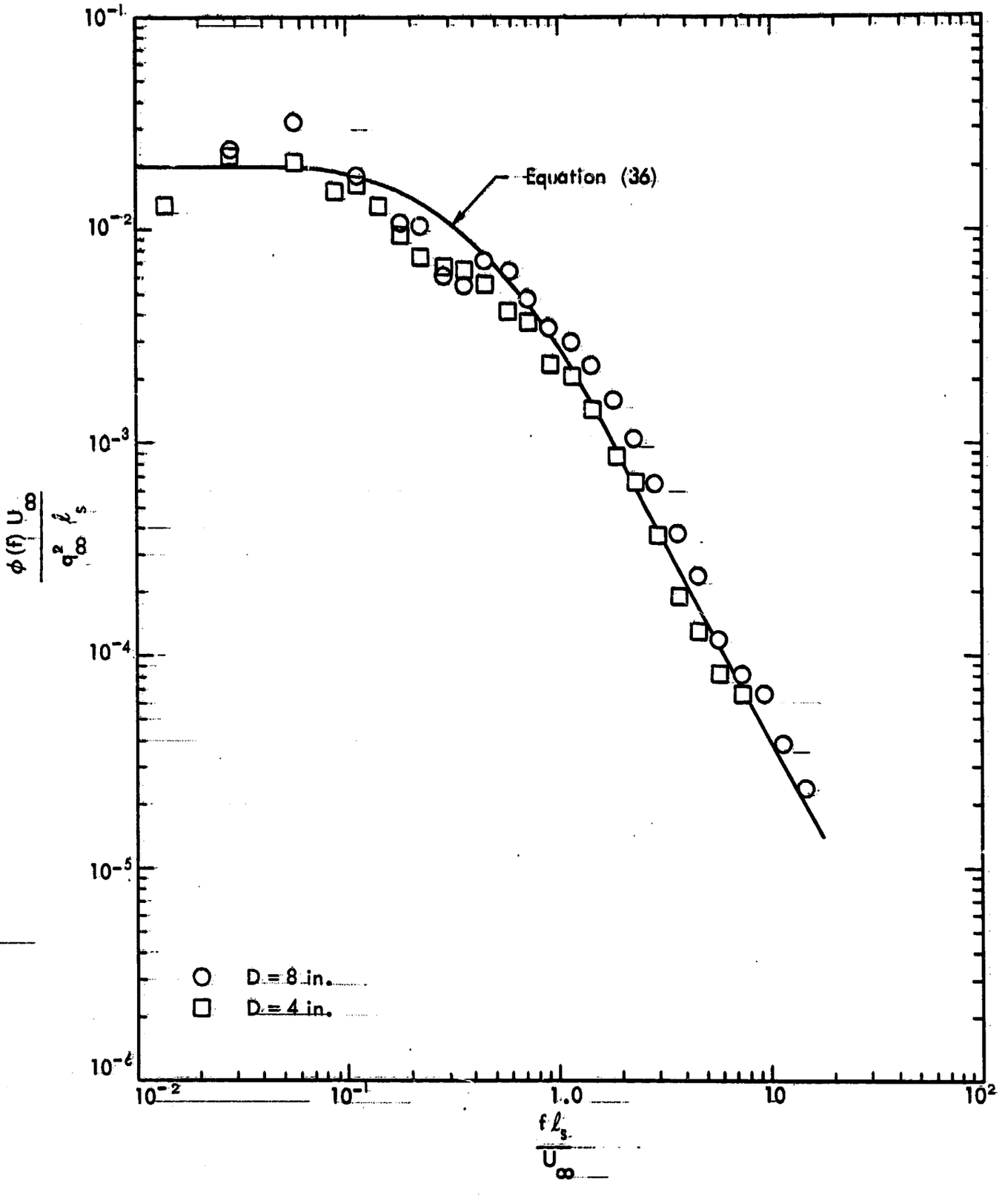

b. r/D = 1.75

Figure 22. Continued

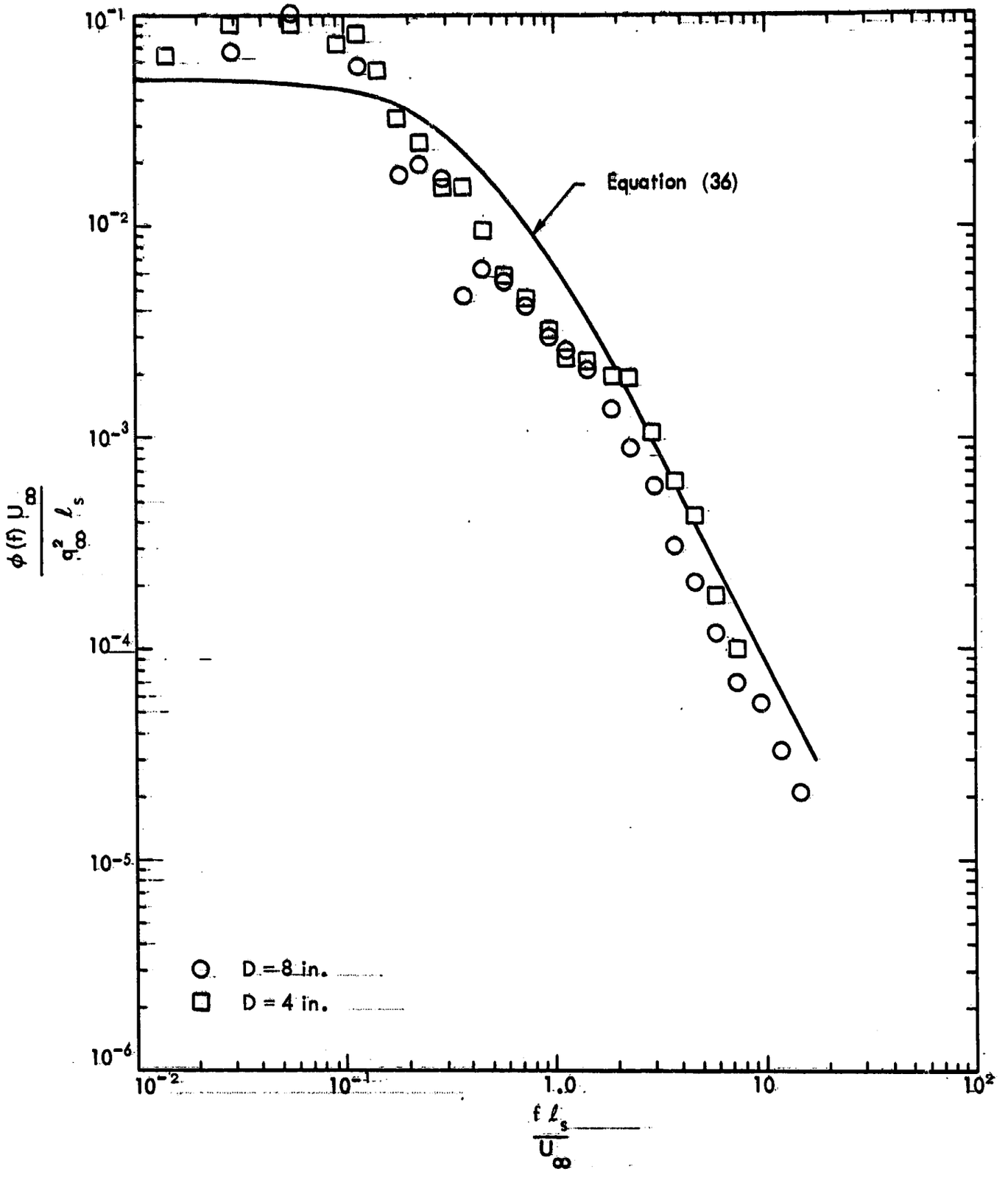

c. $r/D = 1.50$

Figure 22. Concluded

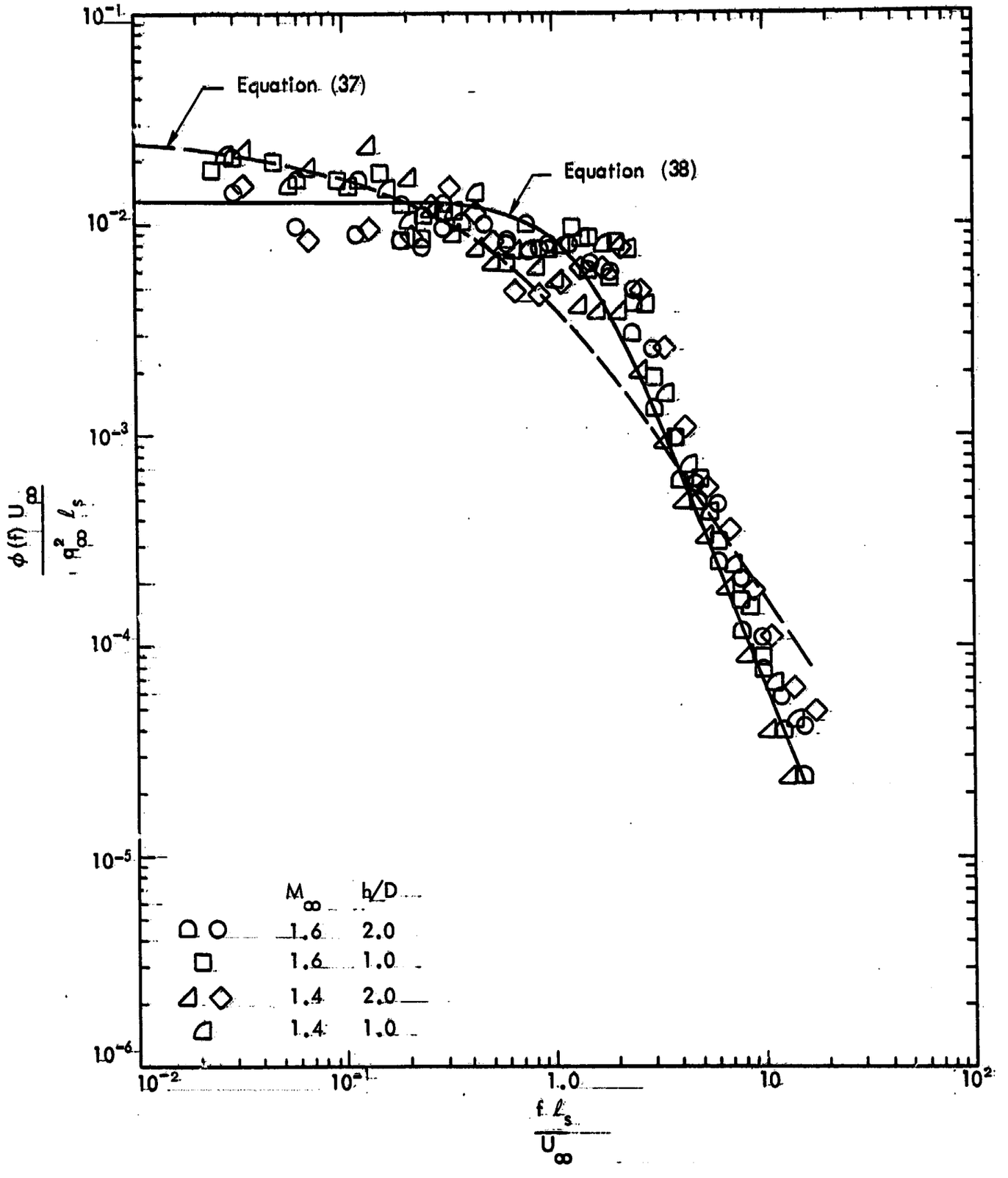

Figure 23. Power Spectra for the Inner Region of Separated Flow Induced by Cylindrical Protuberances Showing the Data Collapse Using ℓ_s and U_∞ as Normalizing Parameters.

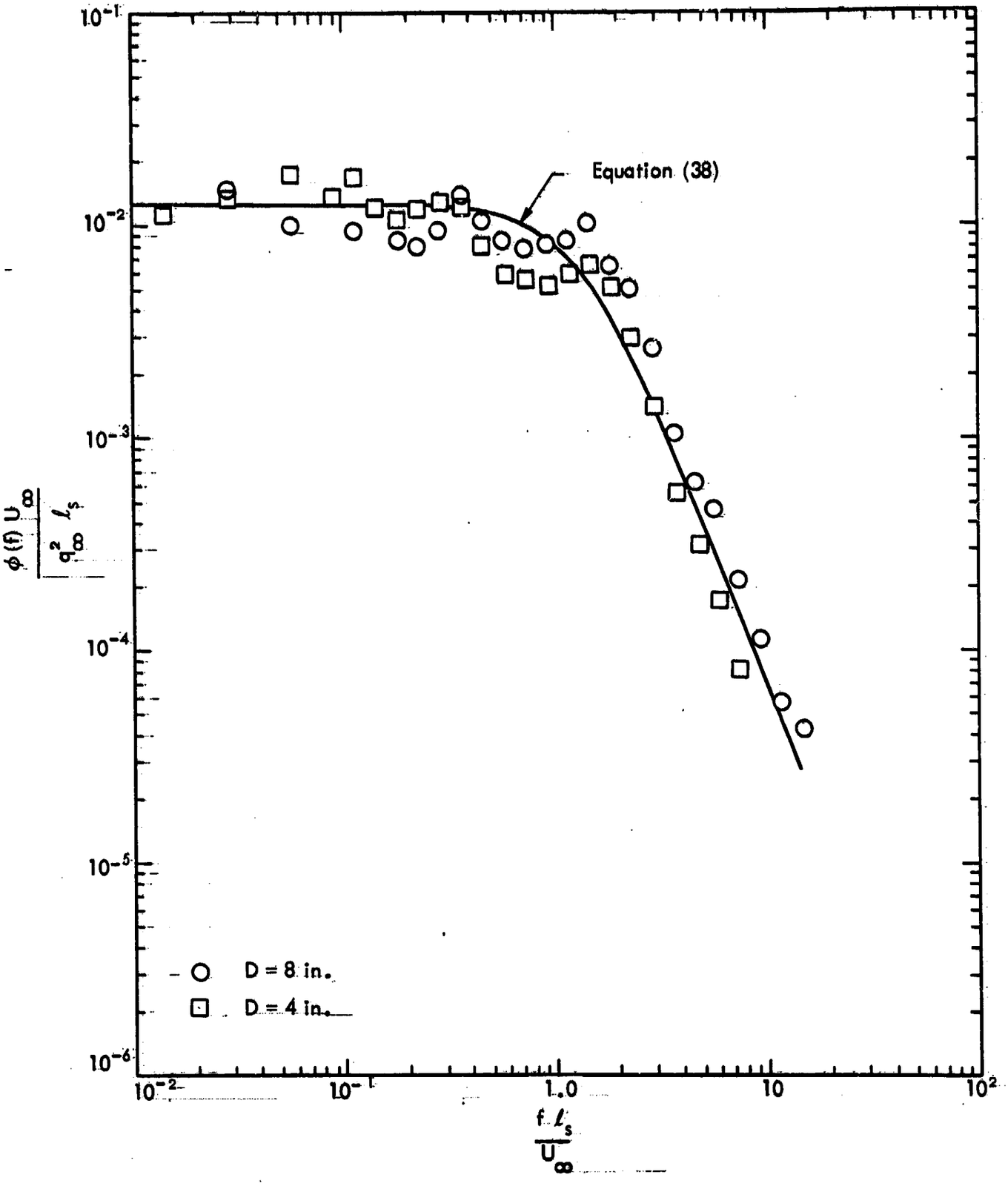

Figure 24. Comparison of Empirical Prediction with Experimentally Measured Power Spectra for the Inner Region of Separated Flow, $M_\infty = 1.60$, $h/D = 2.0$, $r/D = 1.25$

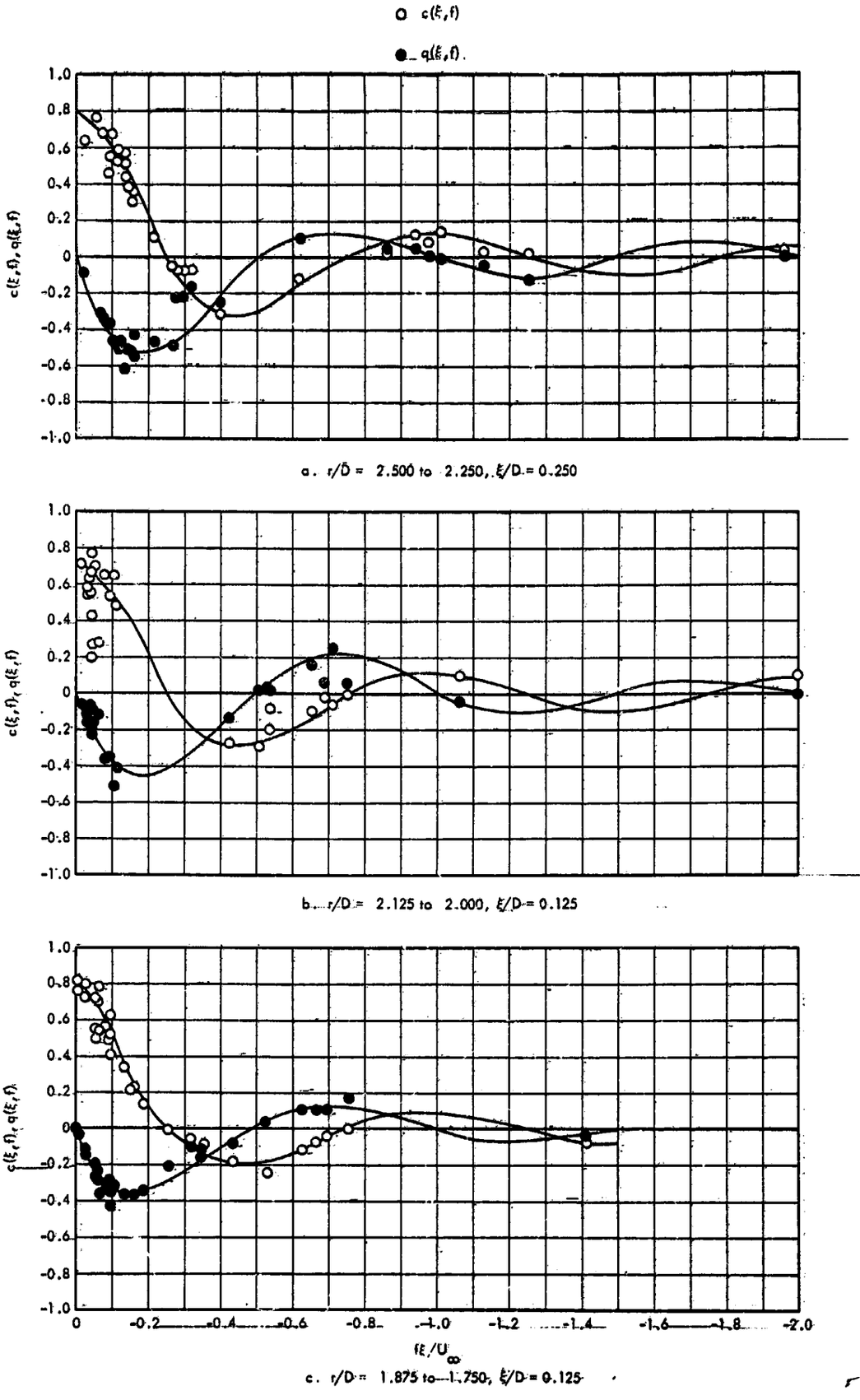

Figure 25. Variation of Longitudinal Cross-Spectra Within the Upstream Separated Flow Field, $M_\infty = 1.60$, $h/D = 2.0$

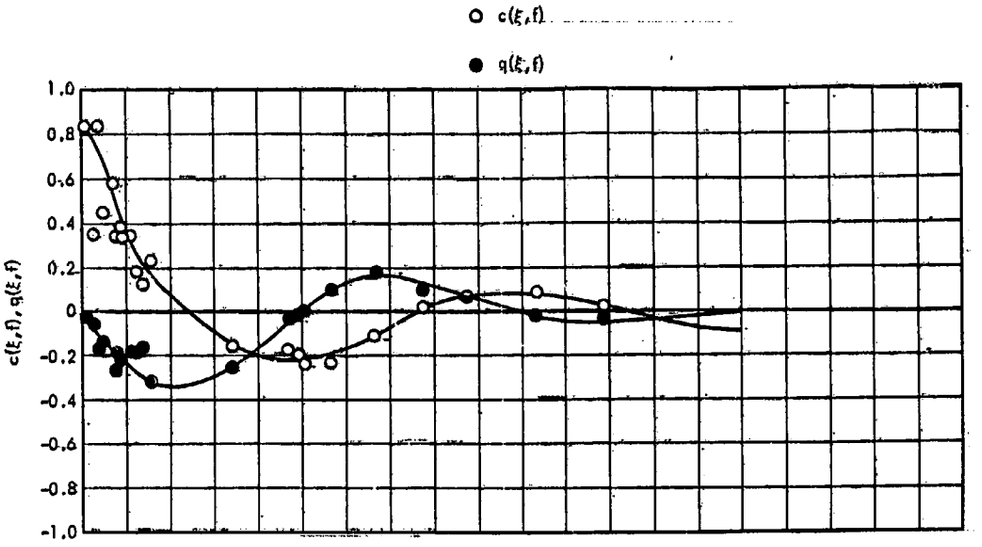

d. r/D = 1.625 to 1.500, ξ/D = 0.125

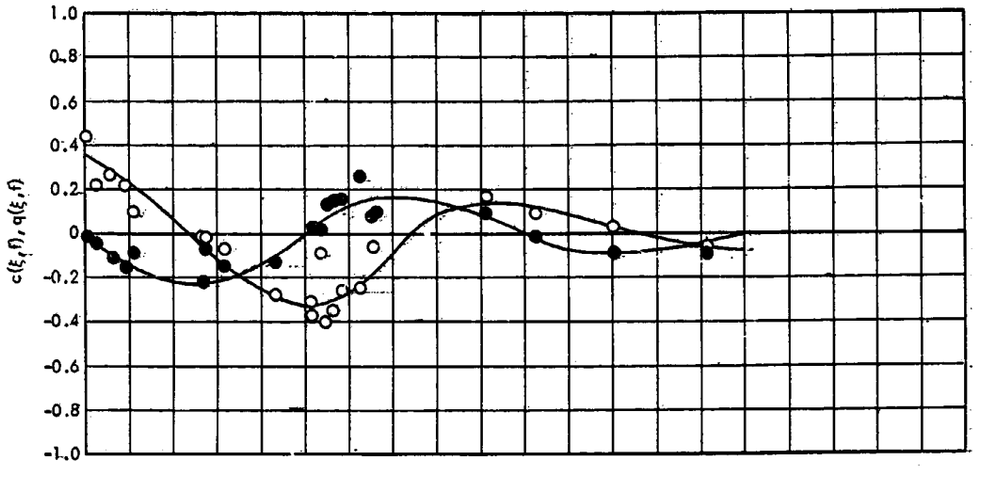

e. r/D = 1.375 to 1.500, ξ/D = 0.125

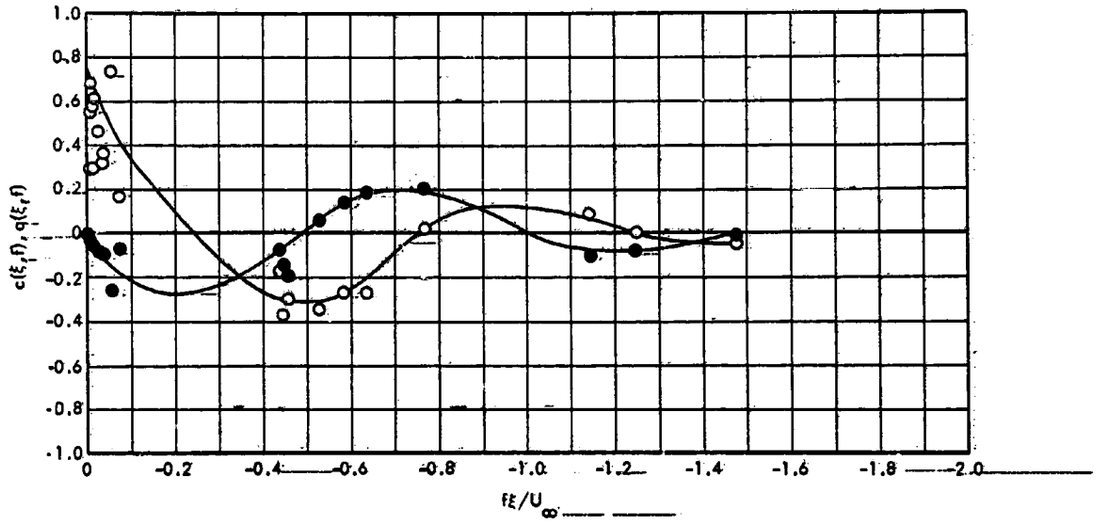

f. r/D = 1.125 to 1.000, ξ/D = 0.125

Figure 25. Concluded

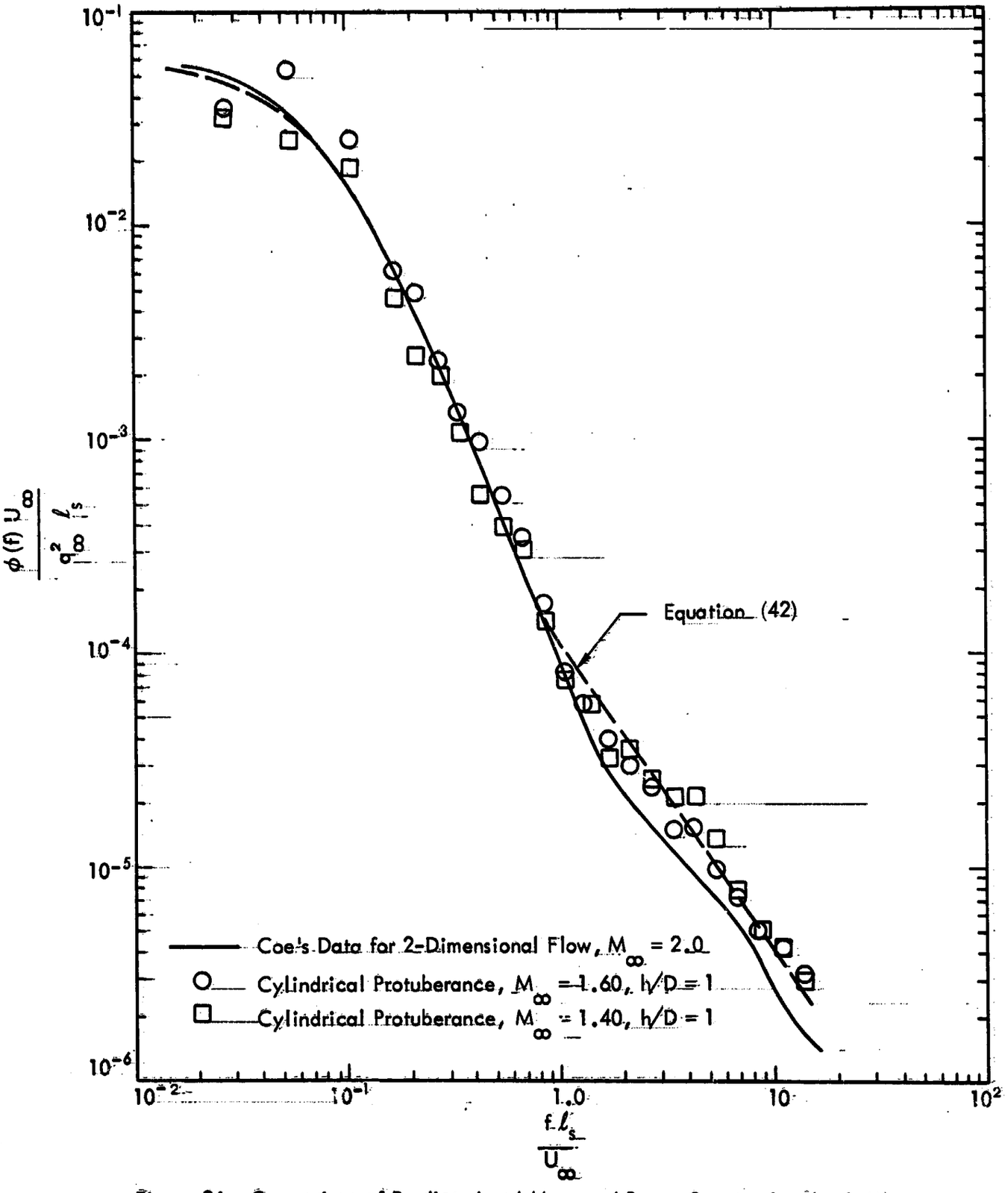

Figure 26. Comparison of Predicted and Measured Power Spectra for Shock-Wave Oscillation Upstream of Two- and Three-Dimensional Separated Flow Fields

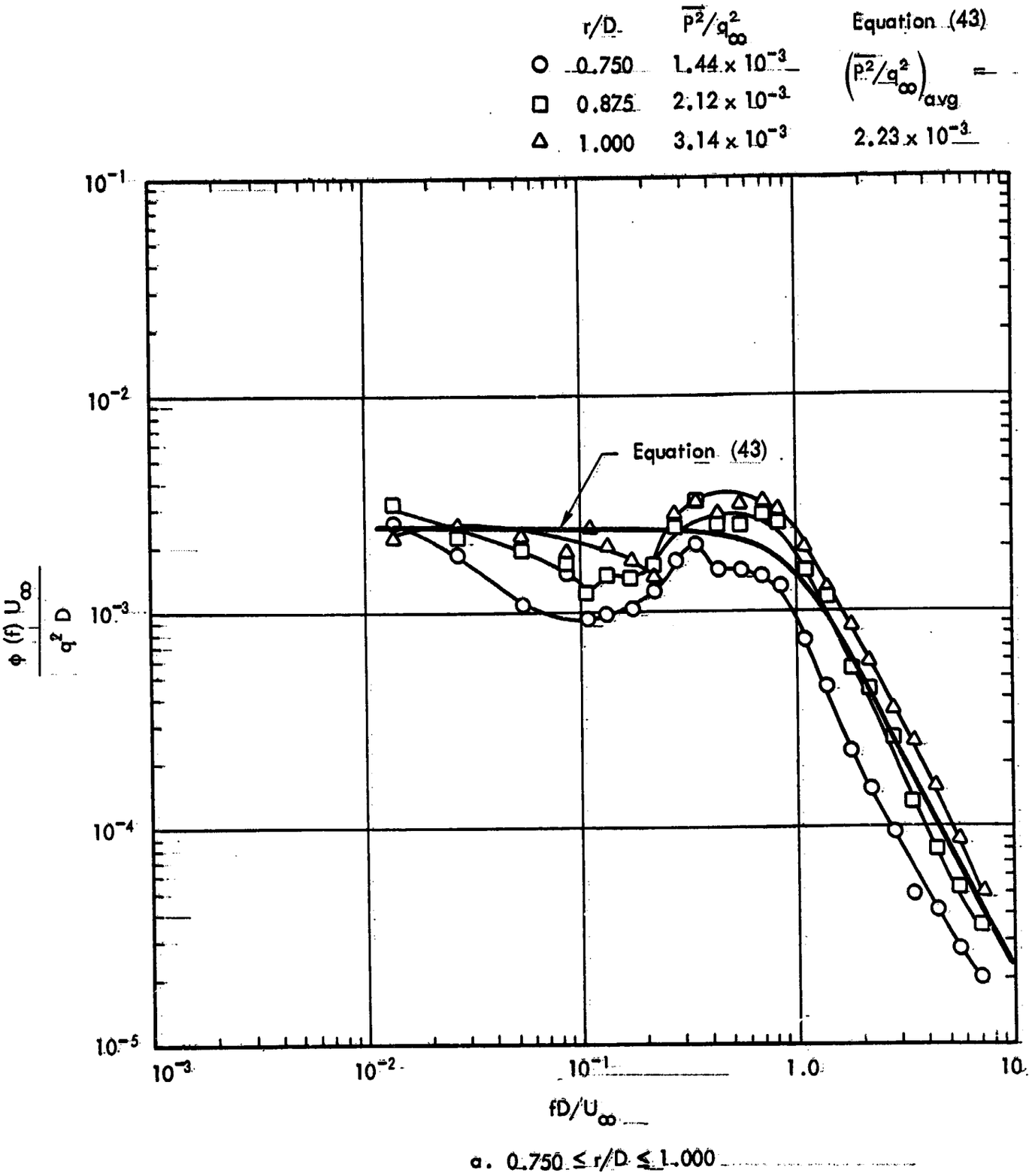

a. $0.750 \leq r/D \leq 1.000$

Figure 27. Comparison of Predicted and Measured Power Spectra for Various Regions of the Wake Downstream of a Cylindrical Protuberance ($M_\infty = 1.60$, $h/D = 1.0$, $D = 8$ in.)

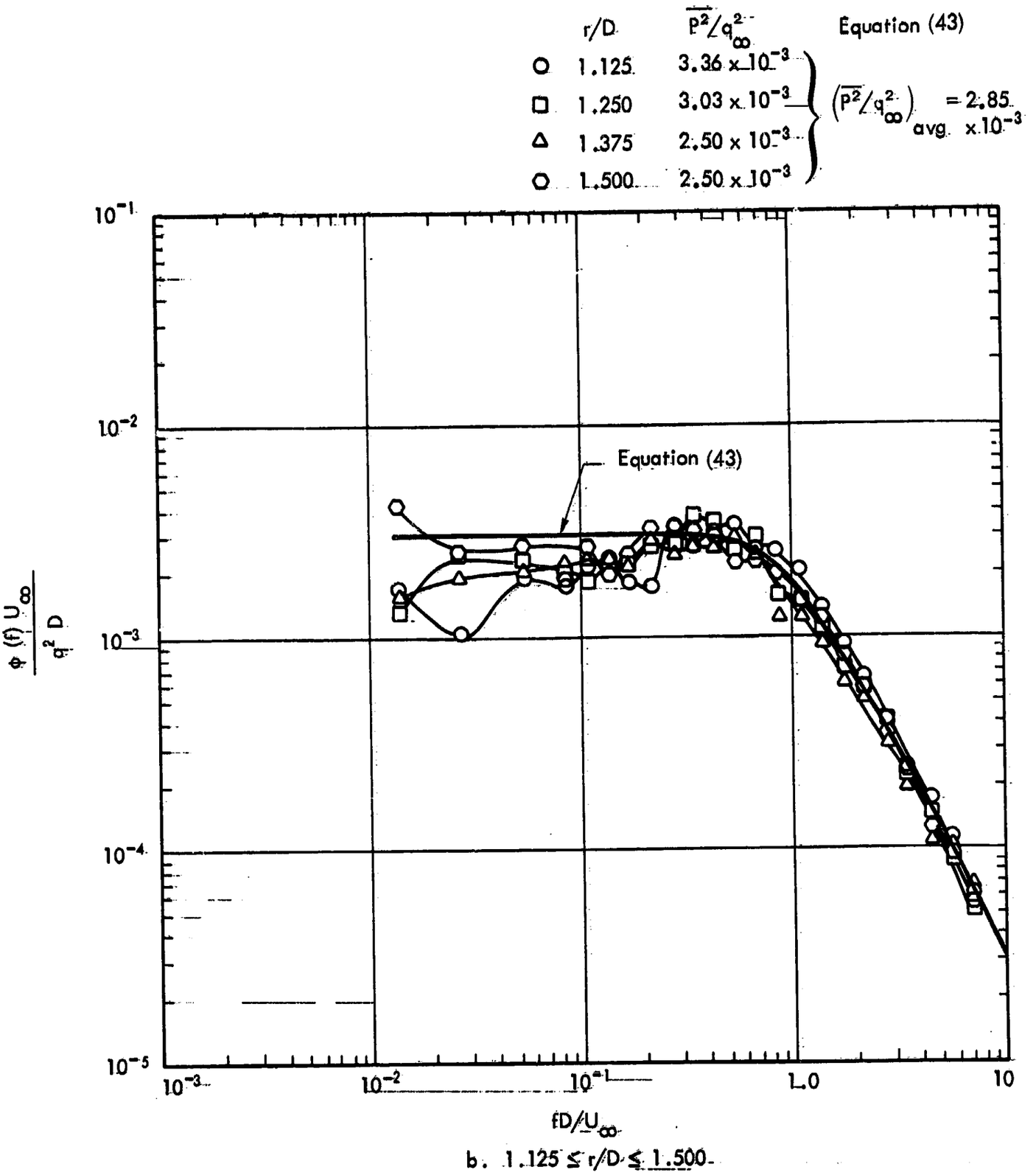

b. $1.125 \leq r/D \leq 1.500$

Figure 27. Continued

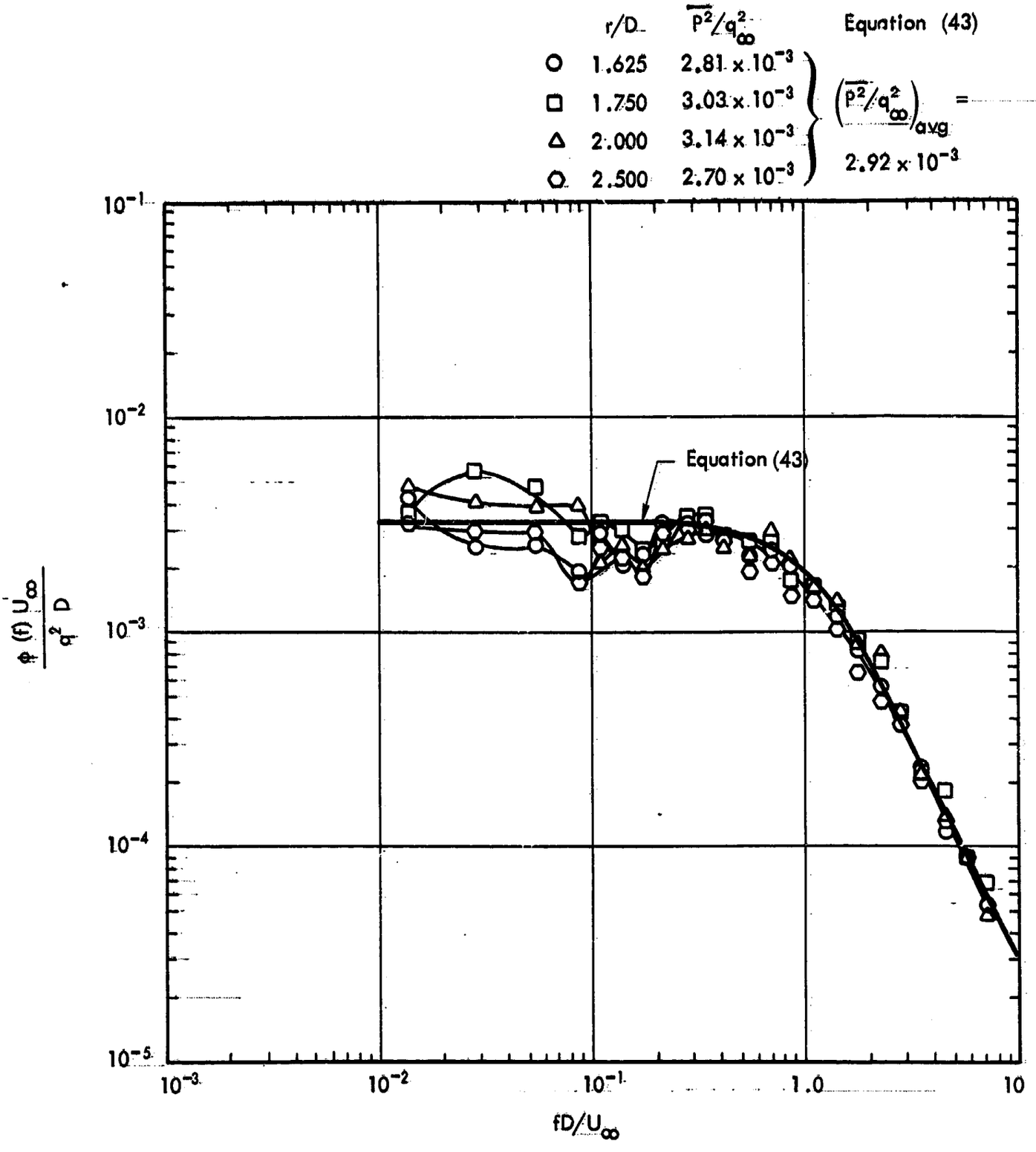

c. $1.625 \leq r/D \leq 2.500$

Figure 27. Concluded

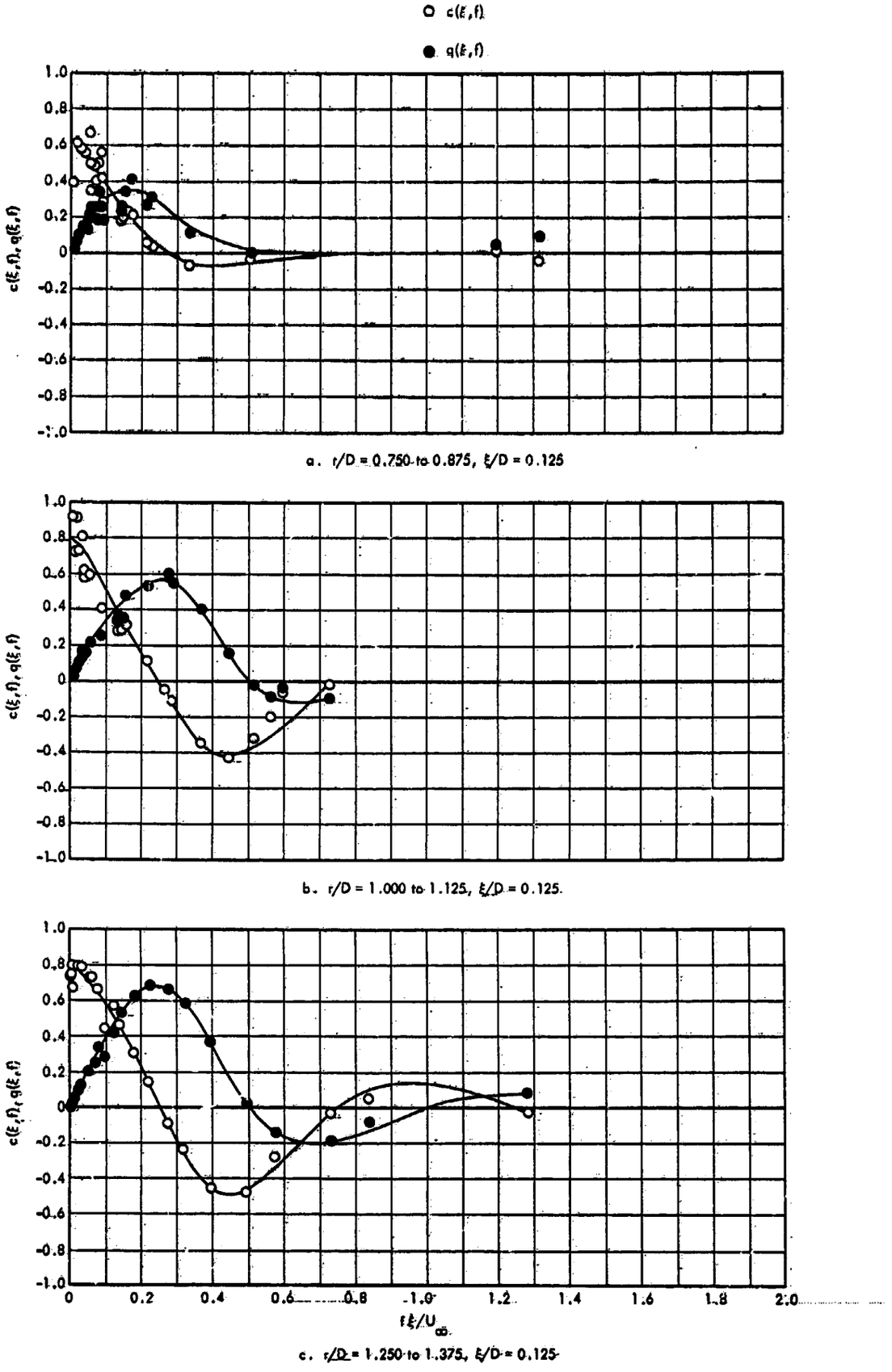

a. r/D = 0.750 to 0.875, ξ/D = 0.125

b. r/D = 1.000 to 1.125, ξ/D = 0.125

c. r/D = 1.250 to 1.375, ξ/D = 0.125

Figure 28. Variation of Longitudinal Cross-Spectra Within the Downstream Wake Flow Field, $M_\infty = 1.60$, $h/D = 2.0$

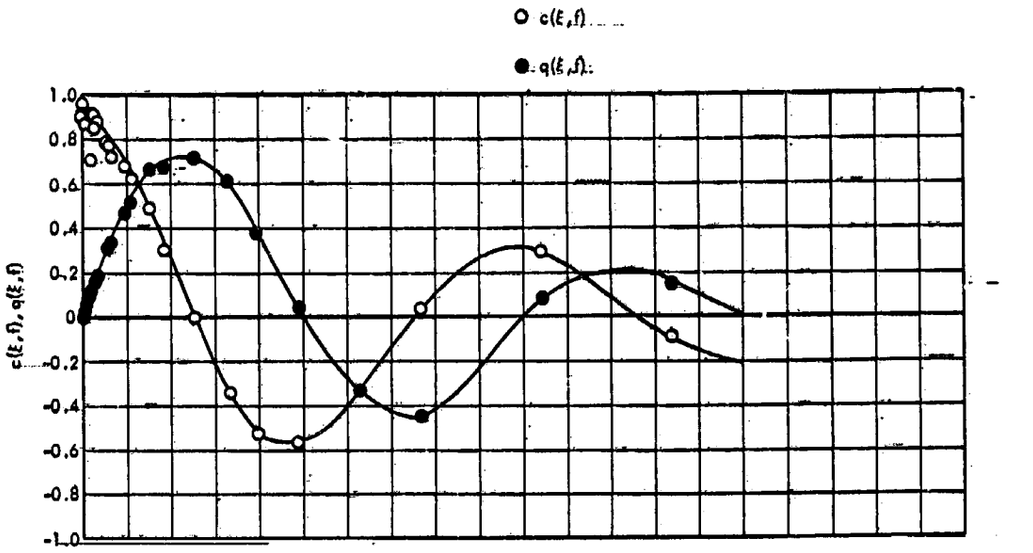

d. r/D = 1.500 to 1.625, ξ/D = 0.125

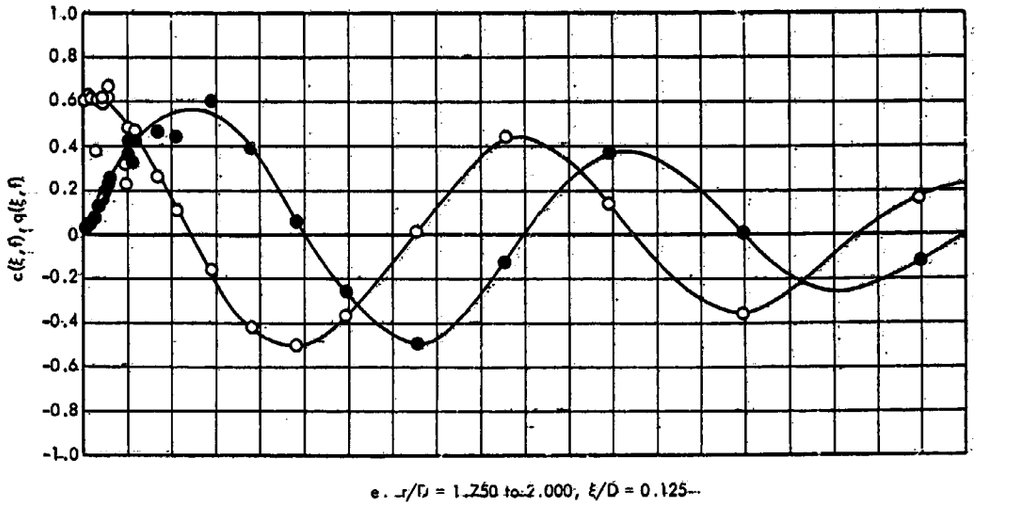

e. r/D = 1.750 to 2.000, ξ/D = 0.125

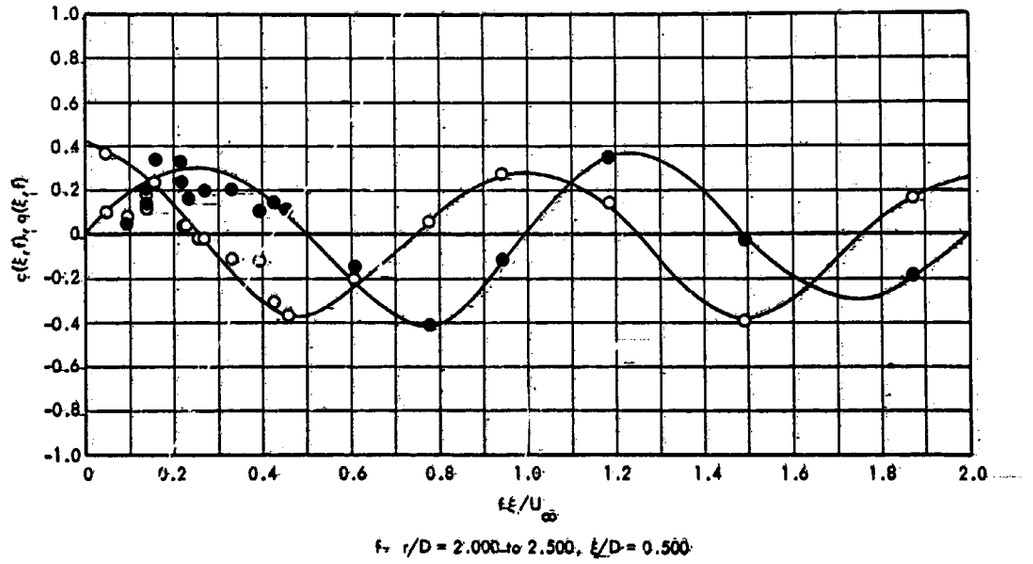

f. r/D = 2.000 to 2.500, ξ/D = 0.500

Figure 28. Concluded

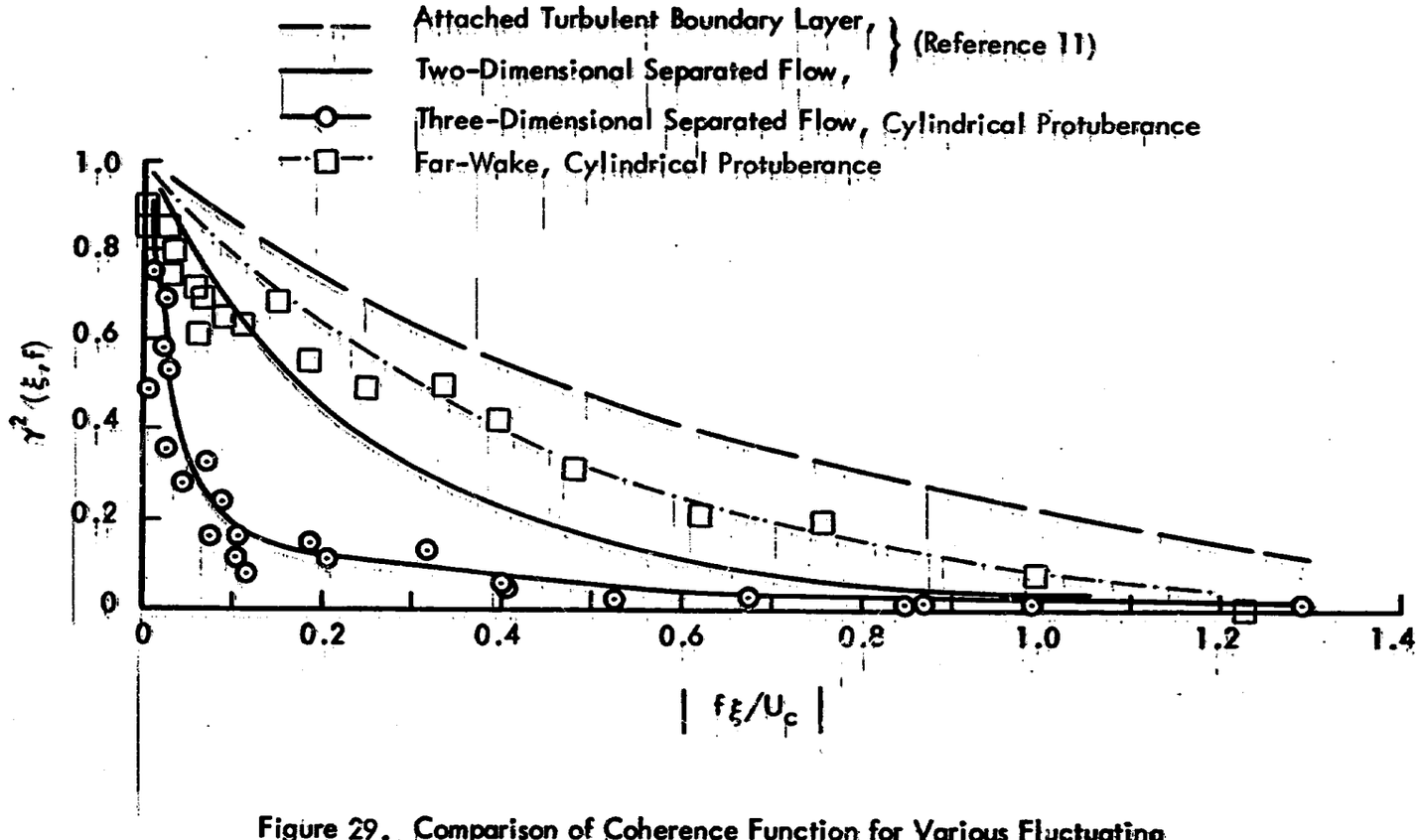

Figure 29. Comparison of Coherence Function for Various Fluctuating Pressure Environments, $M_\infty = 1.60$

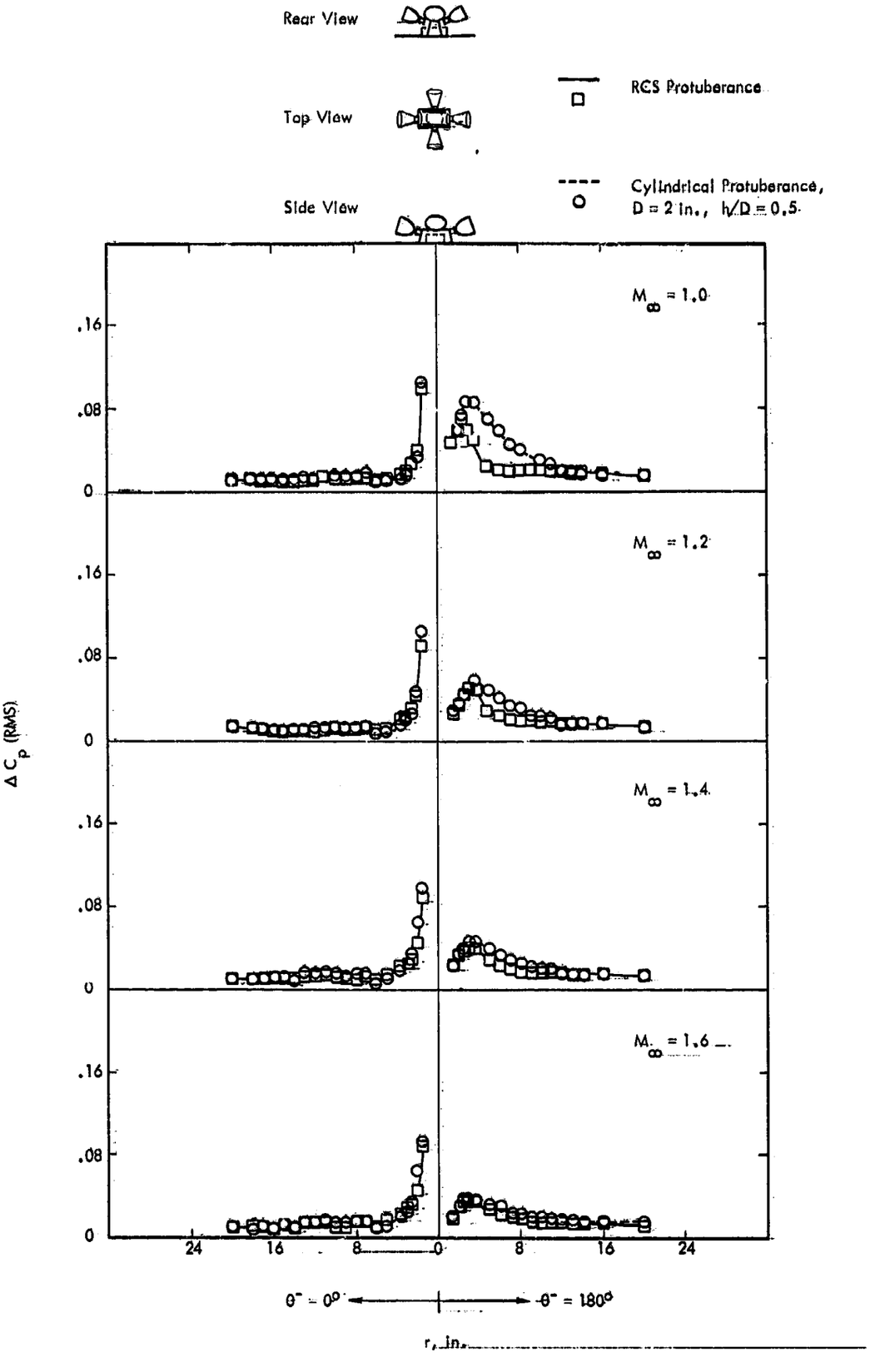

Figure 30. Comparison of the Axial Distribution of RMS Fluctuating Pressure Coefficient for the RCS Protuberance and a Cylindrical Protuberance

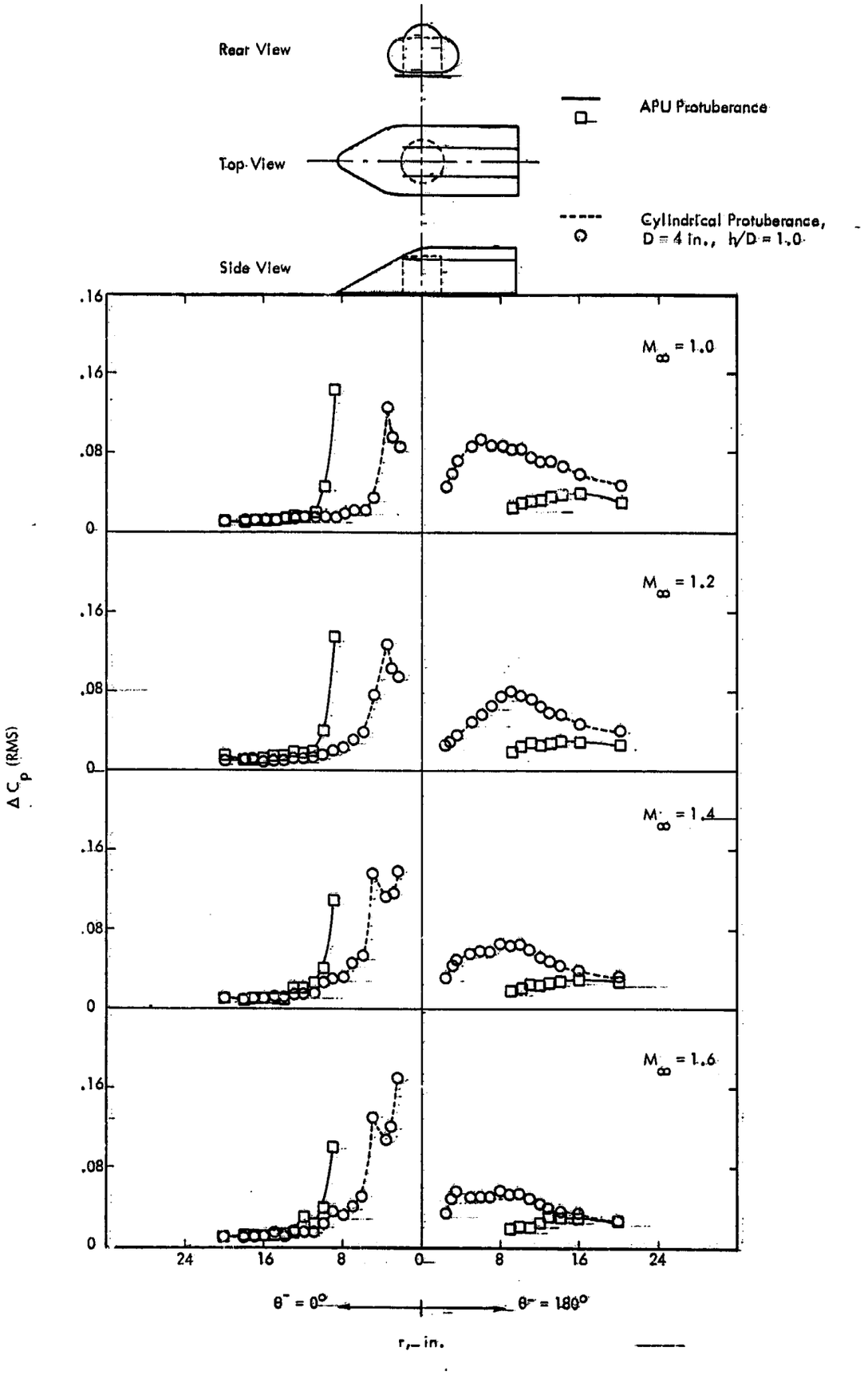

Figure 31. Comparison of the Axial Distribution of RMS Fluctuating Pressure Coefficient for the APU Protuberance and a Cylindrical Protuberance